Technische Universität Dresden

Stochastic harmonic emission model of aggregate residential customers

Ana Maria Blanco Castañeda

von der Fakultät Elektrotechnik und Informationstechnik
der Technischen Universität Dresden

zur Erlangung des akademischen Grades eines

Doktoringenieurs

(Dr.-Ing.)

genehmigte Dissertation

Vorsitzender:	Prof. Dr.-Ing. Wilfried Hofmann		
Gutachter:	Prof. Dr.-Ing. Peter Schegner	Tag der Einreichung:	06.06.2017
	Prof. Dr.-Ing. Matti Lehtonen	Tag der Verteidigung:	25.08.2017

Acknowledgments

I would first like to express my gratitude to my thesis director Prof. Peter Schegner and my thesis advisor Dr. Jan Meyer for their constant support and guidance. I must express my profound gratitude to Dr. Jan Meyer for providing me with unfailing support, stimulating discussions, critical evaluation of the methods and results, and continuous encouragement throughout the process of researching and writing this thesis.

Nobody has been more important to me in the pursuit of this thesis than the members of my family and my friends. I am very grateful to my mother Maria Cristina, who has provided me invaluable emotional support. Without her precious support it would not be possible to finish this task. My profound gratitude goes also to Martin, specially for his patience, motivation and love during the hardest times.

I would like to thank my colleges for their feedback, cooperation and of course friendship.

Finally, I would like to thanks Colciencias for providing the funding for the doctoral studies.

Contents

Nomenclature

List of acronyms

AC	Alternating current
ACF	Autocorrelation function
APT	Apartment
ARIMA	Autoregressive-moving-average model
CDF	Cumulative distribution function
CFL	Compact fluorescent lamp
DC	Direct current
EHV	Extra high-voltage
EMC	Electromagnetic compatibility
EV	Electric vehicle
HV	High-voltage
IEC	International Electrotechnical Commission
IEEE	Institute of Electrical and Electronics Engineers
LED	Light emitting diodes
LV	Low-voltage
MFH	Multi-family house
MV	Medium-voltage
PACF	Partial autocorrelation function
PC	Personal computer
PDF	Probability distribution function
PFC	Power factor correction
POC	Point of connection
PQ	Power Quality
SFH	Single-family house
SMPS	Switch model power supply
RMS	Root mean square

List of symbols

$AHU^{(h)}$	Aggregate harmonic unbalanced factor
C	Capacitance
CAF	Customers aggregation factor

DF	Diversity factor
DM_{E}	Distance measure - Euclidean distance
$DM_{\mathrm{M}g}$	Distance measure - Minkowski distance
DM_{FFT}	Distance measure - Euclidean distance between FFT coefficients
f	Frequency
FC_k	Magnitude of the kth Fourier component (eq. 5.1)
h	Harmonic order
I	Current
$\underline{I}^{(h)}$	Complex harmonic current
$I^{(h)}$	Harmonic current magnitude
IN_{av}	Average annual income per household
K	AR model, constant
ℓ_{TOT}	Total line length (cables and overhead lines)
L	Inductance
m_{cg}	Number of groups of aggregate customers (c.f. section 6.2)
MRL	Mean resultant length
n_{cg}	Number of customers in a aggregate group of customers (c.f. section 6.2)
n_{EV}	Number of aggregate electric vehicles
$n_{\mathrm{u\ TOT}}$	Total number of customers
$n_{\mathrm{u\ SFH}}$	Number of single family houses
$n_{\mathrm{u\ APT}}$	Number of apartments
N_μ	First parameter of a normal distribution (mean value)
N_σ	Second parameter of a normal distribution (variance)
$\mathbf{P}$	Permutation matrix (eq. B.9)
$P_{\mathrm{G\ TOT}}$	Total rated active power of the distributed generators
PF	Power factor
R	Resitance
R^2_{adj}	Coefficient of determination
s	Scaling factor (eq. 5.6)
$S_{\mathrm{r\ T}}$	Rated power of the distribution transformer
$S_{\mathrm{k\ T}}$	Short-circuit power of the distribution transformer
SM_{C}	Similarity measure - Cosine measure
SM_{P}	Similarity measure - Pearson's correlation coefficient
t	Time
T	Period
$\underline{\mathbf{T}}_{120}$	Transformation matrix for symmetrical components
THD	Total harmonic distortion
$u_{\mathrm{k\ T}}$	Short-circuit voltage of the distribution transformer
$\underline{U}^{(h)}$	Complex harmonic voltage
Y	Admittance

Z	Impedance
α	AR model, correlation between successive values
$\varphi^{(h)}$	Harmonic current phase angle
σ	AR model, variance of the normal distribution
ρ_{pop}	Population density
θ_k	Angle of the kth Fourier component (eq. 5.1)
μ	First parameter of a von Mises distribution (measure of location)
κ	Second parameter of a von Mises distribution (measure of concentration)

Functions

$\mathcal{N}(N_\mu, N_\sigma)$	Normal distribution with mean N_μ and variance N_σ
$\mathcal{VM}(\mu, \kappa)$	Von Mises distribution with parameters μ and κ (eq. B.3)

Subscripts

A, B, C	Line conductors
ARI	Arithmetic sum
b	Balanced component
D	Deterministic component
MD	Mean direction
N	Norton
norm	Normalized value with a min-max normalization
norm-z	Normalized value with a z-score normalization
PHS	Phasorial sum
R	Stochastic component
S	Seasonal variation
T	Trend or secular variation
TOT	Total
u1	First unbalanced component
u2	Second unbalanced component
[*number*]	Percentile rank (i.e. $x_{[95]}$: 95$^{\text{th}}$ percentile of x)
[*number,number*]	Difference between percentiles (i.e. $x_{[95,5]} = x_{[95]} - x_{[5]}$)
[max]	Maximum value
[min]	Minimum value

Superscripts

(h)	Harmonic order

1. Introduction

The concern about the causes and effects of harmonics in power systems began in the 1920's when distorted voltage and current waveforms were observed on power lines for the first time [58]. The level of harmonics was very small in the past, but with the increasing number of electronic devices (harmonic sources) used by industrial, commercial and residential customers, the level of harmonic voltages and harmonic currents in the networks have increased, and with them the need of more accurate and complete studies about harmonics.

Research has been focused mainly on the harmonic distortion caused by industrial installations, due to the high power electronic devices that they use. However, the amount of electronic devices used by residential customers have also increased significantly during the last decades. Different electronic household appliances, like computers, compact fluorescent lamps, LEDs, flat panel TVs, smart-phones, etc., and new technologies as electric vehicles and photovoltaic systems are now widely used by residential customers. Fig. 1.1 shows exemplary the increment of some electronic household appliances and electric vehicles during the last years in Germany.

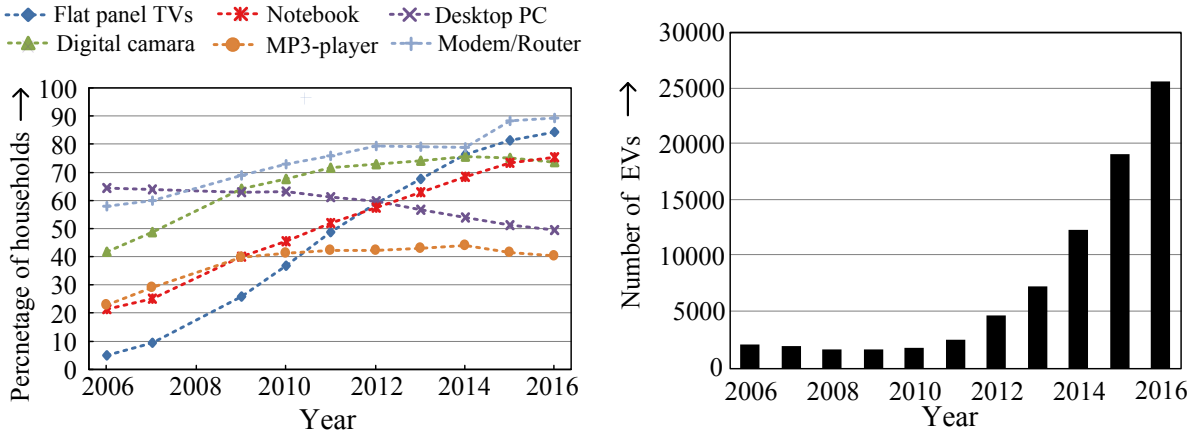

(a) Household appliances [121]

(b) Electric vehicles [120]

Figure 1.1.: Increase of some household appliances and electric vehicles in Germany

The increasing number of harmonic sources in public distribution networks may lead to an unacceptable increase in the voltage and current distortion levels and other unwanted effects, like additional loading of the neutral conductor, overheating of network elements, damage of equipment, etc. Therefore, the causes and effects of harmonic voltages and currents are more and more considered in both the planning and the operation of distribution systems. This analysis is complex, because multiple factors influence the emission and propagation of harmonics through the network, like the network impedance, the voltage distortion and the time-variation of number and type of connected equipment.

The analysis of harmonic propagation in public distribution networks requires the development of aggregate models, that represent the harmonic emission of the multitude of household appliances. The emission of harmonic currents of residential customers is highly time-variant due to the continuous changes in load conditions (e.g. types and number of connected devices) and system parameters (e.g. voltage distortion). These variations have a non-deterministic

character, which is better represented with stochastic models.

There are two common approaches to obtain stochastic models of the harmonic emission of aggregate customers: component-based approach and measurement-based approach. The component-based approach uses a bottom-up methodology, where models of individual household appliances are combined to build the model of multiple customers. This approach requires high amount of input data, like models of individual household appliances and detailed information of customer behavior and device composition, which is usually not easy to acquire. The measurement-based approach is based on long-term measurements of the networks, which include inherently the real harmonic emission of the multitude of household appliances and the behavior of the individual residential customers.

Most of the present models were developed with the component-based approach. The measurement-based approach has not been widely used due to limitations to obtain a representative sample of measurements of the networks. However, with the increasing number of measurement instruments in low and medium voltage networks as well as the integration of harmonic measurement capabilities into smart meters, it is expected that the required measurements will be available in the near future.

Objective of the thesis

The main objective of the thesis is to develop a stochastic model of the low-order harmonic emission of aggregate residential customers for harmonic analysis of low and medium-voltage networks. Different to the present models, this stochastic model is based on a measurement-based approach, where measurements of several low-voltage networks are used to represent the most important characteristics of the harmonic emission of aggregate residential customers.

The stochastic model includes not only the representation of harmonic magnitudes, but also the representation of harmonic phase angles. The inclusion of the phase angles in the model allows a more accurate analysis of the harmonic propagation in the networks, where the real complex summation of harmonic currents is considered.

Outline of the thesis

The document is organized in three parts. The first part (chapters 2 and 3) includes a detailed description of the propagation of harmonic currents in distribution systems, and the present models of the harmonic emission of residential customers available in the literature. Based on a systematic comparison of the component-based and measurement-based approaches, the advantages and disadvantages of both approaches are identified, and the feasibility of the measurement-based approach to generate accurate models of aggregate customers is explained.

The second part (chapter 4) analyzes the characteristics of the harmonic currents of several low-voltage residential networks obtained thorough an extensive measurement campaign in Germany. Different methods are applied in order to characterize the stochastic variation of harmonic magnitudes and phase angles, and their correlation with different electric and non-electric parameters. Based on the most relevant characteristics of the real emission of aggregate residential customers, the main characteristics of the model are identified.

The third part of the document (chapters 5 and 6) contains a detailed description of the modeling methodology applied to obtain the representation of the harmonic emission of aggregate residential customers for the simulation of low-voltage and medium-voltage networks. The model is parameterized with the measurements of German networks, but the methodology can be easily applied to obtain the model of other regions or countries. Finally, the model is used in a practical application example (chapter 7), where the impact of electric vehicles on medium-voltage networks is studied.

2. Fundamentals of harmonic distortion

The term power quality began to be extensively used in the 1970s due to the proliferation of electronic equipment, which represented a major change in the usual design and operation of electric power systems. There is no universally accepted definition of power quality, and usually the definition depends on the point of view of the affected entities, i.e. the energy suppliers, the network operators, or the customers. The International Electrotechnical Commission (IEC) defines power quality in the standard IEC 61000-4-30 as the "characteristics of the electricity at a given point in an electrical system, evaluated against a set of reference technical parameters" [68]. In this way, power quality may be interpreted as the combination of voltage quality and current quality. Voltage and current quality are concerned with deviations of the real voltage and current waveforms from the sinusoidal reference waveform with constant magnitude and frequency [20].

Power quality covers a multitude of electromagnetic disturbances that may deteriorate the voltage and current quality. In order to ensure a "good" quality, all the elements in a power network (environment) should be electromagnetically compatible, i.e. each element should not cause intolerable disturbances to other elements and it should be sufficiently immune to disturbances inside the power network [63]. The sources of the disturbances, the way they propagate in the power network, and the effects that they may produce on other network elements have to be studied in order to establish limits that ensure a proper operation of the whole power system and an acceptable deviation of the voltage and current waveforms.

Fig. 2.1 illustrates the electromagnetic compatibility problem. An emitter (source of disturbance, e.g. a lightning strike, a machine, etc.) produces a disturbance and a coupling path transfers the disturbance to a receiver (other elements in the power network), where it may result in an undesired behavior. The problem concerns all three elements and not only the emitter. The coupling path may alter the original electromagnetic disturbance, which may result in an increase or decrease in the effects on the receiver. Moreover, the receiver should have some immunity to the disturbances since a power network is never disturbance-free.

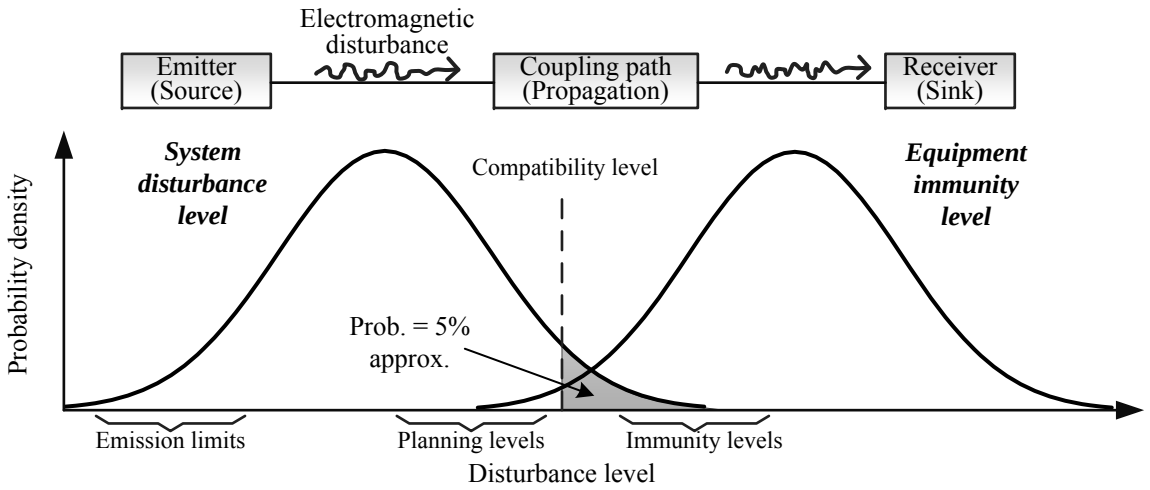

Figure 2.1.: The electromagnetic compatibility problem [63]

Depending on the disturbance level (total disturbance produced by all the emitters) and the equipment immunity level, different limits, as shown in Fig. 2.1, can be defined in order to ensure the electromagnetic compatibility in power networks:

1. Compatibility level is the level of a disturbance which can be expected in a power network, allowing for a small probability (less than 5%) of it being exceeded [63].
2. Emission limits are the maximum disturbance level that any emitter is allowed to produce [62].
3. Immunity level is the level of disturbance that the receiver should tolerate such that it can remain capable of operating at a required degree of performance [62]. The immunity levels should be higher than the accepted compatibility level.
4. Planning level is the level of a disturbance in a specific network that is adopted as reference value by the network operator to set the emission limits of a group of emitters or large emitters which are to be connected to that network [63]. The planning level should be lower than the accepted compatibility level.

There are several electromagnetic disturbances present in the networks. This thesis is focused exclusively on the waveform distortion, specifically on harmonic distortion.

2.1. Waveform distortion and harmonic distortion

Waveform distortion is one of the most common electromagnetic disturbances present in power systems. It is the steady-state deviation of voltages and currents from the ideal sine waveform [48]. Periodic distorted voltages and currents are usually studied using the Fourier transform, which decomposes the original distorted signals into a linear combination of pure sinusoids:

$$x(t) = c_0 + \sum_{k=1}^{\infty} c_k \cdot \sin\left(f_k \cdot 2\pi \cdot t + \theta_k\right) \tag{2.1}$$

where c_0 is the DC component, c_k and θ_k are the amplitude and phase angle of the spectral component of order k with frequency $f_k = (k/N)f_{h1}$, f_{h1} is the fundamental frequency (50 or $60\,\mathrm{Hz}$ in most power systems), and N is the number of fundamental periods within the window width. According to the standard IEC 61000-4-7 [66], $N = 10$ for $50\,\mathrm{Hz}$ systems and $N = 12$ for $60\,\mathrm{Hz}$ systems. In this document, all quantities are referred to $50\,\mathrm{Hz}$ systems.

Using the Fourier transform, the total waveform distortion can be separated into:

- Harmonics: Spectral components with frequencies that are integer multiples of the fundamental frequency. These spectral components are renamed as harmonic components, e.g. the 30^{th} spectral component corresponds to the third harmonic component if $N = 10$ and f_{h1} =$50\,\mathrm{Hz}$.
- Interharmonics: Components with frequencies that are non-integer multiples of the fundamental frequency, e.g. $f_{35} = 3.5 \cdot (50\,\mathrm{Hz})$ =$175\,\mathrm{Hz}$ if $N = 10$ and f_{h1} =$50\,\mathrm{Hz}$. All interharmonics with frequencies below the fundamental frequency ($k = 1, 2, .., 9$) are known as subharmonics.
- Supraharmonics: Spectral components in the frequency range between 2 to $150\,\mathrm{kHz}$ [21].
- DC-offset: The constant component c_0 (non-sinusoidal component).

Fig. 2.2 presents an example of a distorted signal with a fundamental frequency of $50\,\mathrm{Hz}$ composed with a DC-offset, an subharmonic component at $25\,\mathrm{Hz}$, and two harmonic components

at 100 Hz (second harmonic) and 150 Hz (third harmonic), as described in eq. 2.2.

$$x(t) = 20 + 20 \cdot \sin(25 \cdot 2\pi \cdot t) + 80 \cdot \sin(50 \cdot 2\pi \cdot t - 30°) + 40 \cdot \sin(100 \cdot 2\pi \cdot t - 10°) + 50 \cdot \sin(150 \cdot 2\pi \cdot t) + 40°) \quad (2.2)$$

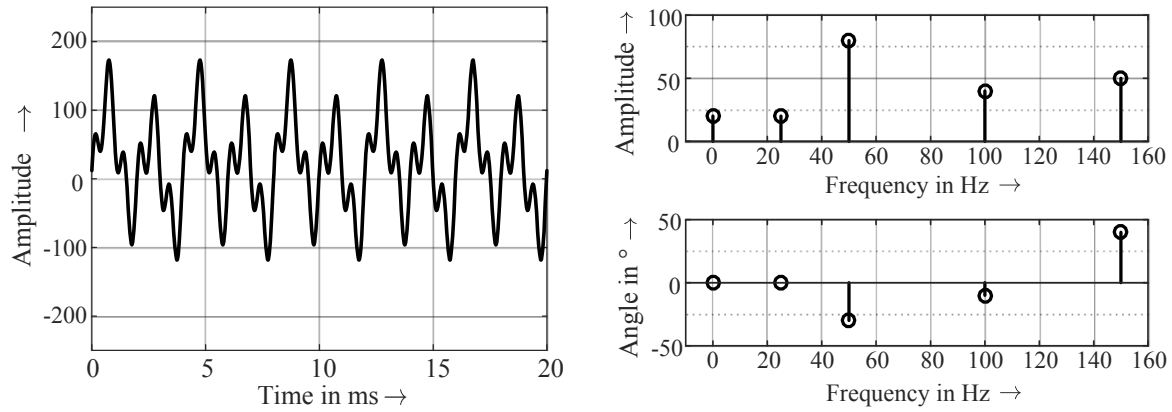

(a) Time-domain signal

(b) Spectrum

Figure 2.2.: Example of the distorted signal in eq. 2.2

In most public power networks, the DC-offset, interharmonics, and supraharmonics are very small and difficult to measure and study. Low-order harmonics (harmonics with frequencies below 2 kHz) are the most studied distortions due to the continuous increase of harmonic sources in the networks (emitters) and the subsequent need to understand their effects on the network elements. The scope of this document is limited to low-order harmonics.

The most applied index to quantify the harmonic distortion of a signal is the *Total Harmonic Distortion* THD. The THD is the ratio of the RMS value of the sum of all harmonic components ($Y^{(h)}$) up to a specified order (H) to the RMS value of the fundamental component ($Y^{(1)}$) [66]:

$$THD_{\mathrm{Y}} = \sqrt{\sum_{h=2}^{H} \left(\frac{Y^{(h)}}{Y^{(1)}} \right)^2} \quad (2.3)$$

The symbol Y should be replaced by the symbol I for currents or by the symbol V for voltages. Usually only the first 40 or 50 harmonics are considered in the calculation of the THD_{Y}. The signal of Fig. 2.2 has a THD of 112.5 %.

The following sections explain the electromagnetic problem related to low-order harmonic distortion in public low-voltage networks, including a description of the harmonic sources, the propagation mechanism, their effects on the network elements, and the related standardization.

2.2. Sources of low-order harmonics

Harmonic distortion is caused by non-linear devices, i.e. devices that draw a current waveform that is not directly proportional to the applied voltage. Electric equipment often has a non-linear behavior. For example, power transformers and generators are non-linear devices since

they use ferromagnetic materials that are operated very close to the non-linear region. This produces a non-sinusoidal magnetizing current even if the applied voltage is sinusoidal.

However, the main source of harmonics in power systems is the electronic equipment used by industrial, commercial, and residential customers. Numerous types of industrial electronic equipment emit harmonic currents, like three-phase power converters and arc welders. However, in public low-voltage networks, the principal sources of harmonics are the multitude of electronic household appliances used by residential and commercial customers, like energy saving lamps (CFLs and LEDs), computers, television sets, battery chargers, electric vehicles, etc.

Electronic appliances usually have a switch mode power supply (SMPS) for their operation. A simple SMPS has a three stage topology, consisting of protection and filtering, rectification, and inverting stages (c.f. Fig. 2.3). The first stage contains different elements that protect the SMPS from e.g. current peaks, and also an EMC filter that reduces the high-frequency components emitted by the SMPS [34, 134]. The rectification stage includes a capacitor-fed diode bridge rectifier and provides smooth DC voltage to the inverting stage. Finally, the inverter stage converts this DC voltage to a stabilized voltage/current signal of certain shape and level required by the load [17]. For harmonic studies, usually the first two stages are represented in detail and the inverting stage is simply represented with a resistor, as shown in Fig. 2.3 [134].

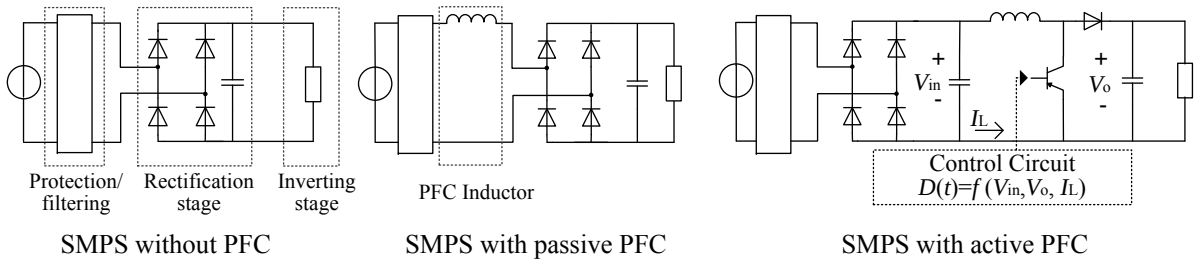

Figure 2.3.: Simplified circuit diagram of electronic appliances with SMPS

Depending on the existence of standardized limits (e.g. IEC 61000-3-2 [69]), some devices also implement a power factor correction stage (PFC). PFC methods can be classified as passive and active according to their components. Passive PFC methods use capacitors and/or inductors either to the input or the output of the rectification stage in order to improve the shape of the current pulse (see Fig. 2.3) [134]. It is a cost-effective and reliable way to lower current distortion, but passive PFC methods nevertheless increase the size and weight parameters of SMPS by using bulky capacitors and inductors. These drawbacks are not present in active PFC topologies, which use different DC-DC converters that shape the input current waveform by high-frequency switching and control circuits [17].

Fig. 2.4 compares the current waveforms and the harmonic current magnitudes of some electronic household appliances with different topologies obtained when an undistorted voltage waveform was used for the measurements. CFLs below and equal $25\,\mathrm{W}$ have a simple SMPS without PFC, while CFLs higher than $25\,\mathrm{W}$ have a SMPS with active PFC due to the requirements of the standard IEC 61000-3-2 [69]. Computers power supplies are available with passive PFC or active PFC topologies. Fig. 2.4-b also compares the total harmonic distortion of the current (THD_I) and the power factor (PF) of the devices (Power factor is the ratio of the total active and apparent power as defined in [70]). Devices without PFC usually have the highest distortion and lower power factor ($THD_\mathrm{I} > 80\,\%$, and $PF < 0.7$), while active PFC topologies have the best performance related to low-order harmonic emission ($THD_\mathrm{I} < 30\,\%$, and $PF > 0.85$).

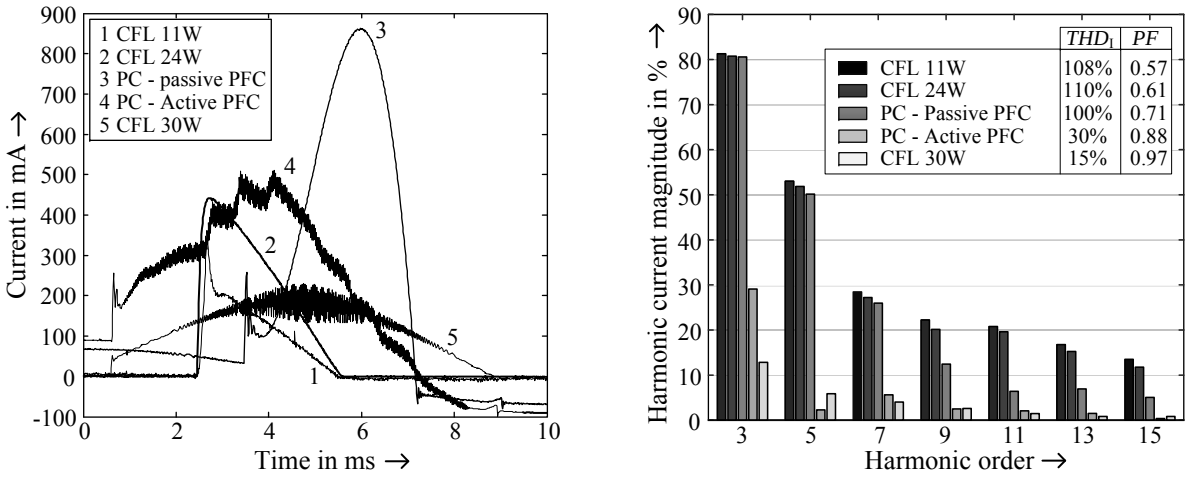

(a) Current waveforms (first half cycle)

(b) Current spectrum

Figure 2.4.: Harmonic currents emitted by five electronic household appliances when an undistorted voltage is applied [17]

2.2.1. Variation of harmonic current emission of electronic household appliances

Harmonic current emission of electronic devices varies with the distortion of the voltage supply. Fig. 2.5 shows the fifth harmonic current emitted by different household appliances when a sinusoidal and a flat-top voltage supply is applied. A flat-top voltage was selected because almost all residential low-voltage networks show a more or less distinctive flat-top voltage that is caused by the massive use of single-phase SMPS. The characteristics of the flat-top voltage waveform used for these measurements are described in [14]. A comparison of Fig. 2.5a and Fig. 2.5b reveals that the harmonic current magnitudes and phase angles change more or less significantly with voltage distortion. This phenomenon is usually known in the literature as *attenuation effect* because in most of the cases, when a flat-top voltage is applied, the harmonic emission of the electronic devices decreases, i.e. it is attenuated. However, as already proved by several authors, depending on the voltage waveform characteristics (magnitude and phase angle of the voltage harmonics), harmonic current emission of electronic devices can increase or decrease [17, 30, 87, 104].

It is also noticeable from Fig. 2.5 that devices of the same topology do not have exactly the same harmonic emission. This is caused by slight changes in the circuit elements or circuit schematic implemented by the different manufacturers. Moreover, some devices have non-steady state harmonic current emission, such as computers, laptops, and battery chargers, which depend strongly on customer behavior and/or operating modes. A specially designed constant resistive load connected to the DC-side was used for the measurements of computers and laptops shown in Fig. 2.5 and Fig. 2.4.

2.2.2. Harmonic current emission of groups of household appliances

The total harmonic current emitted by several devices at one connection point is calculated as the phasor sum of the harmonic currents emitted by the devices. Thus, the presence of different devices with different topologies at one connection point can cause a diversity of harmonic current phase angles, and subsequently may lead to a lower magnitude of the phasor sum than the arithmetical sum of the harmonic current magnitudes. This is known as *cancellation effect* and has a high influence on the total harmonic distortion emitted by larger groups of electronic

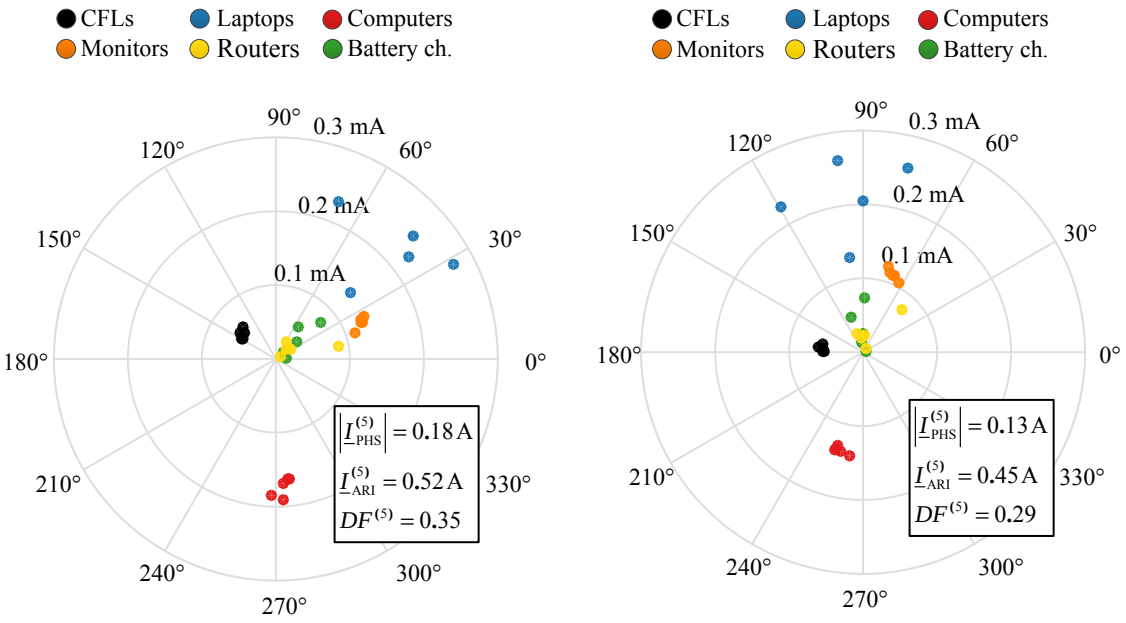

(a) Sinusoidal voltage

(b) Flat-top voltage

Figure 2.5.: Fifth harmonic current of different appliances measured with a sinusoidal and a flat-top voltage waveform. Measurements from [72]

devices in the network [94]. The cancellation effect is commonly quantified by the phase angle diversity factor $DF^{(h)}$ individually for each harmonic order [17]:

$$DF^{(h)} = \frac{\left|\underline{I}^{(h)}_{\mathrm{PHS}}\right|}{I^{(h)}_{\mathrm{ARI}}} = \frac{\left|\sum_{i=1}^{n} \underline{I}^{(h)}_{i}\right|}{\sum_{i=1}^{n} |\underline{I}^{(h)}_{i}|} \tag{2.4}$$

where $\underline{I}^{(h)}_{i}$ represents the harmonic current phasor of the device i, n is the number of devices, and h is the order of the harmonic. The phase angle diversity factor varies between 0 (perfect cancellation) and 1 (no cancellation). Fig. 2.5 shows the $DF^{(h)}$ factors obtained for each group of devices under the different voltage distortions. In both cases, the arithmetical sum of the harmonic currents $I^{(5)}_{\mathrm{ARI}}$ is higher than the magnitude of the phasor sum $\underline{I}^{(h)}_{\mathrm{PHS}}$, which results in a good cancellation between the harmonic currents and, subsequently, in a low diversity factor. The diversity of harmonic phase angles that lead to a cancellation of harmonic currents emitted by different appliances is an effective way to manage harmonic current emission in public low-voltage networks [96].

2.3. Propagation of harmonics in distribution networks

Harmonic analysis is conducted to determine the propagation of harmonic currents through the network and calculate the resulting distortion of the voltage waveform. It must consider not only the harmonic currents emitted by household appliances (emitters of distortion), but also the characteristics of the network (coupling path) and the presence of other linear and non-linear devices. The main objectives of harmonic analysis are [39, 48]:

- Determine individual and total harmonic distortion levels produced by harmonic sources

at individual nodes and at the distribution transformer and verify the compliance with the standards.

- Analyze the effects of harmonic currents and voltages on network elements.
- Specify the design characteristics of harmonic filters to reduce the harmonic distortion levels.
- Assess the connection of new loads /customers in order to maintain the harmonic distortion levels within tolerable limits.

2.3.1. Methods for harmonic analysis

There are three main methods for harmonic analysis: time-domain, frequency-domain, and hybrid methods [91]. In the time-domain method, the dynamic characteristics of the power networks are represented in terms of non-linear differential equations that are usually solved by numerical integration [56]. This method is the most accurate one, but it requires considerable time and computing resources, making it hard to simulate extensive or complex networks. Moreover, the modeling of some loads and network components (overhead lines, cables, transformers, etc.) in the time-domain may require deep knowledge of internal components and circuit schema, which is often not easy to acquire.

Frequency-domain methods are preferred because they require simpler computation programs and short computing times. In this case, the network components are modeled considering their frequency-dependent characteristic. The harmonic sources are usually represented with a Norton model that represents the injection of harmonics with a current source [56] (see Fig. 2.6).

There are several simplifications that may be applied to harmonic studies in the frequency-domain:

- Independence: It can be assumed that the networks respond to each harmonic independently of others, thus each harmonic can be treated separately [131]. With this simplification, an equivalent circuit for each harmonic order is obtained and solved independently to find the respective harmonic voltage at each node. Using the superposition principle, the total distortion in the network is the result of the sum of the responses obtained for each harmonic order [56].
- Network balance: It is common to assume that the network is completely balanced and the original three-phase network can be solved using a single-phase representation [56].
- Background distortion: Real voltages and currents in the medium-voltage networks are also polluted with harmonics, and some of those harmonics cross through the distribution transformer to the low-voltage network. However, it is commonly assumed that the voltage distortion at the low-voltage side of the distribution transformer is negligible (no background distortion).

Fig. 2.6 shows exemplary the representation of a simple balanced network with a unique harmonic source in the frequency-domain. If the independence and network balance conditions are applied, the network can easily be solved by direct methods for each harmonic order:

$$\underline{U}^{(h)} = \left(\frac{\underline{Z}_{\mathrm{S}}^{(h)} \underline{Z}_{\mathrm{N}}^{(h)}}{\underline{Z}_{\mathrm{S}}^{(h)} + \underline{Z}_{\mathrm{N}}^{(h)}} \right) \left(\frac{\underline{U'}_{\mathrm{MV}}^{(h)}}{\underline{Z}_{\mathrm{S}}^{(h)}} + \underline{I}_{\mathrm{N}}^{(h)} \right) \tag{2.5}$$

$$\underline{Z}_{\mathrm{S}}^{(h)} = \underline{Z'}_{\mathrm{MV}}^{(h)} + \underline{Z'}_{\mathrm{T}}^{(h)} + \underline{Z}_{\mathrm{L}}^{(h)} \tag{2.6}$$

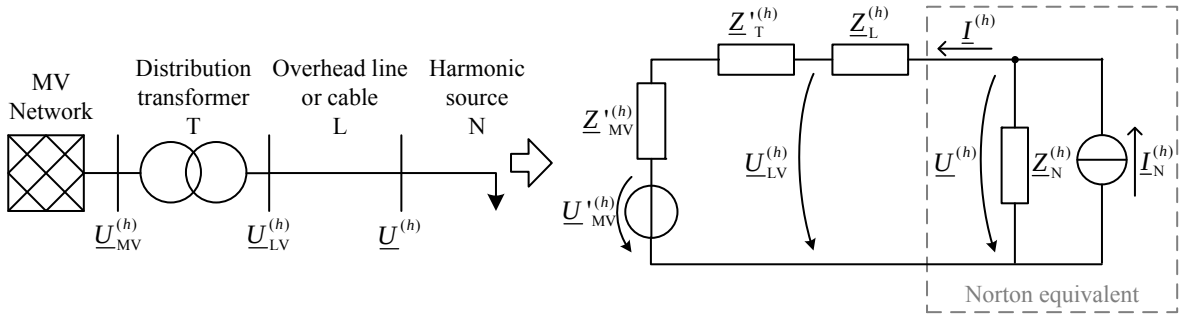

Figure 2.6.: Simple low-voltage network representation for harmonic studies in frequency-domain

The relation between the impedances in the network determines the flow of harmonic currents. For example, if the Norton impedance $\underline{Z}^{(h)}_{\mathrm{N}}$ (equivalent impedance that represents the customers/loads) is considerably bigger than the system impedance $\underline{Z}^{(h)}_{\mathrm{S}}$, the current $\underline{I}^{(h)}_{\mathrm{N}}$ will flow directly towards the medium-voltage network. This assumption is usually accepted in the analysis of residential low-voltage networks, thus the impedance $\underline{Z}^{(h)}_{\mathrm{N}}$ is neglected and the Norton model is commonly simplified with a Current source model. If the background distortion is also neglected, the voltage source in Fig. 2.6 is eliminated.

The flow of harmonic currents can be altered by the presence of other loads, especially the presence of power factor capacitors. A resonance may occur if the natural frequency of the network lines up with the frequency of one harmonic current present in the network, which can increase the harmonic voltages and currents at that frequency considerably. However, the resistance in the network usually provides enough damping to prevent the rise of catastrophic voltages and currents [48].

The accuracy of the frequency-domain technique relies on the accurate representation of all linear and non-linear devices, which is usually a challenging task. Hybrid methods have been developed in order to combine the individual advantages of the frequency-domain and time-domain methods [91]. In this case the linear network components are represented in the frequency-domain while the non-linear devices and the time-varying components are represented in the time-domain. First, the response of non-linear devices is obtained in a time-domain simulation, and the results are integrated to solve the complete network in the frequency-domain. In this way the hybrid method combines the computational efficiency of the frequency-domain method and the accuracy of the time-domain method.

2.3.2. Aggregate harmonic emission models

It is not practical to simulate an entire distribution network using individual models of each device; hence, it is indispensable to develop aggregate models that represent the aggregate harmonic emission of sets of devices. Depending on the goal of the harmonic study, different levels of aggregation, like individual customers, customer groups, or all customers of a low-voltage network might be useful [17].

There are two common methodologies to obtain aggregate harmonic emission models (aggregate model in short): component-based and measurement-based approaches. The component-based approach uses a bottom-up methodology which models each individual device (household appliances) to set up the aggregate model of a customer or a group of customers. The measurements-based approach is based on measurements of the network, which inherently includes the aggregate effect of individual devices connected to a respective measurement point. Moreover, the aggregate model can be deterministic or stochastic. Deterministic aggregate models represent specific harmonic emission levels, for example, the maximum or the 95$^{\mathrm{th}}$ per-

centile of the harmonic emission of aggregate customers during one week, while stochastic aggregate models represent the random variation of emitted harmonic currents through probability distributions. Chapter 3 contains a detailed review of the types of harmonic emission models of residential customers for harmonic studies in low-voltage networks.

The selection of the harmonic emission models depends on the goal of the harmonic analysis. If a rough estimation of the harmonic voltages and currents in the network is sufficient, then deterministic models can be used. However, increasing the simplicity of the models will lead to more uncertain results. There is always a trade off between the complexity of the models and the desired accuracy of the results.

Table 2.1 lists some common harmonic analyses of public medium and low-voltage networks with the most suitable aggregate models. Deterministic models are sufficient in most of the cases, but there are some specific analyses that require a more complete model that represents in high detail the variation of harmonic currents emitted by the customers, including the stochastic variation and/or the daily pattern. The development of accurate deterministic or stochastic models is a complex task that comprises several steps, such as the measurement of household devices, individual and/or aggregate customers, data processing, attempt different modeling methods, model verification, etc.

Table 2.1.: Main harmonic analyses and their related harmonic emission models.

Harmonic analyses	**Harmonic emission model**
Calculate the voltage distortion at different nodes of the medium-voltage distribution network and evaluate the compliance with standards.	Deterministic model of the complete low-voltage network.
Calculate the voltage distortion at different nodes of the low-voltage distribution network and evaluate the compliance with the standards.	Deterministic model of individual customers or aggregate customers.
Analyze the impact of new devices (i.e. photovoltaic inverters or electric vehicles) on the current and voltage distortion levels.	Deterministic or stochastic model of individual customers or aggregate customers that represent the daily variations of harmonic current emission.
Design of filters and other countermeasures to reduce the harmonic distortion in a network.	Deterministic model of individual customers or aggregate customers.
Analyze the effect of harmonic currents on the network elements, like the increase of losses and life loss, increase of neutral currents, etc.	Deterministic or stochastic model of individual customers or aggregate customers that represent the daily variations of harmonic current emission.
Planning of system expansion following the recommendations of technical reports like IEC 61000-3-6 [64] or D-A-CH-CZ [129] rules.	Deterministic model of individual customers or aggregate customers.
Analysis of responsibilities. Calculate the harmonic power flow in the network and decide who is responsible for certain harmonic distortions in the networks.	Stochastic model of individual customers or aggregate customers that represent the daily variations of harmonic current emission.

2.4. Effects of harmonics

Distorted voltages and currents affect every component in the power system. Some of the most common effects are:

- Additional dielectric, thermal, and/or mechanical stress on network components (transformers, lines, capacitors, loads, etc.). They may lead to a decrease of the efficiency (increase of losses), a faster loss of life, and/or the complete failure of the devices [5, 50, 108].
- Overloading of the neutral conductor caused by the flow of triple harmonics. The overloading may lead to the complete failure of a network, given that the overload protection systems are usually set to protect only the line conductors [20].
- Increase of the skin effect and proximity effect in cables and overhead lines due to an increase in the conducted signal frequencies [20].
- Additional audible noise in transformers and other electrical machines [58].
- Incorrect operation of electronic equipment, like household equipment, medical equipment, metering, instrumentation, protection and control instruments. [37, 58].
- Higher thermal and dielectric stress in capacitors. Capacitors are a low-impedance path for harmonics, which increases the current flow through the capacitor causing additional losses and reduced life. Under resonant conditions, the high harmonic voltages and currents can cause the complete failure of capacitors [58].
- Interference in communication circuits due to the direct or indirect coupling of harmonic currents on the power system into the communication system [48, 52]

To avoid these and other possible undesirable effects, different standardization bodies have established limits for the voltage and current distortion in the networks, as well as immunity levels for the different network components. The next section summarizes the most used standards.

2.5. Standardization

The International Electrotechnical Commission (IEC) and the Institute of Electrical and Electronics Engineers (IEEE) are the most prolific organizations regarding publications related to the measurement, analysis, limitation, and mitigation of power quality phenomena. There are also several national and international organizations that have contributed to the understanding and regulation of power quality disturbances. In all cases, the goal is to set emission, immunity, planning and compatibility levels in order to ensure electromagnetic compatibility in the whole power system (c.f. Fig. 2.1). Moreover, guidelines and norms related to the measurement and treatment of power quality phenomena are also required. Table 2.2 lists the most used standards and technical reports related to low-order harmonic distortion in low and medium-voltage networks.

The emission limits are set as the maximum harmonic currents that any harmonic source (individual devices and/or individual customers) can inject into the network. The limits are set considering that the total harmonic currents emitted by all the devices in the network lead to an acceptable voltage distortion in the entire power system, which requires some assumptions about the impedances (system and load) in the power system. The devices should not only

Table 2.2.: Most important standards and technical reports related to harmonic current distortion in low-voltage and medium-voltage networks.

Document no.	Title	Type
Emission		
IEC 61000-3-2	Limits for harmonic current emissions (equipment input current $\leq$ 16 A per phase)	IS
IEC 61000-3-12	Limits for harmonic currents produced by equipment connected to public low-voltage systems with input current >16 A and $\leq$ 75 A per phase	IS
IEEE Std 519-2014	IEEE Recommended practice and requirements for harmonic control in electric power systems	NS
IEC TR 61000-3-6	Assessment of emission limits for the connection of distorting installations to MV, HV and EHV power systems	TR
IEC TR 61000-3-14	Assessment of emission limits for harmonics, interharmonics, voltage fluctuations and unbalance for the connection of disturbing installations to LV power systems	TR
Immunity		
IEC 61000-4-13	Harmonics and interharmonics including mains signalling at a.c. power port, low frequency immunity tests	IS
Compatibility levels		
IEC 61000-2-2	Compatibility levels for low-frequency conducted disturbances and signalling in public low-voltage power supply systems	IS
IEC 61000-2-12	Compatibility levels for low-frequency conducted disturbances and signalling in public medium-voltage power supply systems	IS
IEEE Std 519-2014	IEEE Recommended practice and requirements for harmonic control in electric power systems	NS
Planning levels		
IEC TR 61000-3-6	Assessment of emission limits for the connection of distorting installations to MV, HV and EHV power systems	TR
IEC TR 61000-3-14	Assessment of emission limits for harmonics, interharmonics, voltage fluctuations and unbalance for the connection of disturbing installations to LV power systems	TR
D-A-CH-CZ TR	Technical rules for the assessment of network disturbances	TR
Measurement		
IEC 61000-4-7	General guide on harmonics and interharmonics measurements and instrumentation, for power supply systems and equipment connected thereto	IS
IEC 61000-4-30	Power quality measurement methods	IS
IEEE Std 519-2014	IEEE Recommended practice and requirements for harmonic control in electric power systems	NS
IEEE Std 1159-2009	IEEE Recommended practice for monitoring electric power quality	NS

IS: International standard, NS: National standard, TR: Technical report

comply with the emission limits, they should also operate correctly in the already harmonic distorted environment. Therefore, the immunity levels are set as the maximum harmonic voltage distortion at which any device can operate satisfactorily.

Emission limits and immunity levels are set according to the compatibility levels. Compatibility levels are usually based on the 95^{th} percentile of harmonic voltage distortion levels of power systems [64] (c.f. Fig. 2.1). The voltage distortion levels are obtained through measurements of several networks with different characteristics and/or through extensive simulations. However, compatibility levels should also consider the costs that device manufacturers, customers, and utilities have to assume. If the compatibility levels are set too high, the cost of improving the immunity of devices will increase. If the compatibility levels are set too low, then the cost of limiting the harmonic emission of devices or the measures to reduce the harmonic distortion in the networks (e.g. filters) will increase [20].

Planning levels are set by each network operator according to the compatibility levels and the characteristics of their own networks. These levels are useful when defining internal quality objectives and setting emission limits for the connection of new customers [63]. Some technical reports provide different methods for setting the planning levels, but network operators are free to set the limits according to their experience and knowledge about their network.

The emission, immunity, and compatibility levels defined in the standards are compulsory in some countries, but in other countries they are only considered as recommended values. In any case, the measurement of harmonic voltages and currents is essential to supervise and control the harmonic distortions in the networks. Continuous monitoring of harmonic distortion is recommended, not only to verify the compliance of planning levels, but also to evaluate the performance of the network, assess the effect of the connection of new loads or changes in the network configuration, identify problems, etc. [48]. Moreover, the measurement of single devices is also required to characterize the harmonic sources and verify the fulfillment of emission limits. The requirements of the measurement instruments and the proper procedure to analyze the data is also covered in the standardization.

2.6. Chapter summary

Low-order harmonic distortion is one of the most studied electromagnetic disturbances in public low-voltage and medium-voltage networks due to the continuous increase of electronic appliances (harmonic sources) used by residential and commercial customers. Electronic appliances are non-linear devices that inject harmonic currents into the network, which propagate in the network and produce the distortion of the voltage waveform.

Analyses of harmonic currents propagation in distribution networks are carried out not only to evaluate the levels of voltage distortion with respect to the standards, but also for many other studies, like the effect of distorted voltages and currents on the network elements, the impact of the connection of new customers or new devices, design of filters, etc. These analyses require accurate models of all network components, especially the harmonic sources. For analysis of extensive and complex distribution networks, it is not suitable to simulate each individual electronic appliance; instead aggregate models that represent the harmonic emission of sets of devices are required. Developing aggregate models is a complex task that can be achieved by two different approaches: component-based and measurement-based approaches. The next chapter describes both approaches and their advantages and disadvantages.

3. Overview of harmonic emission models of residential customers

Harmonic emission models can be classified into two main groups: equipment models and aggregate models. Equipment models correspond to the models of individual devices (household appliances), which are mainly used to:

- understand the response of household appliances under different voltage distortions (attenuation effect) and network conditions (i.e. [86, 102, 136]),
- study the effects of harmonic currents on specific devices, like the increase in losses or the decrease in operational performance (i.e. [55, 83]),
- study the cancellation effect between different types of devices in the networks (i.e. [17, 61, 94]),
- analyze the impact of the introduction of new technologies on the distribution networks (i.e. [77, 79, 133])

Aggregate models represent the aggregate harmonic emission of a set of devices/customers. They are used to analyze complex networks because it is not practical to simulate an entire network using individual models of each device. Some of the analyses that can be done with aggregate models are listed in Table 2.1.

The next sections contain the state of the art of both types of models for harmonic studies, including a more comprehensive description of aggregate load models. The focus is put on models of residential customers, which is linked to the objective of this thesis.

3.1. Equipment models

Household appliances consist of resistive and inductive loads (linear loads) like stoves, ovens, and refrigerators, and several electronic loads (non-linear loads) like CFLs, LEDs, personal computers, and battery chargers.

For harmonic analysis, linear-loads are usually considered as constant impedance loads and modeled with a RL equivalent if the inductive loads are not operating within their saturation range. If the electric motors are operated in saturation, the inductive loads are considered as non-linear loads and their model is more complex (examples of these models can be found in [125]).

However, in harmonic analysis the modeling of electronic equipment is more important because they are the main sources of harmonic currents. These non-linear devices can be represented with time-domain or frequency-domain models. Most time-domain models represent the internal electronic circuit of the device, which is then solved with specialized circuit simulation programs like Pspice, EMTP, and Simulink. This type of model allows for a very good approximation of the behavior of the device under different voltage and network conditions, but it requires considerable time and computing resources. Besides, complete information about the internal electronic circuit schema and its components is required to build up the model,

and such information is difficult to acquire for most household appliances. Moreover, time-domain models cannot be easily integrated with most power system analysis programs, which are configured to use only frequency-domain models. Examples of some time-domain models of household appliances can be found in [17, 34, 88].

Frequency-domain models are widely used for harmonic analysis due to the simplicity of their formulation and later simulation. As explained in chapter 2, the Norton model is used to represent harmonic sources in the frequency-domain. The Norton model contains an admittance in parallel with a current source, as shown in Fig. 3.1.

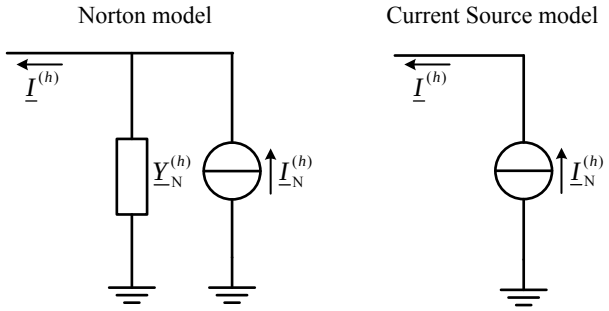

Figure 3.1.: Norton model and Current source model

The Decoupled Norton model can be mathematically represented as [78]:

$$\begin{bmatrix} \underline{I}^{(1)} \\ \underline{I}^{(3)} \\ \vdots \\ \underline{I}^{(n)} \end{bmatrix} = \begin{bmatrix} \underline{I}_{\mathrm{N}}^{(1)} \\ \underline{I}_{\mathrm{N}}^{(3)} \\ \vdots \\ \underline{I}_{\mathrm{N}}^{(n)} \end{bmatrix} - \begin{bmatrix} \underline{Y}_{\mathrm{N}}^{(1)} & 0 & \dots & 0 \\ 0 & \underline{Y}_{\mathrm{N}}^{(3)} & \dots & 0 \\ \vdots & \vdots & \dots & \vdots \\ 0 & 0 & \dots & \underline{Y}_{\mathrm{N}}^{(n)} \end{bmatrix} \cdot \begin{bmatrix} \underline{U}^{(1)} \\ \underline{U}^{(3)} \\ \vdots \\ \underline{U}^{(n)} \end{bmatrix} \tag{3.1}$$

where n is the maximum harmonic order considered in the model. The Decoupled Norton model does not consider the couplings between different harmonic orders, i.e. each harmonic order is threated separetelly. The Decoupled Norton model may be further simplified to a Current source model. The Current source model represents the non-linear device as an admittance for the fundamental current and as a current source for the harmonic currents (i.e. $\underline{I}_N^{(1)} = 0$ for $h = 1$ and $\underline{Y}_N^{(h)} = 0$ for $h \neq 1$) [58]. The Current source model is only valid if the non-linear device is not sensitive to distorted voltages, which is usually not the case for most electronic equipment [17].

In order to include the variation of harmonic emission of devices with the voltage distortion, the Decoupled Norton model is extended. In this case, the admittance matrix is modified to represent the relation between the emitted harmonic currents and the supplied voltage as [78]:

$$\begin{bmatrix} \underline{I}^{(1)} \\ \underline{I}^{(3)} \\ \vdots \\ \underline{I}^{(n)} \end{bmatrix} = \begin{bmatrix} \underline{I}_{\mathrm{N}}^{(1)} \\ \underline{I}_{\mathrm{N}}^{(3)} \\ \vdots \\ \underline{I}_{\mathrm{N}}^{(n)} \end{bmatrix} - \begin{bmatrix} \underline{Y}_{\mathrm{N}}^{(11)} & \underline{Y}_{\mathrm{N}}^{(13)} & \dots & \underline{Y}_{\mathrm{N}}^{(1n)} \\ \underline{Y}_{\mathrm{N}}^{(31)} & \underline{Y}_{\mathrm{N}}^{(33)} & \dots & \underline{Y}_{\mathrm{N}}^{(3n)} \\ \vdots & \vdots & \dots & \vdots \\ \underline{Y}_{\mathrm{N}}^{(n1)} & \underline{Y}_{\mathrm{N}}^{(n3)} & \dots & \underline{Y}_{\mathrm{N}}^{(nn)} \end{bmatrix} \cdot \begin{bmatrix} \underline{U}^{(1)} \\ \underline{U}^{(3)} \\ \vdots \\ \underline{U}^{(n)} \end{bmatrix} \tag{3.2}$$

This model is known as the Coupled Norton model. To calculate the model parameters, several measurements of the electronic equipment under different voltage distortion levels are required. It has been proved that the Coupled Norton model is more accurate than the Decoupled Norton model or the Current source model [3, 51, 78].

Several models exist to represent individual linear and non-linear devices using time-domain and frequency-domain models, some of the most relevant models in the literature are presented in [2, 15, 30, 34, 36, 88, 103, 124, 125, 133].

3.2. Aggregate harmonic emission models

Aggregate models represent the harmonic emission of all individual devices connected at some node in the network. Depending on the goal of the harmonic study, different levels of aggregation, like single customers, customer groups, or the entire low-voltage network, might be useful. Fig. 3.2 shows the possible aggregation levels. If the harmonic current propagation in low-voltage networks shall be analyzed, an aggregate model of individual customers or groups of few customers is required in order to obtain the necessary detail in the simulation. If e.g. the analysis of the harmonic situation in medium-voltage network is needed, one aggregate model containing all customers of a low-voltage network is usually sufficient.

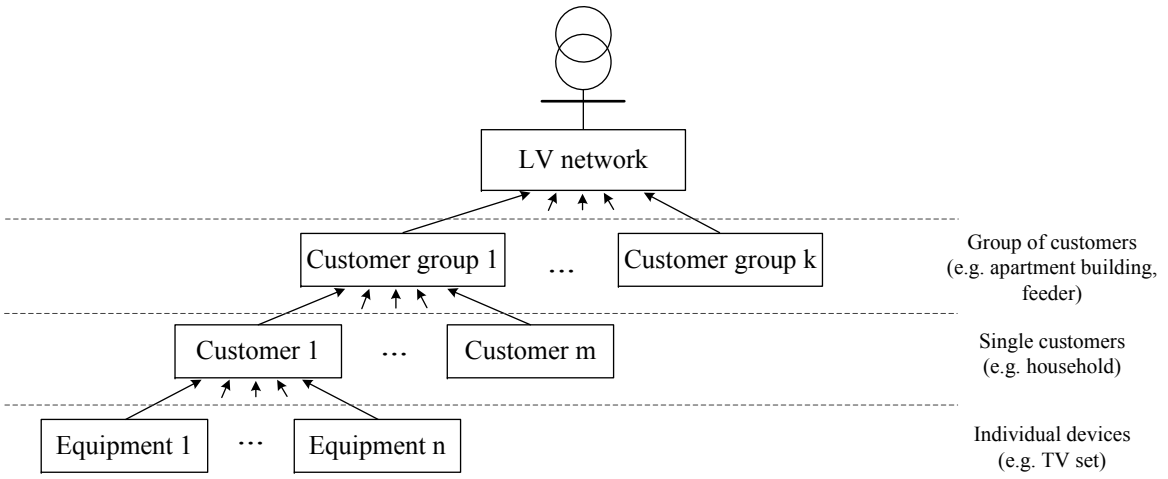

Figure 3.2.: Aggregation levels of aggregate harmonic emission models

An aggregate model can represent different characteristics of the load composition and the customer's behavior. The more characteristics the aggregate model can represent, the more complex the model is and the more computation resources requires the simulation. A balance between the accuracy of the model and its complexity always has to be found. The most important characteristics that an aggregate model can include are:

- Balanced/unbalanced condition

  The aggregate model can represent the balanced or unbalanced condition of the load. A balanced aggregate model is generally simpler to develop and implement. However, it is often inadequate to analyze networks with numerous single-phase household appliances as in residential networks [48].

- Stochastic/deterministic behavior

  Current and voltage harmonics at network/customer buses have a stochastic (random) nature due to continual changes in network configuration and load condition. Therefore, stochastic aggregate models are preferred to quantify harmonic levels in distribution networks [10]. However, stochastic aggregate models require stochastic analysis of the harmonic power flow (e.g. Monte Carlo simulations), which is more difficult to implement and demands more time and computing resources. Therefore, deterministic aggregate models are widely used due their simplicity, but they can only be applied if network and load variations are negligible.

- Stationary/non-stationary condition

  The harmonic emission of most customers is a non-stationary process, i.e. the statistical

properties of the harmonic emission (mean, standard deviation, etc.) change over time. An aggregate model may include the daily/monthly/yearly variations of the harmonic emission of the customers.

There are two main approaches to obtain aggregate models:

- Component-based approach

  This approach is based on a bottom-up methodology where models of single devices (i.e. each household appliance) are used to build the aggregate model of an individual customer or a group of customers connected at some point in the network (c.f. Fig. 3.3). Each component (each device) is modeled individually using a time-domain or frequency-domain technique, as shown in the previous section. An aggregate model is approximated by combining the models of the components in certain proportions based on, for example, load surveys [38].

- Measurement-based approach

  The aggregate model is based on measurements of the network (see Fig. 3.5). The measurements are later analyzed using descriptive statistics or probability functions, which indicate the amount of harmonic currents emitted by several residential customers. The precision and reliability of the model depend on the number of measured sites and the measured window.

An overview of the different types of aggregate models available in the literature is presented in the following sections. The aggregate models are divided first according to the applied modeling approach (Component-based or Measurement-based approach), and then subdivided into deterministic and stochastic aggregate models. The emphasis is laid on modeling of residential customers.

3.3. Component-based approach

This approach uses a bottom-up methodology where the models of the equipment (linear and non-linear devices) are first developed, and then those models are aggregated to build the model of an individual customer. The aggregation is usually done with information about usage behavior (when and how the devices are used) and load composition (types and number of equipment for individual customers or a customer group). The model of individual customers can be further aggregated to obtain the model of a customer group or the whole low-voltage network (c.f. Fig. 3.3).

The equipment models can be time-domain or frequency-domain models, as explained in section 3.1. In some cases, the individual devices are first grouped according to their circuit topologies (i.e. SMPS topologies) or harmonic emission characteristics, in order to reduce the amount of required equipment models.

The modeling of each device or device group is not an easy task. First there is a high variety of devices with different circuit topologies which have to be characterized and modeled individually. There are also differences between devices within the same topology due to differences in the electrical components used by each manufacturer. Besides, some devices have non-steady state harmonic current emission, like PCs and laptops, which depends strongly on customer behavior and/or operating modes.

Another challenge of the component-based approach is the acquisition of information about usage behavior and device composition. This information can be obtained from surveys, but might not always be available with the required detail.

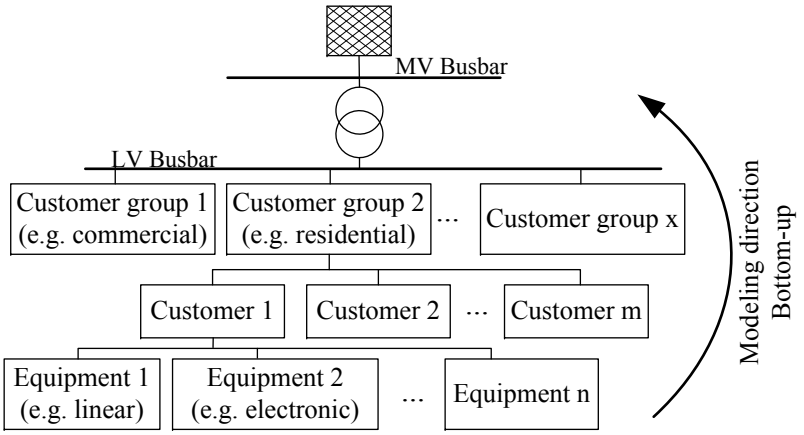

Figure 3.3.: Component-based approach

If the above aspects are properly treated in the model, this approach provides reliable aggregate models to simulate different loading conditions or the impact of future technological and legislative changes on harmonic network performance.

Some models based on the component-based approach are deterministic aggregate models where some specific combinations of equipment are used to represent some states of the residential customers, like low and high load states corresponding to the night and the evening load characteristics, respectively. However, most aggregate models use a stochastic approach to represent the random variations of load composition and harmonic emission of different devices. Some of the deterministic and stochastic aggregate models obtained with the component-based approach are described below.

3.3.1. Deterministic aggregate models - component-based approach

One of the first deterministic models obtained with a component-based approach was presented in [25], where time-domain models of some electronic household devices were used to simulate specific real-life combinations of devices, which were identified through interviews of the households in the area of study. The harmonic emission of the different combinations was compared with real measurements on a residential low-voltage network, showing that some of the defined combinations match the real emission of the residential customers. The authors proposed to use a table with different combinations of devices to estimate the daily variations of harmonic currents. Moreover, the reference tables could also be used to identify the penetration of different non-linear devices and evaluate the impact of new devices on the network.

A similar methodology was later applied by [12], but in this case a more complete set of equipment models was used. The household appliances were modeled with a fingerprint, which is a database that contains a large set of harmonic current measurements of a device under different voltage distortions. The fingerprints were introduced in a simulation program, which can select the harmonic current emission of each device according to the present voltage distortion at the connection node. Some device combinations were defined based on residential load compositions known by the local network operator. At the end, the harmonic emission of each device combination case was obtained and used as the model of each residential customer in the simulation of a low-voltage network. This aggregate model is proposed to compare the harmonic current emission in the low-voltage networks with the limits of available standards.

A more recent development explained in [31, 32, 33] uses time-domain models of different

household devices and more detailed information about the daily variation of load composition in order to recreate the variation of harmonic emission during the day. In this case, the household appliances were grouped into five general categories, which are further divided into subcategories as shown in Fig. 3.4. Then, time-domain models of each category were developed in order to accurately represent the emitted current waveform of each type of device. Parameters of the models were obtained from manufacturers' data sheets and measurements, and each equipment model can be adjusted to represent any subcategory. Finally, these models were aggregated based on load curves and information about the load structure. The output of the model is the current waveform of the aggregate devices and, hence, its harmonic content.

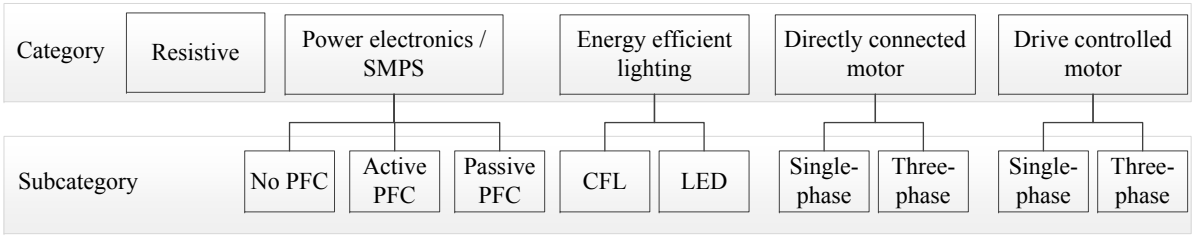

Figure 3.4.: Device categories and subcategories used by [32]

The previous models make a noble effort to model the household appliances, but they oversimplify the stochastic variation of harmonic currents emitted by residential customers or their typical daily variations. They only check some specific combinations of devices, which can over- or underestimate the real harmonic emission of residential customers.

3.3.2. Stochastic aggregate models - component-based approach

Stochastic aggregate models are widely used in order to represent the variation of the harmonic emission of the customers in more detail. One of the first stochastic aggregate models obtained with a component-based approach was presented in [9], where the household appliances were divided into four categories according to their operational modes and switching states. For example, there are some devices that have a constant emission of harmonic currents during the whole working cycle (one operational mode and one switching state), but other devices emit random currents during different operational modes, like personal computers. In this way, the authors defined the following four categories:

1. Constant number of constant currents
2. Random number of constant currents
3. Constant number of random currents
4. Random number of random currents

The probability distribution of each device category was defined and the current injected by several customers was obtained through Monte Carlo simulations. In this case, also information about the type and number of devices connected to the network during the day was necessary to complete the model.

In [24] and [111] the household appliances were also modeled using probabilistic approaches, but the devices were not grouped in advance, which requires a more extensive database of models. In [24] each device was modeled with a bivariate normal distribution which represents the emission of harmonic currents of the device under different voltage distortions, while in [111] linear and non-linear devices were modeled with fuzzi admittance and fuzzi harmonic

current sources, respectively. The aggregate models were obtained using information about the load composition of residential customers. The model of [24] was verified using measurements of a German medium-voltage network, providing satisfactory results for that specific network. In [111] only a numerical example was given and no comparison with real measurements was made.

In [113] the aggregate model was developed based on the assumption that the random harmonic emission of residential customers is almost exclusively due to the random on/off states of the household appliances, which could be modeled with probability distributions. The distributions were obtained based on information of residential customers characteristics and habits, like the size and occupancy pattern of the household, type and number of devices per house, estimated working cycle duration, and number of switch-on events per day of each device. The household appliances were represented with Decoupled Norton models, which parameters were obtained from measurements of several devices. The electric models of the different household appliances and the probability distributions of on/off states were used to obtain the aggregate model of a single-house. Finally, single-house models were aggregated to obtain the aggregate harmonic emission at the secondary side of the distribution transformer. Both models, single-house and aggregate model, were validated with some field measurements. The model was also used to investigate the impact of new technologies and changes on the network parameters [74]. Similar approach was also used by [135].

The model developed in [7, 8] represents not only the harmonic emission of the different appliances, but also the customer's behavior and load composition using probability distributions. In this case, all the devices connected at some point of connection (POC) are divided into linear and non-linear devices. The non-linear devices were further divided into 4 groups, namely magnetic ballasts, single-phase SMPS, three-phase converters, and adjustable speed drives. The h^{th} order harmonic current injected by m different non-linear device groups was obtained as following:

$$\underline{I}_{\text{AHL}}^{(h)} = \sum_{i=1}^{m} a_i \cdot \underline{I}_i^{(h)} \tag{3.3}$$

where a_i is a weighted coefficient representing the fraction of the respective non-linear device group into the power demand ($\sum_1^m a_i = 1$) and $\underline{I}_i^{(h)}$ is the harmonic current phasor of the corresponding non-linear device group. The harmonic currents $\underline{I}_i^{(h)}$ were established as average deterministic values obtained from measurements. The harmonic current distortion at the POC depends on the power participation of the non-linear devices in the total demand of the aggregate customers. The total harmonic current at POC was represented as:

$$I_{\text{POC}}^{(h)} = K_{\text{E}} \cdot I_{\text{AHL}}^{(h)} \tag{3.4}$$

where K_{E} is the fraction of non-linear devices participating in the total demand of the aggregate model. To represent the random behavior of harmonic currents, the variables a_i and K_{E} are random variables whose characteristics were derived from field measurements of different customers (residential, office, hotel, etc.) or using the customer's load information. Moreover, the model considered the harmonic emission during two time periods, corresponding to high and low power demand of the aggregate load.

In general, the stochastic aggregate models obtained with a component-based approach are very flexible since different load conditions can be established and also the influence of new loads can be easily analyzed. However, these models require a high amount of input data which is usually not easy to acquire.

3.4. Measurement-based approach

This approach is based on measurements of the network, which inherently include the operating changes of the individual household appliances, variation of customer behavior, effect of line impedances, cancellation and attenuation effects, etc. The measurements can be taken at different levels as shown in Fig. 3.5. In general, both modeling directions, top-down and bottom-up, are possible. If the measurements are taken on the substation or feeder level, the measurements can be decomposed to find approximate models of customer groups (feeder section) or even individual customers. Vice versa, measurements taken at the POC of customers can be used to build the model of customer groups or the whole low-voltage network.

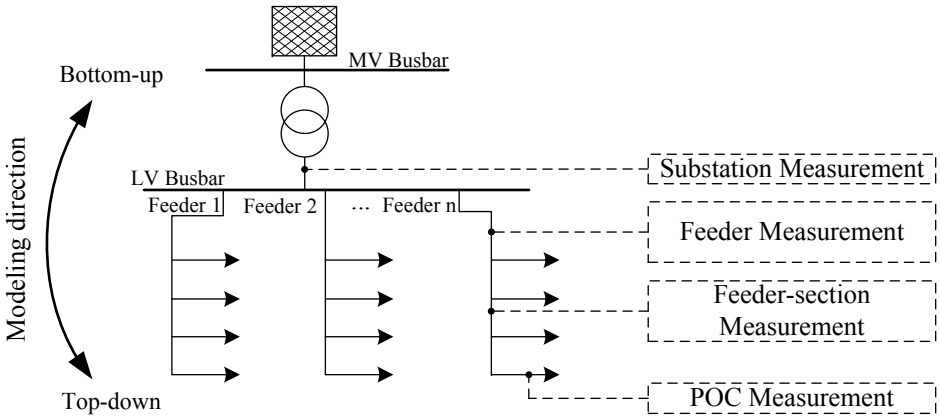

Figure 3.5.: Measurement-based approach

Aggregate models based on the measurement-based approach can also be grouped into deterministic and stochastic aggregate models.

3.4.1. Deterministic aggregate models - measurement-based approach

The simplest deterministic aggregate models obtained with the measurement-based approach are based on the statistical analysis of measurements from several substations or feeders. The customers are represented by a Current source model, the magnitude of which corresponds to the mean or the 95^{th} percentile value of the measured harmonic magnitudes (the 95^{th} percentile value is prefered in order to compare the results with the limits given in most of the national and international standards). The daily variations and the correlation of the measured harmonic currents with other electrical and non-electrical parameters are usually not deeply analyzed and it is always assumed that the data is stationary and normal distributed. These models should be used carefully, because they can overestimate or underestimate the real harmonic emission of the residential customers, and it is recommended to use them only to have a general idea of the behavior of the network. Some examples of such models can be found in [22, 40, 82].

Other deterministic aggregate models define the equivalent Norton model of the aggregate customers using snapshots of the network; that is, the equivalent Norton model of the group of customers at a specific point in time. The first of these models was presented in [84], where the Norton equivalent model (c.f. Fig. 3.1) was broken down into 5 elements, as shown in Fig. 3.6. The Norton impedance consists of a parallel combination of resistor, inductance, and capacitor, and the current source is divided into the sources i_r and i_g. The source i_r represents to the harmonic currents that are coupled with the voltage u, while i_g represents to uncoupled harmonics with the voltage u. In this case the model is defined in the time-domain.

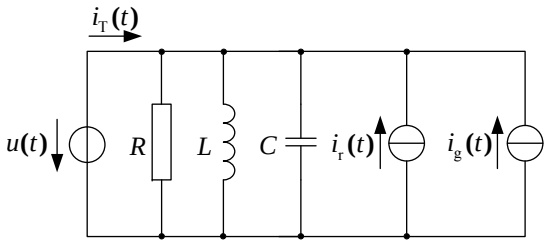

Figure 3.6.: General load model defined by [84]

The parameters of the elements were obtained by solving the differential equations of the circuit using measured voltage and current waveforms. In [49, 116, 117, 118] other techniques were applied to find the parameters of the elements, like least square errors, z-transform and Kalman filtering algorithms, using measured voltage and current waveforms, or the complete spectrum of both signals including the harmonic phase angles. However, it was proved by [59, 127] that the estimated parameters are highly dependent on the measured waveforms and the network characteristics. To consider the daily variations of the load, this model should be extended.

Another way to get the Norton model parameters consists of making measurements of harmonic voltages and harmonic currents under two different operating conditions of the network [90, 107, 127]. The change in the operating conditions can be obtained by switching a shunt capacitor, disconnecting a parallel transformer, or some other action that makes a significant change in the supply network harmonic impedance. However, the model parameters change depending on the performed switching action, which makes accuracy and reliability of the obtained model questionable [1].

A more recent model presented in [3, 4] represents the aggregate load using a Coupled Norton model. The model was calculated from several measurements of the aggregate customers, which allows the solution of the linear system in equation 3.2. The measurements should represent different operating conditions of the aggregate customers in order to solve the linear system. This can be done by selecting the measurements with the higher variation of voltage and current distortion inside the considered time interval.

None of the modeling techniques of deterministic measurement-based models have been used to create a general model of residential customers. All the methods were developed and tested using measurements of a single network, and none of the models consider the possible changes in the model parameters with the number of residential customers, temporal variations (daily and seasonal variations), network conditions, etc.

3.4.2. Stochastic aggregate models - measurement-based approach

The first stochastic aggregate models obtained by a measurement-based approach used joint probability distributions to represent the magnitude and phase angle of harmonic currents measured over long periods of time (at least one week). Some authors (e.g. [35, 76, 114]) used normal or uniform distributions to represent the variation of harmonic magnitudes and phase angles and it was assumed that both variables were independent and stable during time. However, it was later proved in [27] that this methodology does not work properly with residential customers, because their harmonic currents are non-stationary, which results in multimodal distributions of harmonic magnitudes and phase angles; therefore, the time characteristic (trend, seasonal and daily variations) should be considered in the model.

In [6] the daily emission of aggregate residential customers was divided into three periods (high, medium, and low power demand) and described with normal distributions. The prob-

abilistic spectrum was used as input in a Monte Carlo simulation to find the harmonic voltage distortion (THD_u) at each network bus in a radial distribution network. The method gave a very good approximation of the 95$^{\text{th}}$ percentile of THD_u, but it failed to represent the change of THD_u during the day. In [93] a similar method was used, but in this case the daily harmonic emission was divided into stationary (periods of the day where the harmonic magnitudes do not change significantly) and transitional intervals (interval between stationary intervals). Each interval was modeled using also a normal distribution.

Time-series methods have also been applied to represent the variations of harmonic currents over short (daily), medium (seasonal), and long terms (annual). Time-series methods separate a time-series $y(t)$ into different types of behavior patterns [110]:

$$y(t) = y_{\mathrm{T}}(t) + y_{\mathrm{S}}(t) + y_{\mathrm{D}}(t) + y_{\mathrm{R}} \tag{3.5}$$

- $y_{\mathrm{T}}(t)$ is a deterministic function that represents the trend or secular behavior i.e. the increase or decrease of the time-series over several years.
- $y_{\mathrm{S}}(t)$ is a deterministic function that represents the seasonal variations.
- $y_{\mathrm{D}}(t)$ is a deterministic function that represents the variations of the time series during the day.
- y_{R} is a stochastic component that represents the random variations around the deterministic components.

Fig. 3.7 shows exemplary the variation of the fundamental current of a low-voltage substation with residential customers over four years. The data clearly show a trend, a seasonal variation and, zooming in, the daily variations, which can be represented by deterministic functions. The daily variations are caused by the variation in the amount and type of household appliances used during the day, while the seasonal variations are caused by the variation in the temperature and sunshine hours that lead to a variation in the amount of lighting and heating devices used in a year. The trend component is usually caused by the introduction of new technologies (e.g. energy-saving products) or new regulatory policies that slowly change the amount and type of devices in the network or the customer's behavior.

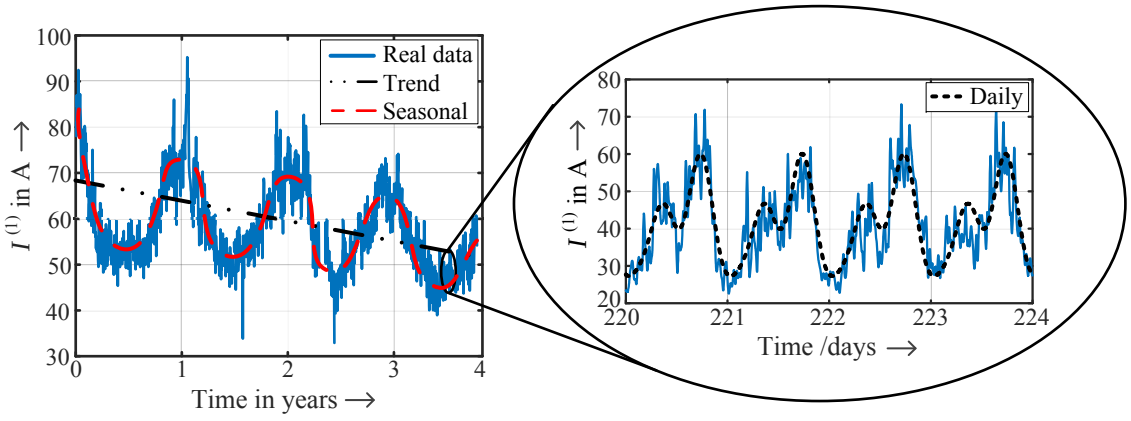

Figure 3.7.: Time-series decomposition

For harmonic studies, usually measurements of only a few days or weeks are available for the analysis; therefore, the trend and seasonal variations are usually not analyzed. The daily variations are obtained using polynomial fitting methods, moving average techniques, or Fourier analyses. The stochastic component is modeled with the residuals (residuals are obtained after subtracting the deterministic part of the original data) using probability functions, autoregressive-moving-average (ARIMA) models, Markov chains, etc.

In [26], measurements of a feeder of a medium-voltage substation with residential customers were used to verify the validity of the modeling technique. The daily component $D(t)$ was obtained using the arithmetic mean of the samples taken over six weeks, while the stochastic part was assumed to have a Gaussian distribution. The model was used in a Monte Carlo simulation to determine the probability density function of the resultant of the sum of harmonic currents injected at different buses and the harmonic voltages at network buses. The model provided an effective description of the behavior of the harmonic currents and harmonic voltages.

A similar method was later applied in [130] using measurements of 18 low-voltage substations with residential customers. In this case, only the 5^{th} harmonic currents were modeled. The statistical analysis of the measurements showed that not all the substations have the same daily pattern for the 5^{th} harmonic; therefore, the 5^{th} harmonic daily curves are first clustered in 3 groups according to their characteristics. For each group, the time-series model was obtained and then verified with simulations. Other references with time-series analysis of harmonic voltages and currents can be found in [71, 97, 98, 119].

A model based on the bottom-up approach was presented in [16], where measurements at the POC of residential customers were used to build the model of aggregate residential customers. Based on statistical analysis of extensive measurement data, the model distinguishes three customer classes with different levels of harmonic emission (customers with low, medium and high harmonic emission) and sub-models of 24 hours. Each sub-model consists of two distribution functions representing the stochastic behavior of one customer class and one hour individually for magnitude and phase angle of the harmonic current of a specific order. The modeling methodology was validated by comparing simulation and measurements for an aggregate of ten customers belonging to one customer class. It shows a sufficient accuracy of better than 10% for the most important 95^{th} and 99^{th} percentiles.

Finally, in [57] a different method was used to represent the random variation of harmonic currents. In this case the authors did not use probabilistic functions or time-series methods, but instead they generated a database with the measured daily harmonic emission of the different feeders or substations with residential customers. During a simulation, the magnitude and phase angle of the harmonic currents for a selected time step was chosen randomly from the database. This method was validated with a Monte Carlo simulation of a network, resulting in a very good response. The reliability of this modeling technique depends on the amount of measurements available in the database.

3.5. Chapter summary

Harmonic propagation studies require aggregate models that simulate the harmonic emission of the multitude of customers in the network. There are two common methodologies to obtain aggregate models: component-based and measurement-based approaches. The component-based approach uses a bottom-up methodology where the household appliances are characterized and modeled individually. The aggregate model is approximated by combining the models of the components in certain proportions based on, for example, load surveys. The model requires a high amount of input data (e.g. accurate models of each household appliance, information about customer's behavior and load composition, etc.), which is usually difficult to acquire. However, this kind of model is very useful for testing different loading conditions and analyze the influence of technological and legislative changes on loads, changes in the customers behavior, implementation of demand side management strategies, and other analyses that require a detailed representation of the type and amount of household devices connected to the network.

On the other side, the measurement-based approach uses measurements of the networks (individual customers, feeder section, or complete low-voltage networks), which inherently include the operating changes of the individual household appliances, effect of line impedances, cancellation and attenuation effects, etc. The measurement-based approach can use a bottom-up or a top-down methodology depending on the type of available measurements. These models can represent more accurately the harmonic emission of aggregate residential customers, since this approach does not make any assumption about the customer's behavior, load composition or the harmonic emission of the household appliances. However, the precision and reliability of the model depend on the number of measured sites and the measured window. With the increasing number of measurement instruments in the network as well as the integration of harmonic measurement capabilities into smart meters, it is expected to be easier to obtain the required comprehensive measurements in order to develop accurate and reliable models.

Component-based and measurement-based approaches can be applied to generate deterministic or stochastic models of the harmonic emission of the aggregate customers. Depending on the desired analysis, the type and the characteristics of the model should be carefully selected. For example, if a rough estimation of the voltage distortion in the network is needed, then deterministic models are sufficient. But if the impact of, for example, electric vehicles and photovoltaic inverters is desired, then stochastic models that represent the daily variation of harmonic current emission are more suitable. Stochastic models are more accurate than deterministic models, since they represent the natural random behavior of harmonic currents, but they usually require more time and computing resources.

During the last decades, component-based models have been broadly studied and there are very well documented modeling methodologies to develop aggregate models for different regions or countries. On the other hand, the measurement-based approach has also been studied and some methods to represent the harmonic emission of aggregate customers based on network measurements have been discussed, but all analyses have been based only on measurements of few networks, and there is no clear and complete modeling methodologies to develop general aggregate models based on network measurements.

The objective of this thesis is to develop a stochastic model of the harmonic emission of aggregate residential customers using the measurement-based approach, and give a modeling methodology that can be applied to develop models for other regions or countries. Several measurements of low-voltage residential networks are available for the model, therefore a top-down methodology is applied. The measurements are first characterized and analyzed in order to identify the different electrical and non-electrical parameters that influence the emission of harmonic currents in residential low-voltage networks (chapter 4). Based on the characteristics of the data, a modeling methodology is proposed and developed in chapters 5 and 6. Finally, the model is tested in an application example in chapter 7.

4. Characteristics of harmonic currents in residential low-voltage networks

In order to develop the measurement-based model of the harmonic currents of aggregate residential customers, it is indispensable to count with measurements of several residential networks that represent the variety of networks and residential customers present in the area, in this case, in Germany. Once the measurements are obtained, the first step in the modeling consists in the characterization of the measured harmonic currents and the identification of the most important parameters that should be included in the model.

This chapter describes the measurement campaign and characterizes the measured harmonic currents of residential networks available for the model. Specifically, the following characteristics are studied:

- Influence of different electrical and non-electrical parameters on the magnitude and phase angle of harmonic currents (section 4.2).
- Level of unbalance of the harmonic currents (section 4.3).
- Behavior of harmonic current magnitudes and phase angles over time (section 4.4).
- Correlation between harmonic magnitudes and phase angles (section 4.5)

Based on the characteristics of the harmonic currents, the characteristics of the model are defined, and the most appropriate model methodology can be selected.

4.1. Measurement campaign

Measurements of several residential low-voltage networks were carried out in different cities and towns in Germany with the collaboration of 32 network operators. The sites were selected in agreement with the network operators in order to have a representative sample of different types of low-voltage networks or feeders with mainly residential customers. A residential site is defined in this work as a low-voltage network or feeder where at least 80% of the customers are residential customers. Certainly, public low-voltage networks are composed of a mixture of residential and commercial customers, but for this project only networks with predominantly residential customers were selected. The characteristics of the measured residential networks are summarized in appendix A.

The measurements were made at the low-voltage side of the distribution transformer, either at the whole low-voltage network or at one of its feeders. The RMS voltage and RMS current, the harmonic voltages and harmonic currents up to 50^{th} order, the active and apparent power and the total voltage and current distortion (THD) were recorded, but for the development of the aggregate model only the magnitude and phase angle of the harmonic currents are used. Additionally, information about the electrical characteristics of the network or feeder, the social environment and the climate conditions during the measurements were also available.

Measurements have been performed using a single type of power quality analyzer complying with IEC 61000-4-30 class A [68]. The measurement interval is between 1 and 4 weeks with an

aggregation interval of 1 minute. The measurement campaign was carried out during winter, where the emission levels in Germany are in general slightly higher compared to the summer months [44]. Moreover, the measurements were made during the same year and during the same season in order to reduce the influence of seasonal variations and trends. The characteristics of the measured sites, the measurement device and the description of the measurement procedure including the accuracy and plausibility check can be found in appendix A.

After checking accuracy and plausibility of the data, 37 residential sites were selected for the analysis. Those sites have fulfilled the following characteristics:

- The amount of residential customers of each site is considerably higher than the amount of individual offices and small commercial customers. The amount of residential customers represents at least the 80% of the total amount of customers. The site does not contain any type of institution (schools, associations, etc.), big supermarkets, construction zones, storage heaters or any other special type of customers.
- The total power of the photovoltaic systems in the residential site is lower than 10% of the rated power of the corresponding distribution transformer.
- More than 95% of the measured values (voltage and current odd harmonics up to the 15$^{\text{th}}$ order) were still available after the accuracy test.
- At least one complete week of measurements is available. Measurements made on holidays, like Christmas and new year, were excluded.

4.2. Influence of electrical and non-electrical parameters

Power quality parameters are influenced by the electrical and non-electrical environment [45]. As shown in Fig. 4.1, the electrical environment includes the network, customer and generation configuration, while the non-electrical environment can be divided into the social environment and the climate conditions. The figure also shows different parameters that can be used to characterize the electrical and non-electrical environment.

It is indispensable to identify the influence that the electrical and non-electrical environment has on the magnitude and phase angle of harmonic currents, and thus decide which parameters should be included in the model. In this case, only the influence of network configuration, customer configuration and social environment is considered. The influence of the generation configuration and the climate conditions can be neglected due to the characteristics of the measurements, which were selected with low amount of photovoltaic inverters and were made during winter time to reduce the influence of seasonal variations.

For a comprehensive analysis of the influence of the electrical and non-electrical environment on the harmonic emission of the selected residential sites, some statistical values that show the central tendency and the variation of the harmonic magnitudes and phase angles are required. For harmonic magnitudes, the median ($I^{(h)}_{[50]}$) and the percentile range between the 95$^{\text{th}}$ and 5$^{\text{th}}$ percentiles ($I^{(h)}_{[95,5]}$) were selected as measures of the central tendency and dispersion of the data respectively. Those measures are robust to outliers and they do not assume a normal distribution of the data. For harmonic phase angles, the mean direction and the mean resultant length, as defined in the directional statistics, were calculated. The mean direction $\varphi^{(h)}_{\text{MD}}$ shows the central tendency of the phase angles, i.e. the direction where most of the phase angles are located. The mean resultant length $MRL^{(h)}$ measures the concentration of the phase angles around the mean direction. $MRL^{(h)}$ varies in the interval $[0, 1]$, and the closer it is to 1, the more concentrated the data is around the mean direction. A $MRL^{(h)} = 0.8$ is used as threshold to

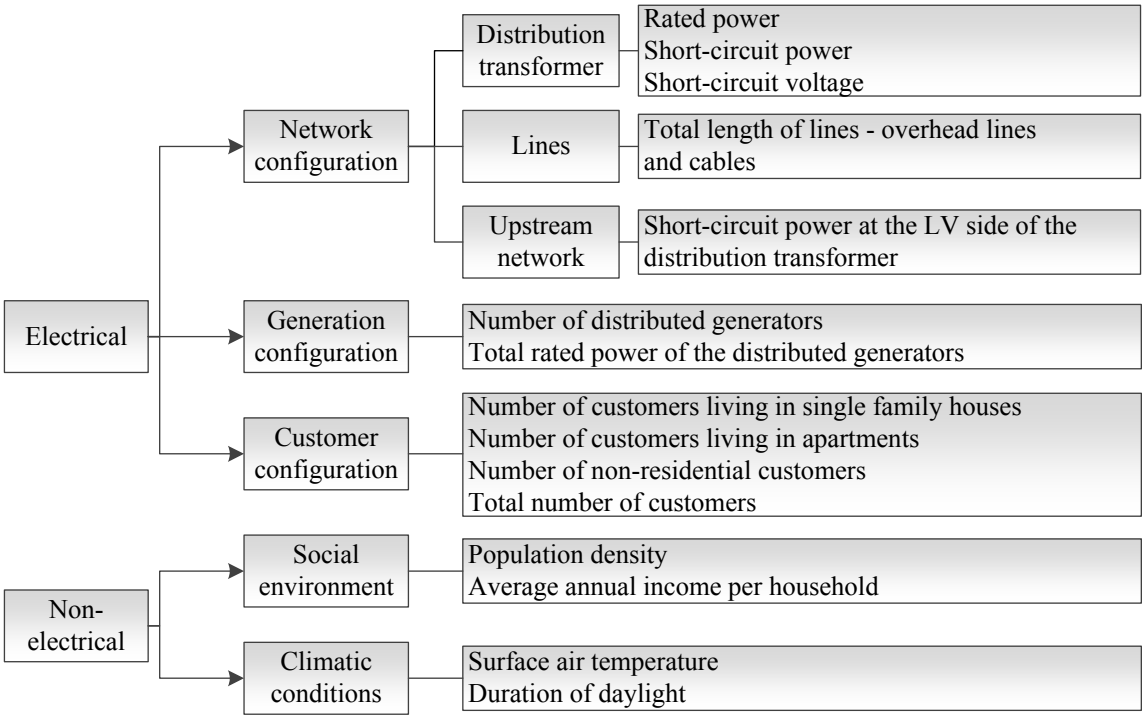

Figure 4.1.: Available electrical and non-electrical parameters of each of the measured sites

define an acceptable dispersion of the harmonic phase angles, where a unique direction of the phase angles can be defined. If $MRL^{(h)} < 0.8$, the mean direction is not reported. Appendix B.1 describes the mean direction and the mean resultant length in more detail.

As example, Fig. 4.2 shows the polar plots of the 3rd and 15th harmonics of one site and one line conductor and their corresponding statistics. The heat-map representation is used to visualize the different densities of the data clouds. The third harmonic phasors are concentrated on a similar direction and $MRL^{(3)}$ is almost equal 1. Therefore, the mean direction indicates properly the direction of the data-cloud and the central tendency of the harmonic phase angles. On the other side, the 15th harmonic is high dispersed in the complex plane and there is not a clear direction of the data-cloud. $MRL^{(15)}$ is below 0.8 and, consequently, a mean direction of the phase angles is not reported.

The selected statistics were calculated for each site, each line conductor and each harmonic order using the data of one week. Fig. 4.3 compares the median of the harmonic magnitudes and the mean direction of harmonic phase angles obtained for the first 15 odd harmonics on the polar plane (one point for each line conductor and each site). The magnitude decreases with the harmonic order (notice the change in the scales on the polar plots), being the third harmonic the dominating harmonic in residential low-voltage networks. Most of the sites have similar phase angles, especially for the fundamental current (between $-20°$ and $0°$), third (between $180°$ and $210°$) and fifth (between $300°$ and $330°$) harmonic currents. The difference between sites increases with the increase of the harmonic order, and for the 11th, 13th and 15th harmonics, a common direction between all sites cannot be defined.

Fig. 4.4 shows the percentage of sites with high ($MRL < 0.8$), medium ($0.8 \leq MRL < 0.89$), low ($0.89 \leq MRL < 0.95$) and very low ($MRL \geq 0.95$) dispersion of the phase angles. The definition of the dispersion levels were obtained through systematic simulation of different types of data distributions, as explained in appendix B.1. The 13th and 15th harmonics show the highest number of sites with high dispersion of harmonic phase angles, but it represents less that 30% of the cases. This indicates that in most of the sites, the phase angles of the first 15

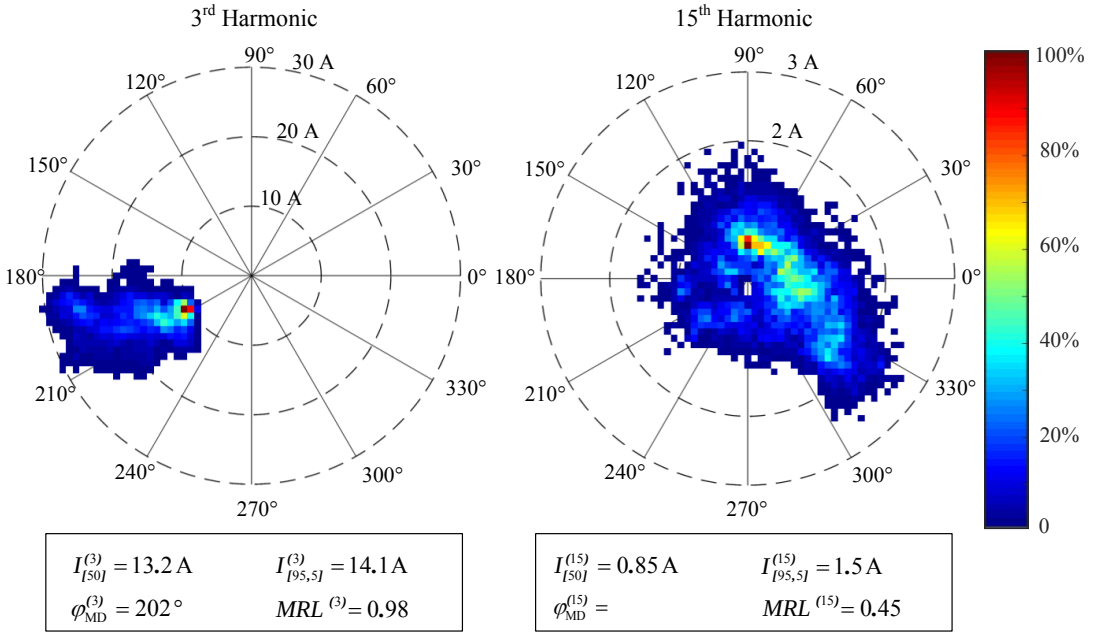

Figure 4.2.: Example of the selected statistics for harmonic magnitudes and phase angles

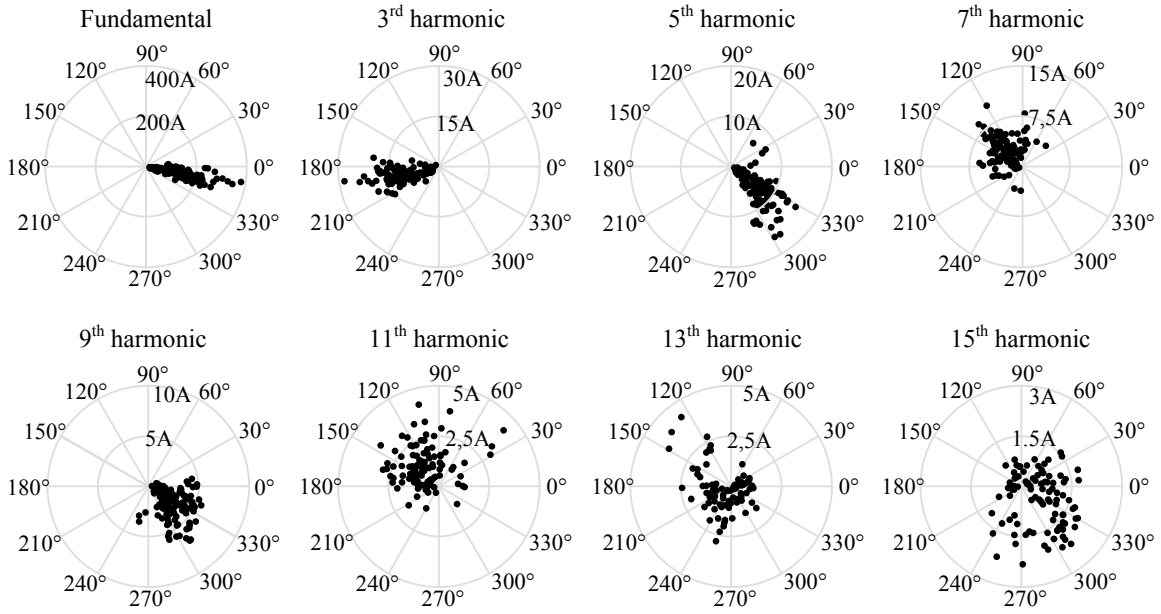

Figure 4.3.: Median and mean direction of the harmonic currents of all residential sites

odd harmonics are concentrated in a similar direction, and, contrary to a common assumption, the phase angles are not randomly dispersed in the interval $[0, 360°]$.

4.2.1. Influence of customer configuration

The obtained statistics are clustered according to the different electric and non-electric characteristics of the networks in order to identify the most influencing factors on the magnitude and phase angle of harmonic currents. First, the influence of the customer configuration is analyzed. To facilitate the analysis, the customer configuration is divided into four categories:

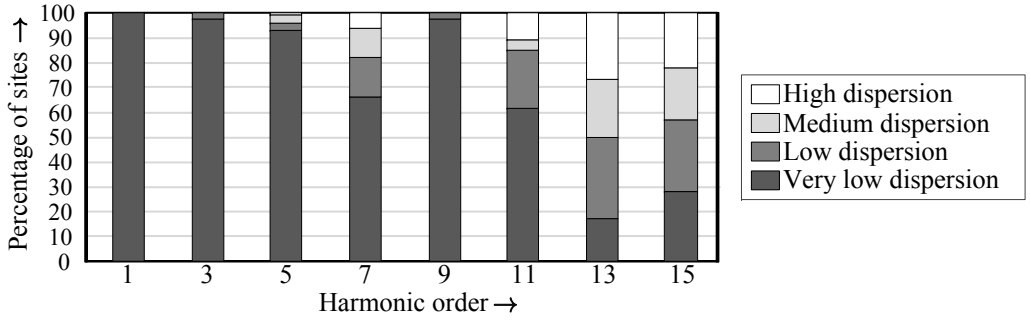

Figure 4.4.: Percentage of sites with high, medium, low and very low dispersion of phase angles

- C1 - Residential sites where the number of customers living in single-family houses (SFH) represents at least 80% of the total number of customers: $n_{\mathrm{u\ SFH}} \geq 0.8 \cdot n_{\mathrm{u\ TOT}}$.
- C2 - Residential sites where the number of customers living in apartments (APT) represents at least 80% of the total number of customers: $n_{\mathrm{u\ APT}} \geq 0.8 \cdot n_{\mathrm{u\ TOT}}$.
- M1 - Residential sites where the number of customers living in single-family houses predominates: $0.5 \cdot n_{\mathrm{u\ TOT}} \leq n_{\mathrm{u\ SFH}} < 0.8 \cdot n_{\mathrm{u\ TOT}}$.
- M2 - Residential sites where the number of customers living in apartments predominates: $0.5 \cdot n_{\mathrm{u\ TOT}} \leq n_{\mathrm{u\ APT}} < 0.8 \cdot n_{\mathrm{u\ TOT}}$.

Fig. 4.5 shows the central tendency and the variation of the third harmonic of each line conductor (three values per site) related to the number of customers and the customer configuration category. As expected, the median value and the variation of harmonic magnitudes increase with the number of customers, because it implies a higher number of electric devices in the network. However, the increase has a non-linear characteristic due to the complex aggregation of harmonic currents and the diversity of residential customers. The dashed lines in the figure show exemplary the tendency of the increment of the harmonic current magnitudes with the number of customers for customer configuration C1 and C2.

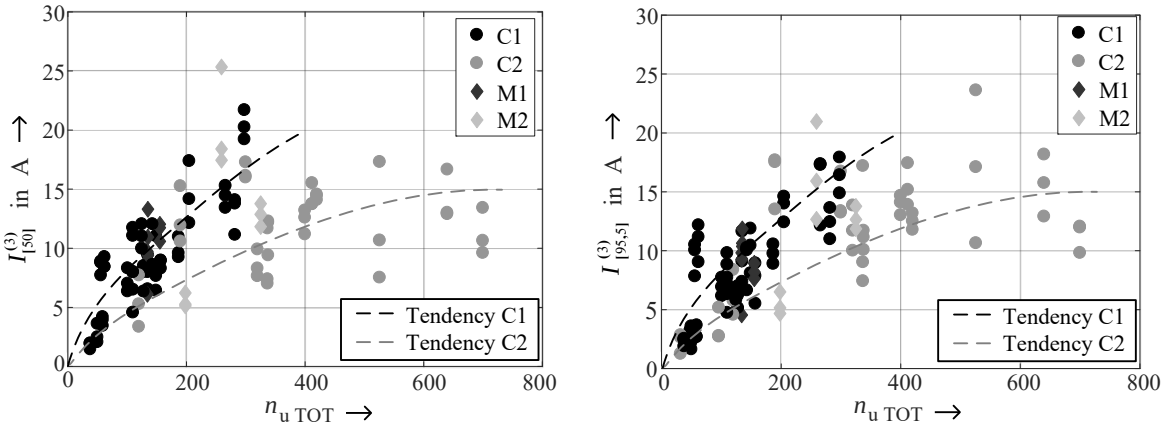

(a) Median harmonic magnitude

(b) Percentile range

Figure 4.5.: Magnitude of the third harmonic related to the number of customers and the consumer configuration

Fig. 4.5 also reveals that the type of housing is an important factor. Networks with predominantly single-family houses (groups C1 and M1) show a higher harmonic emission in comparison with networks with apartments (groups C2 and M2). Usually, single-family houses have a higher floor area than apartments and are usually occupied by families with 3 to 5 members,

which results in a higher amount of electric devices per customer, and consequently higher harmonic currents in the networks. Moreover, customers living in apartments are more diverse than customer living in SFH, which results in a higher cancellation of harmonic currents. The same relations were also found for the other harmonic orders.

The influence of the number of customers and the type of housing on the harmonic phase angles of the third harmonic is shown in Fig. 4.6. For customer configuration C1, the mean direction of the phase angles seems to get concentrated around 190° and the dispersion decreases (increase of MRL) with the increase in the number of customers. However, this behavior (concentration of phase angles and decrease in the dispersion) is not observable in the other cases, i.e. for the other harmonic orders and for customer configuration C2. In general, there is no clear relation between the number of customers and the mean direction and mean resultant length of the phase angles.

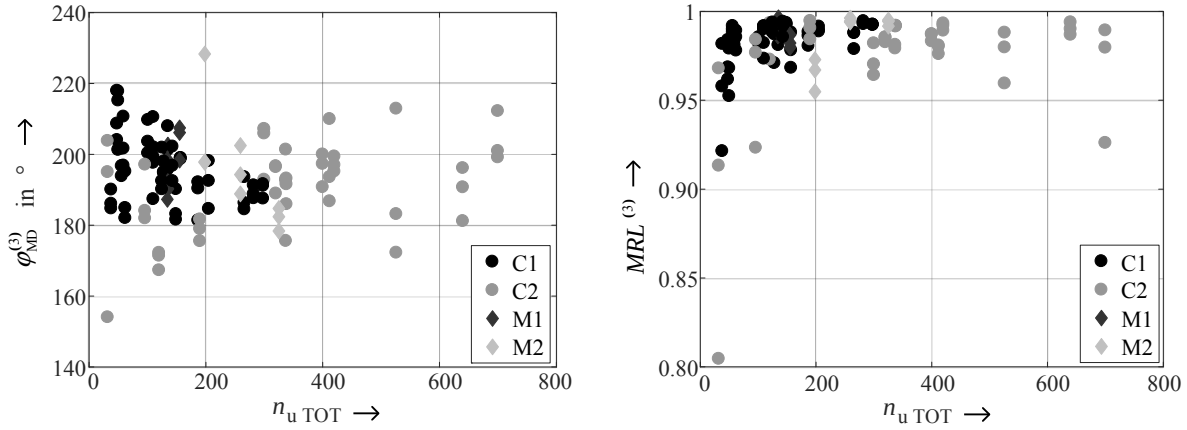

(a) Mean direction

(b) Mean resultant length

Figure 4.6.: Mean direction and mean resultant length of the third harmonic phase angles related to the number of customers and the consumer topology

In conclusion, the customer configuration has a high influence on the harmonic currents of aggregate residential customers, and this aspect should be considered in the model. The harmonic current magnitudes increase with the number of customers, and the magnitude is higher in networks with single-family houses. Harmonic phase angles are more robust to the customer configuration, showing a less variation with the number of customers. However, the smallest considered network contains 38 customers and it is possible that the variation of harmonic magnitudes and phase angles increases for networks with smaller number of aggregate customers. This aspect will be studied in more detail in chapter 6.

4.2.2. Influence of network configuration

Traditional residential low-voltage networks are radial networks with different characteristics (size of the distribution transformer, length and type of the line conductors, number of feeders, etc.) that depend on the geographical conditions, the number of customers, the distribution of the customers in the area, possible expansion strategies, and many other planning criteria [43]. The characteristics of the network have a considerable influence in many power quality phenomena. Related to harmonics, the impedance of the lines, transformer and loads have a high influence in the way the harmonic currents propagate in the network and in the resulting voltage distortion along the network. However, as discussed in section 2.3, due to the high impedance of residential loads in relation to the network impedance (impedance of the lines and the distribution transformer), most of the low-order harmonic currents produced by the

household appliances flow directly to the distribution transformer. Then, the harmonic currents measured at the distribution transformer are approximately the result of the phasorial sum of the harmonic currents emitted by all the electronic devices in the network, and it is expected that the impedance of the lines and the distribution transformer do not have a considerable influence on the phasorial sum of those harmonic currents.

This aspect is verified by analyzing the influence of the length of the lines and the size of the distribution transformer on the measured harmonic magnitudes and phase angles. Fig. 4.7 shows exemplary the median harmonic magnitudes of the third harmonic related to the short-circuit power of the distribution transformer ($S_{\mathrm{k\,T}}$) and the total length of the lines in the network or feeder (ℓ_{TOT}). Similar graphs were generated for the other harmonic orders, as well as graphs to identify the influence of the network configuration on the mean direction and variation of harmonic phase angles. However, no clear relation between both network parameters with the harmonic current magnitudes and phase angles could be found. Therefore, the network configuration is not considered further in the analysis and it is not included in the model.

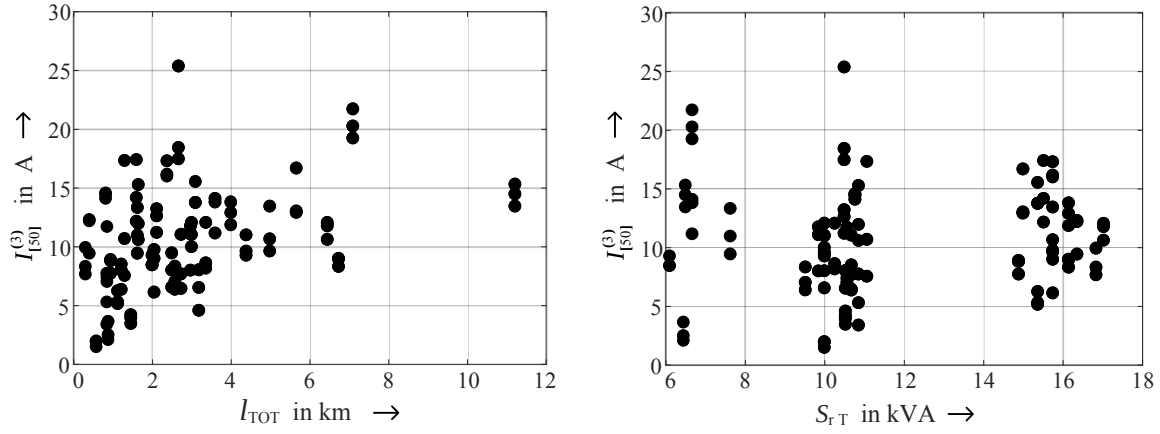

(a) Length of the lines

(b) Transformer size

Figure 4.7.: Harmonic magnitudes related to the network configuration

4.2.3. Influence of social environment

Income and population density may have a significant influence on the amount of electric devices per customer and the corresponding usage behavior, which can consequently influence the level of harmonics in the network. The average annual income (IN_{av}) gives an approximate measure of the purchasing capacity of the customers to acquire household appliances and how much electricity consumption they could afford. Information about the income of each customer may be more appropriate for this analysis, but since this information is not available, only the official average annual income of the region or city is used. The population density (ρ_{pop}) indicates the type of settlement (e.g. highly urbanized area, rural area, etc.) which can also indicate the way in which the customers consume energy. The definition of type of settlements used in this work is described in appendix A.

Fig. 4.8 shows the median of the third harmonic magnitude related to both parameters, but there is no clear influence of income and population density on the harmonic emission. The same result was obtained for the other harmonic orders. The reason is the low income inequality in Germany which results in a similar amount and type of household equipment per customer and also a similar energy consumption. There are still some differences between customers, as seen before, depending on the type of dwelling and the number of inhabitants per

house, but the income of the customers has no clear influence on their harmonic emission in Germany. Moreover, there are no visible differences in the amenities that people from rural and urban areas have. Therefore, these variables can be neglected from the following analysis and modeling, but they should be considered depending on the social characteristics of the considered country or region, especially if high social inequality is present.

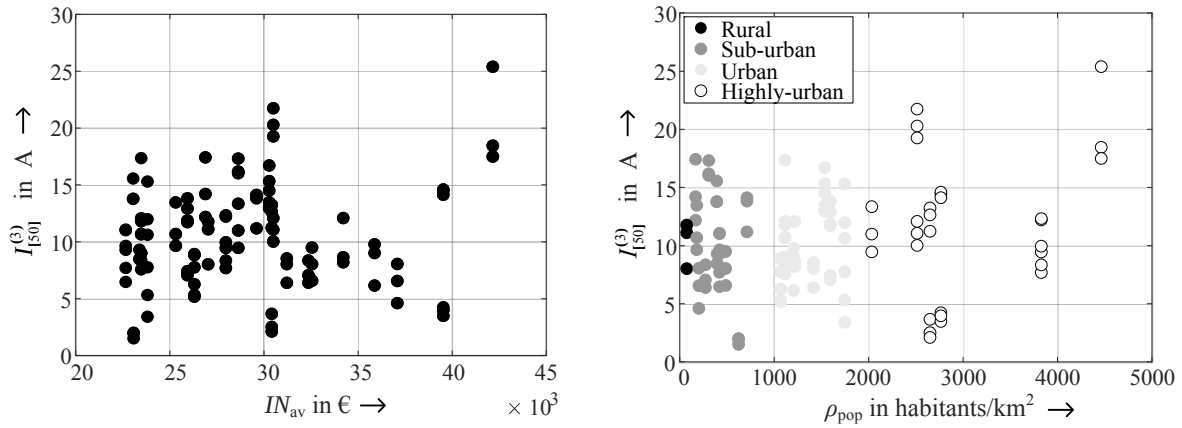

(a) Income

(b) Type of settlement

Figure 4.8.: Harmonic magnitudes related to the number of customers and short circuit power of the distribution transformer

4.3. Harmonic unbalance

Most of the models available in the literature assume perfect balanced conditions, but as already identified in the previous sections the unbalance of harmonic currents is considerable. In this section, a more systematic analysis of the unbalance of harmonic currents is developed in order to decide if this aspect should be considered in the model.

The unbalance is assessed using the symmetrical components of the harmonics currents instead of the original phasors, in order to take into account not only the differences between magnitudes but also the contributions of the angular displacement (differences between phase angles) to unbalance. The symmetrical components are calculated based on the Fortescue transformation, but the results are reorganized to facilitate the analysis. The original phase currents are transformed in a balanced ($\underline{I}^{(h)}_{\mathrm{b}}$), first unbalanced ($\underline{I}^{(h)}_{\mathrm{u1}}$), and second unbalanced ($\underline{I}^{(h)}_{\mathrm{u2}}$) components. The balanced component corresponds to the so called "characteristic" harmonic sequences (e.g. zero-sequence for the third harmonic, negative-sequence for the fifth harmonic, positive sequence for seventh harmonic and so on). The first and second unbalanced harmonic components can give information about the amount of linear and non-linear loads which are not connected in a balanced way. Appendix B.2 contains the mathematical procedure to calculate the symmetrical components for harmonic currents.

Fig. 4.9 shows exemplary the symmetrical components of the third harmonic of one site calculated for one week. The balanced component (zero-sequence component of the third harmonic) is a kind of average of the original line currents (all depicted in gray) which follows a similar daily pattern. On the other hand, the unbalanced components (positive and negative components of the third harmonic) do not follow the same pattern as the balanced component and their values are considerably lower than the balanced current. In this case, the balanced component dominates, which indicates that the third harmonic current is mainly composed of a zero sequence. The phase angle of the balanced component is also similar to the phase angle

of the line currents, but for the unbalanced components the phase angles take values in all the interval [0 °, 360°].

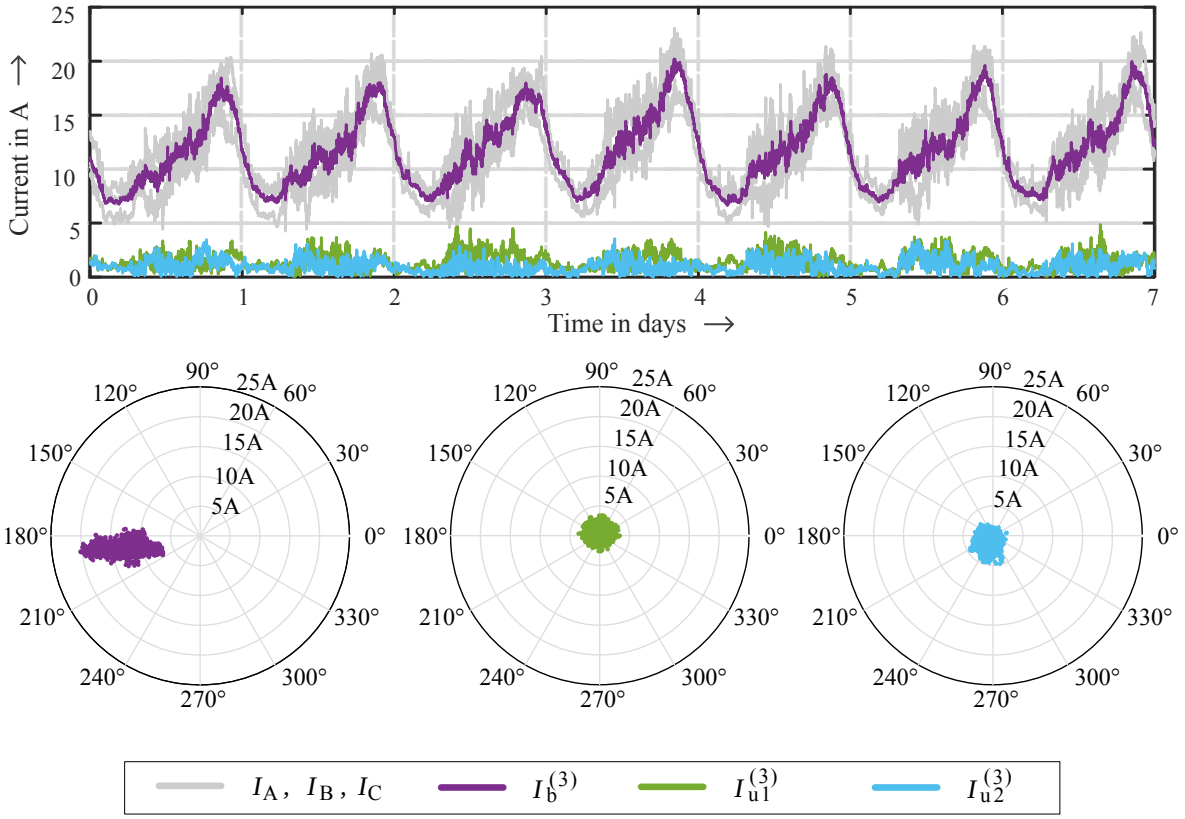

Figure 4.9.: Symmetrical components of the third harmonic of one site

Similar as for the phase currents, the magnitude of the balanced component depends on the number of customers and the type of customers in the network. Fig. 4.10 shows the variation of the median value of the magnitude of the balanced and unbalanced components of the third harmonic for all sites in relation with the number of customers and separated according to the type of customers C1/M1 and C2/M2. The balanced component magnitude increases with the number of customers, just as shown for the magnitude of phase currents in Fig. 4.5. However, the magnitude of the unbalanced component do no increase at the same rate as the balanced component and the difference between balanced and unbalanced components magnitudes increase with the amount of customers.

Comparison of the times-series plots and statistics of the symmetrical components of the other harmonic orders revealed that the balanced component of harmonic currents behave very similar to the phase currents, showing a similar variation of magnitudes and phase angles. The magnitude of the balanced component shows a clear daily pattern for most harmonic orders, and the phase angles show a similar mean direction as the phase currents. The unbalanced components, on the contrary, do not present a clear daily pattern, and nor a mean direction of the phase angles can be defined (mean resultant length is always below 0.8).

Based on the balanced, first and second unbalanced components of each harmonic, the aggregate harmonic unbalance factor (AHU) is proposed to evaluate the unbalance of the harmonic currents [19]:

$$AHU^{(h)} = \frac{\sqrt{\left(I_{u1}^{(h)}\right)^2 + \left(I_{u2}^{(h)}\right)^2}}{I_b^{(h)}} \cdot 100\% \tag{4.1}$$

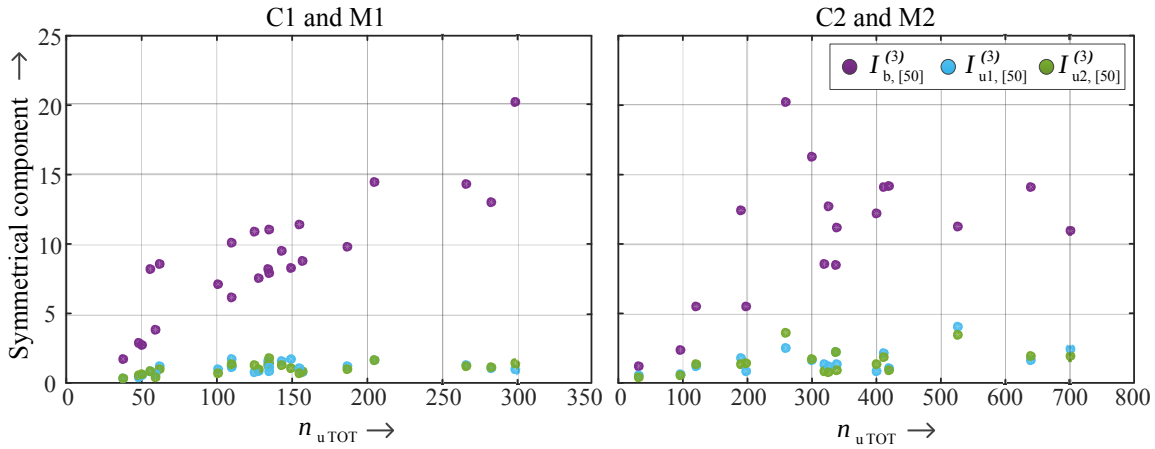

Figure 4.10.: Median of the symmetrical components of the third harmonic for all sites

where $I_b^{(h)}$, $I_{u1}^{(h)}$ and $I_{u2}^{(h)}$ are the magnitudes of the phasors $\underline{I}_b^{(h)}$, $\underline{I}_{u1,}^{(h)}$ and $\underline{I}_{u2,}^{(h)}$ respectively. The AHU factor shows the relation between the unbalanced components with the corresponding balanced component. If the AHU has a value higher than 100%, the harmonic current is dominated by unbalanced components.

The AHU factors were calculated for the first 15 odd harmonics for each site using the 1 minute measurements of one week (10080 values per site and per harmonic). Fig. 4.11 shows the boxplot of the AHU factors of the fundamental, third and fifth harmonic currents for all sites classified according to the customer type. The boxplot representation allows the comparison of the median value (middle line in the box), the variation of the data (the tops and bottoms of each box are the 25th and 75th percentiles of the samples), and the presence of extreme values (dots) more than 1.5 times the interquartile range away from the top or bottom of the box which are represented by whiskers.

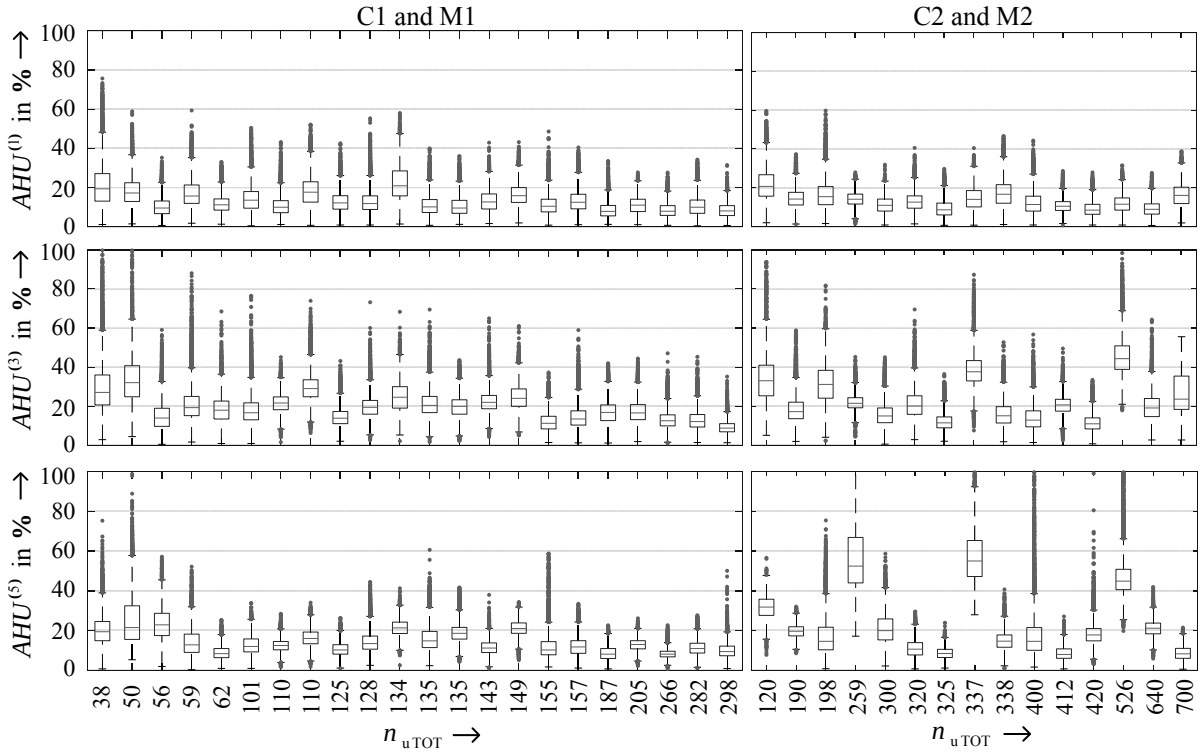

Figure 4.11.: Boxplots of the AHU factors calculated for each site during one week

The *AHU* factor varies considerably between sites. It is mostly below 60% but it can reach values higher than 100% which indicates that the harmonic current during that time does not have the assumed sequence (unbalanced components are higher than the balanced component). However, these high values occur usually during short periods of time. The fundamental current unbalance is in general lower than the harmonic unbalances. Comparing the boxplots it is noticed that the sites with high unbalances in the fundamental current do not necessarily correspond to the sites with high unbalances in the harmonic currents.

The boxplots are organized according to the total amount of customers of the respective site. The fundamental and third harmonic *AHU* factors of customers C1 show a decreasing trend with the number of customers, which coincides with the observations made previously on Fig. 4.10. However, the decrease in the harmonic unbalance with the amount of customers is not so clearly visible looking at the boxplots of the other harmonic orders, especially the unbalances obtained for customers living in apartments (C2).

In general, most of the sites showed harmonic unbalances between 10% and 50%. Therefore, this aspect can no be longer neglected in the harmonic modeling and analysis of residential distribution systems.

4.4. Time-series characteristics

Time-series plots were initially used to identify the daily behavior of the harmonic current magnitudes during all measured days. As already discussed by several authors (e.g. [26, 44, 57, 93]), the fundamental current and the first odd harmonic current magnitudes in residential low-voltage networks show a clear 7-day pattern, which is linked to the daily behavior of residential customers. Fig. 4.12 shows the time-series plot of a typical residential site.

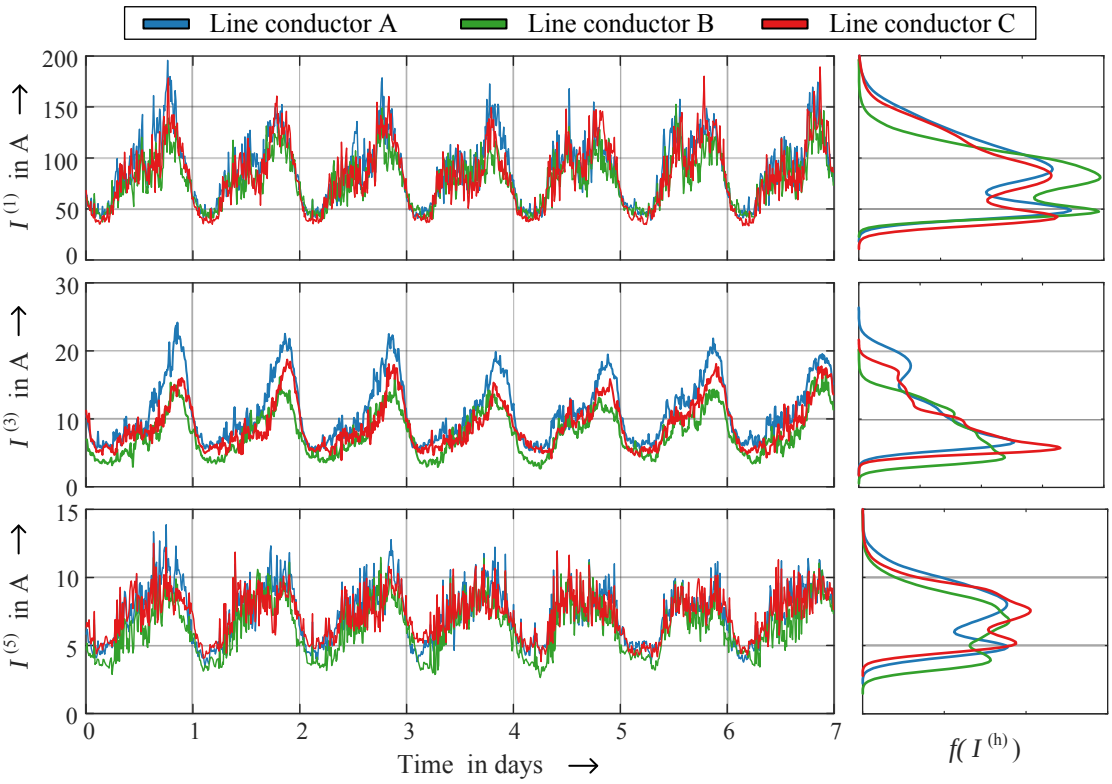

Figure 4.12.: Time-series plots and corresponding PDFs of harmonic currents magnitudes of a typical residential site.

The fundamental current magnitude shows a daily pattern very similar to the well known load profile of residential customers. This pattern shows 2 or 3 peaks which are linked to the times of high activity of most residential customers, i.e. preparation of meals, demand of lighting, entertainment in the evening, etc [42]. In contrast, the third harmonic magnitude shows a daily curve with only one peak which is related to the high use of electronic appliances in the evening. The fifth harmonic magnitude is more similar to the fundamental current, but the difference between the two peaks is not as clear as for the fundamental current magnitude, but still a daily pattern can be recognized.

The daily behavior of harmonic currents results in a non-normal distribution of the data, as can be noticed in Fig. 4.12/right. The distribution of harmonic magnitudes during one day is a mixture distribution with two or three components. Therefore, as discussed by e.g. [27, 93], the use of univariate distributions to represent harmonic current magnitudes may result in high inaccuracies, and more accurate methods are required to model the real behavior of harmonic currents.

Distance and similarity measures can be used to evaluate the similitude of the daily patterns of the harmonic current magnitudes, either for each site or between sites. There are different types of measures in the literature, but only measures that preserve the time-stamp characteristics should be selected, i.e. the peaks and valleys of the daily curves should not be shifted. For this analysis the Euclidean distance (DM_{E}) and the Pearson's correlation coefficient (SM_{P}) are used to evaluate the resemblance of the daily curves. The Euclidean distance evaluates the geometrical distance between two curves, while the Pearson's correlation coefficient evaluates the correlation between curves. Appendix B.4 contains a review of the chosen distance and similarity measures.

The data of each site was first normalized and smoothed using the min-max normalization (c.f. section B.3) and a simple moving average with a window of 10 minutes. The normalization and smoothing reduce the effects of noise and amplitude scaling, giving more reliable results (c.f. section B.4).

It is indispensable to define thresholds for the distance and similarity measures in order to evaluate the resemblance of the daily patters i.e. thresholds that can be used to accept or reject the similarity between daily curves. Based on the normalized and smoothed daily curves of the fundamental current and the third harmonic current magnitudes of all sites, 1500 pairs of curves with acceptable similarity were chosen. The similarity between these curves was evaluated using time-series plots, as shown in Fig. 4.12, and it was accepted that a pair of curves was similar based on a visual comparison of their patterns. The measures DM_{E} and SM_{P} were calculated for each pair of curves. Fig. 4.13-a and Fig. 4.13-b show the CDFs of the calculated measures. According to them, around 95% of the curves showed a DM_{E} lower than 8 and a SM_{P} higher than 0.7 ($SM_{\mathrm{P},[5]} \approx 0.7$ which implies that more than 95% of the cases showed a SM_{P} higher than 0.7). Based on the maximum possible Euclidean distance for normalized curves in the range $[0, 1]$ (c.f. section B.4), a DM_{E} of 8 corresponds to the 21.1% of the maximum possible distance.

Based on the 95$^{\mathrm{th}}$ and 99$^{\mathrm{th}}$ percentiles of the DM_{E} measure, and the 1$^{\mathrm{st}}$ and 5$^{\mathrm{th}}$ percentiles of SM_{P} measure, the thresholds of both measures were defined, as shown in Fig. 4.13-c. The similarity between two pairs of curves is accepted if DM_{E} is lower than 11 (<30% of the maximum Euclidean distance) and SM_{P} is higher than 0.55. Both factors should be evaluated simultaneously, as each of them evaluates different characteristics between the curves.

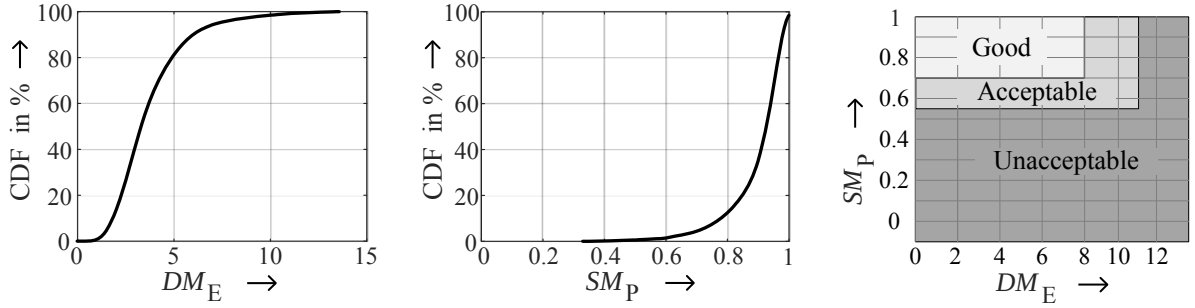

(a) Euclidean distance (b) Correlation coefficient (c) Thresholds

Figure 4.13.: Threshold of distance and similarity measures

4.4.1. Differences between curves of single sites

First, the distance and similarity measures were calculated between the daily curves of each site and each line conductor, in order to evaluate the similarity of the daily variation of the harmonic current magnitudes of each site. The Euclidean distance between day i and day j is defined as $DM_{\mathrm{E},i,j}$ and the corresponding Pearson's correlation coefficient as $SM_{\mathrm{P},i,j}$. If there are N number of days, then $N-1$ distances (or correlation coefficients) are calculated for each day, i.e. the distance between day i and j for all $j \neq i$. In order to give an unique index for each day, the mean Euclidean distance and the mean Pearson's correlation coefficient for a day i is defined as [44]:

$$\overline{DM}_{\mathrm{E},i} = \frac{1}{N}\sum_{j=1}^{N} DM_{\mathrm{E},i,j} \qquad \text{for } i,j = 1,2,...,N \text{ and } i \neq j \tag{4.2}$$

$$\overline{SM}_{\mathrm{P},i} = \frac{1}{N}\sum_{j=1}^{N} SM_{\mathrm{P},i,j} \qquad \text{for } i,j = 1,2,...,N \text{ and } i \neq j \tag{4.3}$$

Comparing the values $\overline{DM}_{\mathrm{E},i}$ and $\overline{SM}_{\mathrm{P},i}$ with the thresholds in Fig. 4.13-c, the similarity of day i with respect to the other days is accepted or rejected. The harmonic currents of a site have a daily pattern only if at least 80% of the days are similar between them, i.e. the 80% of the days have good or acceptable $\overline{DM}_{\mathrm{E},i}$ and $\overline{SM}_{\mathrm{P},i}$ values.

Fig. 4.14 shows the percentage of sites with clear daily patterns for each harmonic order. The procedure was repeated using only workdays (from Monday to Friday) and also with the balanced component I_{b}. Results reveal that the fundamental and third harmonic magnitudes show a clear daily pattern, while the 13$^{\mathrm{th}}$ harmonic magnitude showed the worst similarly between days. All results improve if only workdays are considered, which indicates that there is a noticeable difference between workdays and weekends, especially for the 5$^{\mathrm{th}}$, 7$^{\mathrm{th}}$ and 11$^{\mathrm{th}}$ harmonics.

Results also improved if the balanced component is considered. The balanced component follows a similar daily pattern as the phase currents, but it is more stable over time, which results in a more clear daily pattern. The similarity of daily curves of the first and second unbalanced components was also assessed, but for those components the percentage of sites with clear daily patterns is for all harmonics below 5%, therefore the first and second unbalanced components do not have a daily pattern.

The time-series plots of harmonic phase angles revealed that the phase angles do not show a clear daily pattern, and their behavior seems more random. This observation was verified with the distance and similarity measures.

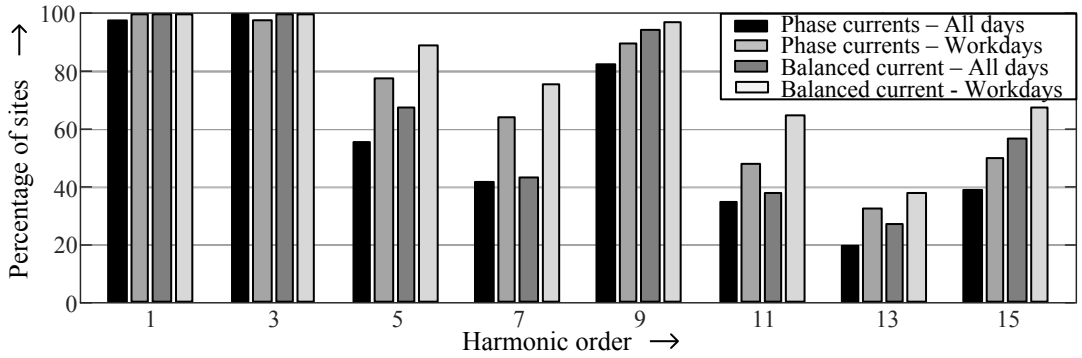

Figure 4.14.: Percentage of sites with clear daily patterns

4.4.2. Differences between sites

It is also interesting to know if the daily patterns of the harmonic current magnitudes of different networks are similar, so that a general daily behavior for residential sites can be defined. In order to calculate this similarity, the mean Euclidean distance and mean Pearson's correlation coefficient were calculated between all daily curves of the balanced component of sites with clear daily patterns, i.e. sites that were approved in the previous subsection. Table 4.1 shows the percentage of days with acceptable similarity. According to this, for most harmonic orders the similarity between daily curves is high and there is a high similarity between sites. This can be explained by the similar daily behavior that residential customers have in general.

Table 4.1.: Percentage of similar days

	Harmonic order							
	1	3	5	7	9	11	13	15
Percentage of days	100	100	97.4	93.3	97.6	84.5	81.7	73.9

Consequently, a model based on the time-series characteristics of the harmonic current magnitudes seems adequate. Moreover, including the daily variations of harmonic currents in the models will provide flexibility to analyze the influence of certain loads that are operated during specific periods of time, for example, photovoltaic systems or electric vehicles.

4.5. Correlation between harmonic magnitudes and phase angles

The possible correlations between harmonic magnitudes and phase angles should be identified in order to include the relationship between variables in the model. Moreover, the correlations between variables may lead to the simplification of the model, in which only some variables have to be modeled in detail, and the others are calculated based on the correlations.

Three different correlations are analyzed:

- Relation between magnitudes and phase angles of the same harmonic order.
- Relation between magnitudes of different harmonic orders.
- Relation between phase angles of different harmonic orders.

The Pearson correlation coefficient SM_{P} (see definition in appendix B.4) is used to identify the correlation between the different variables in a systematic way. In this case, a good correlation between variables is accepted if $|SM_{\mathrm{P}}| > 0.7$. Lower values of $|SM_{\mathrm{P}}|$ indicate that between

variables there is a non-linear relationship or that there is no relationship at all. The analysis is complemented using scatter plots, which allow a easy verification of conclusions drawn with the $|SM_{\mathrm{P}}|$ values and the identification of the possible non-linear relationships between variables.

The correlation analysis is applied to the data of one complete week, and the data of only one workday during two different periods (1-3 a.m. and 7-9 p.m.). The data of one day during different time periods is used in order to verify that the correlation is independent of the time, and to reduce the possible influence of other factors, like the voltage distortion. Moreover, the analysis is applied to the phase currents and the corresponding symmetrical components.

Fig. 4.15 shows the percentage of sites with good correlation between magnitudes and phase angles of the same harmonic, for the data of line conductor A ($I_{\mathrm{A}}^{(h)}$), the balanced component ($I_{\mathrm{b}}^{(h)}$) and the first unbalanced component ($I_{\mathrm{u1}}^{(h)}$). The results obtained for the line conductors B and C are similar to the results of line conductor A, while the results of the second unbalanced component are similar to the results of the first unbalanced component. The amount of sites with good correlations do not exceed 40% in any of the considered cases. The correlation seems to improve for the balanced component, but still most of the sites do not show a clear linear relationship between magnitudes and phase angles of the same harmonic order.

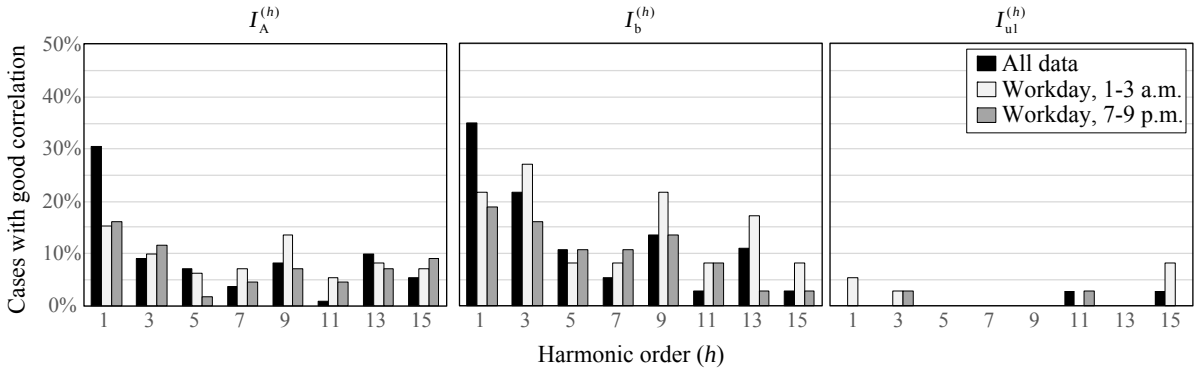

Figure 4.15.: Amount of sites with good correlation between magnitudes and phase angles

Scatter plots confirm the results obtained with the $|SM_{\mathrm{P}}|$ values. Fig. 4.16 shows exemplary the scatter plots of the magnitudes and phase angles of the third harmonic of three different sites (line conductor A). There are some sites with clear correlation between variables, like site C in the figure, but in most of the cases the correlation is not clear. In general, the relation between variables is different for each residential site, and no unique relation between variables for all residential networks can be easily defined.

The relation between magnitudes of the same harmonic order, and between phase angles of the same harmonic order were analyzed in the same way, but no clear relation between magnitudes or phase angles could be identified, except for the relation between the first and second unbalanced component of the fundamental currents, which show a clear linear relationship for most than 70% of the sites.

It is possible that the relation between variables is linked to the electrical characteristics of the network, the voltage distortion and/or the impedance characteristic; therefore, the relation between variables for each site is different. Detailed and controlled measurements in different networks should be perform in order to verify the correlations between variables. In this thesis, each variable will be treated independently and the correlation between variables will be neglected.

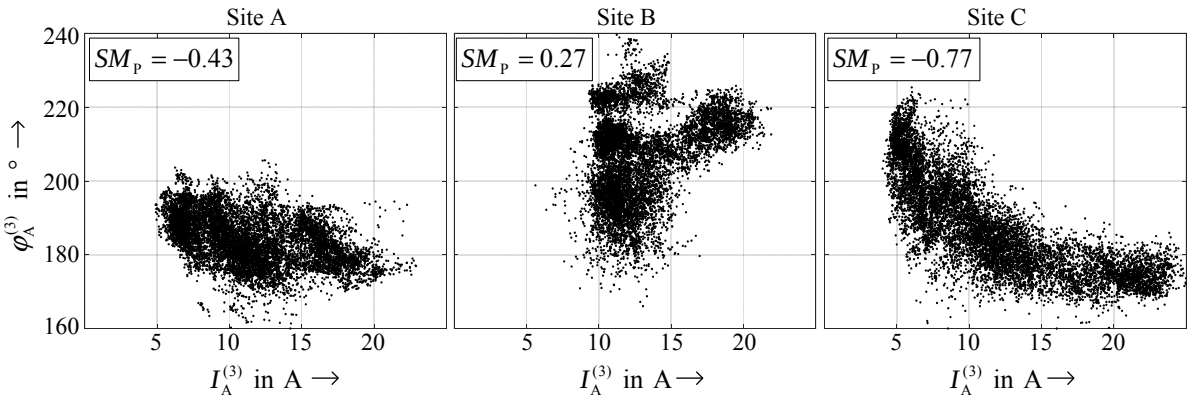

Figure 4.16.: Relation between magnitude and phase angle of the third harmonic of three residential sites

4.6. Chapter summary

Measurements of 37 residential low-voltage networks are available to develop a harmonic emission model of aggregate customers using a measurement-based approach. The measurements were made during the winter time to reduce the influence of seasonal variations. Moreover, only networks with mainly residential customers and with none or few photovoltaic systems were selected, in order to analyze and model the real harmonic current emission of pure residential customers. According to the initial characterization, the harmonic currents of aggregate residential customers have the following characteristics:

- The harmonic current magnitudes depend on the type and number of customers connected to the network. Harmonic current magnitudes increase with the number of customers. Moreover, networks with mainly single-family houses have higher harmonic current magnitudes than networks with apartments.
- The harmonic phase angles do not vary randomly in the complex plane, but they are concentrated in a prevailing direction for most harmonic orders. Most of the residential sites show a similar direction of harmonic phase angles, especially for the fundamental, third, fifth, seventh, and ninth harmonic orders. For higher harmonic orders, the variation of phase angles is higher for each site, and there are more differences between sites. There is no clear relation between the type and number of customers with the harmonic phase angles.
- Harmonic current magnitudes show a daily pattern for most harmonic orders, which is linked to the daily activities of residential customers. There are also differences between workdays and weekends, which results in variations of the daily patterns. Harmonic phase angles do not show a clear daily pattern.
- The unbalance of the fundamental and the harmonic currents is significantly high, usually higher than 10%. The unbalance increases with the harmonic order.
- Magnitudes and phase angles do not show a clear correlation. Magnitudes and phase angles may be treated as independent variables.

Based on the characteristics of the harmonic currents, a modeling methodology can be defined, which is explained in the next chapter.

5. Model of residential low-voltage networks

The main characteristics of the harmonic currents of aggregate residential customers were identified based on the analysis of several measurements of residential low-voltage networks. The model is developed in order to obtain an accurate representation of the harmonic magnitudes and phase angles of the first 15 odd harmonics, including as many characteristics as possible.

Fig. 5.1 shows the general scheme of the model. The input parameters are the harmonic order, the number of customers, and the type of customer; the outputs are the daily harmonic magnitudes and phase angles. The structure and components of the stochastic model are fixed, but the values of the parameters vary for each harmonic order and according to the type and number of customers.

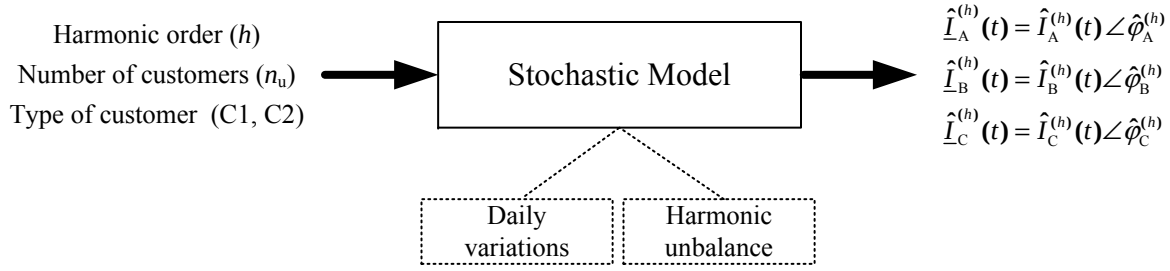

Figure 5.1.: Basic scheme of the stochastic model

The model represents the random variations of harmonic magnitudes and phase angles of aggregate customers, considering the daily variations of harmonic magnitudes and the harmonic unbalances between line conductors. The representation of the daily variation of harmonic magnitudes is of great importance for accurate analyses, especially in penetration studies of new technologies, e.g. photovoltaic inverters and electric vehicles, which have specific schedules for the generation or demand of energy. The inclusion of harmonic unbalance in the model allows more accurate and realistic analyses, especially if the propagation of harmonic currents to the upstream medium-voltage network is of interest.

The model is developed for harmonic propagation analyses of medium and low-voltage networks, with the additional characteristic that it can be implemented in widely used analysis programs, like DigSilent, Neplan, etc. As measurements of the low-voltage residential networks are available (measurements at the low-voltage side of the distribution transformer), first the model of the whole residential low-voltage network is obtained, and then, using a top-down approach, the model is modified to represent groups of customers, i.e. feeder or feeder sections (c.f. Fig. 3.5). The model of the complete low-voltage network will allow the analysis of medium-voltage networks, while the model of groups of customers can be used for the analysis of low-voltage networks. The model of residential low-voltage networks is explained in this chapter, and the model of groups of residential customers is explained in chapter 6.

It is important to mention that an unique model that represents with high detail all types of residential networks is virtually impossible, because, as shown in the previous chapter, each residential network has slightly different harmonic emission characteristics. The harmonic emission of residential networks depends on the electrical characteristics of the network (impedances, possible resonances, influence of other non-residential customers, etc.), the social environ-

ment, the climate conditions, but mainly on the random behavior of the customers, which can not be exactly determined. Therefore, the objective is to develop a generic model that represents the typical harmonic emission of most residential networks.

Different modeling techniques were applied in order to obtain a generic model of harmonic currents. The different modeling techniques were first applied to each of the available residential sites, i.e. each residential site was modeled individually. Then, the parameters of the site models were compared, and a generic model was formulated. Below, only the selected generic model, which had the best results among different models, is presented. Some of the other approaches, which were not successful, are shortly discussed along the chapter.

This chapter is divided in three sections. The first section describes the stochastic model, including all equations and parameters required to estimate the harmonic current magnitudes and phase angles. The second section explains in detail how the stochastic model was parameterized for German cities based on the available measurements. The model with the presented parameters is valid for Germany and other cities, where the electric and non-electric environment is similar as in Germany. However, the parametrization procedure can be used to get the model parameters of other regions with different harmonic current characteristics. Finally, the third section validates the stochastic model comparing the output of the model with measurements of different residential low-voltage networks.

5.1. Characteristics of the stochastic model

The Norton equivalent (c.f. Fig. 2.6) is selected to represent the aggregate residential customers. As only measurements during normal operating conditions of the harmonic currents are available, only the current source parameters can be estimated. The impedance of the Norton equivalent should be obtained with dedicated measurement systems (e.g. [105, 123, 128]). However, as the impedance of the network at low-order frequencies is considerably lower than the impedance of the customers in typical residential networks [90], most of the harmonic currents produced by the residential customers flow directly toward the distribution transformer, and the simplified current source model can be used to get approximate results (c.f. section 2.3).

The aggregate customers are represented then by independent current sources for each harmonic order. In this model, the behavior of magnitudes and phase angles of each harmonic order is modeled independently, in accordance with the correlation analysis presented in the previous chapter. The other advantage of this approach is the easy implementation of the model in most analysis programs, because most of them use current sources to represent harmonic polluting loads.

Different to other approaches, this model includes the harmonic unbalances. This is done modeling the symmetrical components, instead of the phase currents. As shown before, the balanced component is a kind of average of the phase currents with similar magnitude and phase angle. Actually, the balanced component shows a more clear and stable daily pattern (c.f. Fig. 4.14) than the phase currents, which can be represented by time-series modeling techniques. The magnitude and phase angle of unbalanced components show a more random behavior, and they can be modeled with more simple models or distribution functions.

Fig. 5.2 shows the flow diagram of the stochastic model, which is divided into three blocks: estimation of balanced and unbalanced harmonic magnitudes (Block I), estimation of balanced and unbalanced harmonic phase angles (Block II), and transformation to phase currents (Block III):

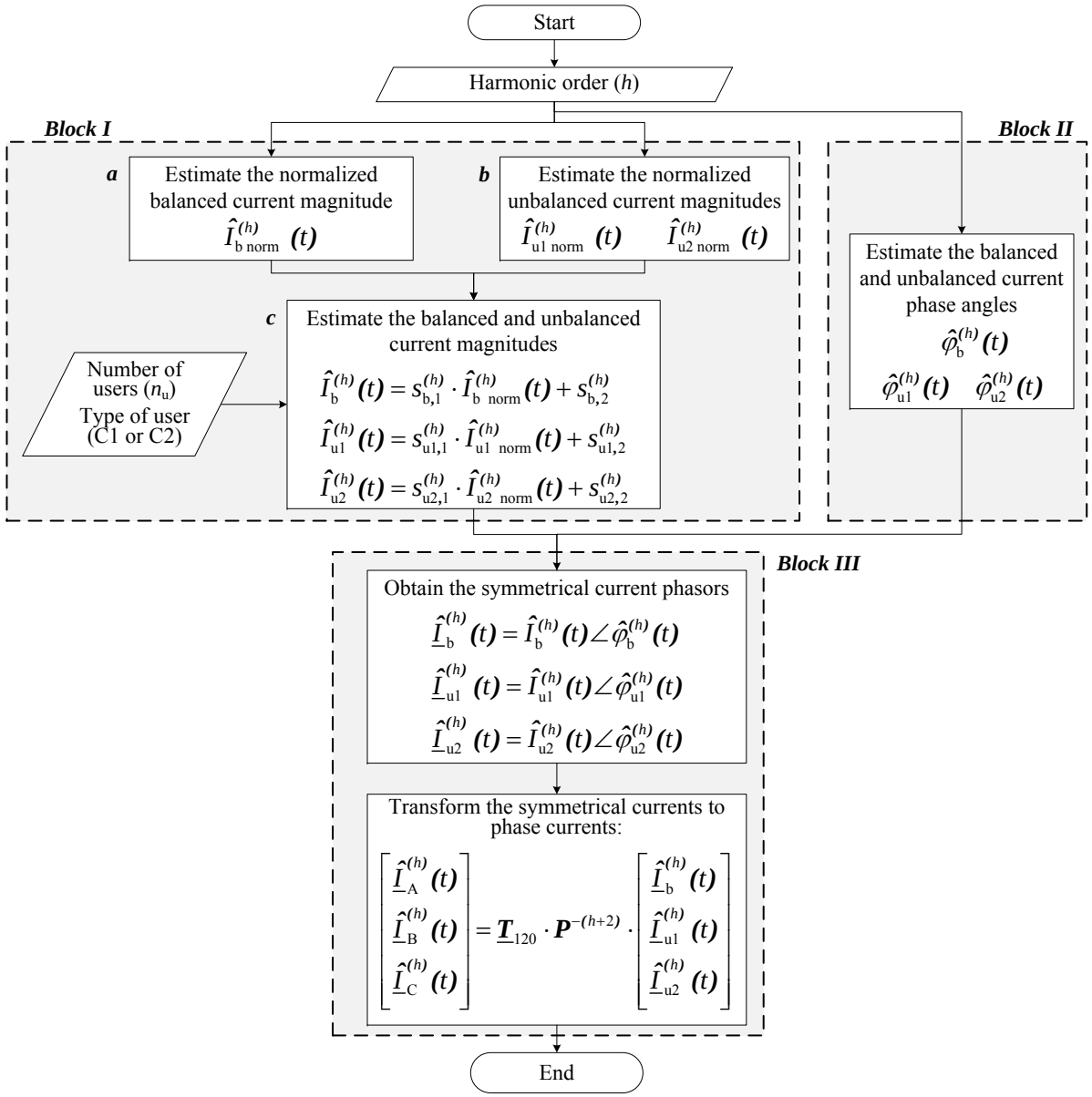

Figure 5.2.: Flow diagram of the stochastic model.

Block I - Estimation of harmonic magnitudes

The balanced and unbalanced current magnitudes ($\hat{I}^{(h)}_{\text{b}}$, $\hat{I}^{(h)}_{\text{u1}}$, $\hat{I}^{(h)}_{\text{u2}}$) are estimated based on normalized balanced and unbalanced currents ($\hat{I}^{(h)}_{\text{b norm}}$, $\hat{I}^{(h)}_{\text{u1 norm}}$, $\hat{I}^{(h)}_{\text{u2 norm}}$), which are defined in the interval [0 1]. Once the normalized magnitudes are obtained, they are scaled according to the number and type of customers.

- Normalized balanced current magnitude $\hat{I}^{(h)}_{\text{b norm}}$

  The normalized balanced current magnitude is described with a stochastic time-series model, which consists of two main parts: a deterministic component that describes the daily variations of harmonic magnitudes, and a stochastic component that represents the random variations around the deterministic component (c.f. equation 3.5 and Fig. 3.7). In this case, the trend (annual changes) and the seasonal variations are neglected as only the measurements of few weeks are available. However, if measurements over long periods

of time are available, the trend and the seasonal variations can be included, extending the model for more diverse analysis, like forecasting. A discussion about the identification of trends and seasonal variations can be found in [46, 47, 81].

Equation 5.1 shows the generic model formulation. The deterministic component $\hat{\underline{I}}^{(h)}_{\mathrm{b\ norm\ D}}(t)$ is a Fourier series, which describes the daily pattern with a constant value FC_0 and three cosine functions, each with magnitude FC_k and angle θ_k. The stochastic component is represented with an autoregressive model of first order $\hat{\underline{I}}^{(h)}_{\mathrm{b\ norm\ R}}(t)$, also called a Markov process [110]. The autoregressive model represents the dependence of successive observations, i.e. a value of the process is expressed as a finite, linear aggregate of previous values of the process and a pure random part described with a normal distribution $\mathcal{N}(0, \sigma)$ [23]. The function $\hat{\underline{I}}^{(h)}_{\mathrm{b\ norm\ R}}(t)$ is described with the parameters α_{b} and σ_{b}, where α_{b} describes the relation between successive values, and the parameter σ_{b} is the variance of the normal distribution.

$$\begin{aligned}
\hat{I}^{(h)}_{\mathrm{b\ norm}}(t) &= \hat{\underline{I}}^{(h)}_{\mathrm{b\ norm\ D}}(t) + \hat{\underline{I}}^{(h)}_{\mathrm{b\ norm\ R}}(t) \\
\hat{\underline{I}}^{(h)}_{\mathrm{b\ norm\ D}}(t) &= FC_0^{(h)} + \sum_{k=1}^{3} FC_k^{(h)} \cos(2\pi \cdot k \cdot f_{\mathrm{D}} \cdot t + \theta_k^{(h)}) \\
\hat{\underline{I}}^{(h)}_{\mathrm{b\ norm\ R}}(t) &= \alpha_{\mathrm{b}}^{(h)} \hat{\underline{I}}^{(h)}_{\mathrm{b\ norm\ R}}(t-1) + \mathcal{N}(0, \sigma_{\mathrm{b}}^{(h)})
\end{aligned} \tag{5.1}$$

The period of the deterministic component T_{D} is 1 day, and their corresponding frequency f_{D} is obtained as $f_{\mathrm{D}} = \frac{1}{T_{\mathrm{D}}}$. As measurements every 1 minute are available, the frequency of the deterministic component is $f_{\mathrm{D}} = \frac{1}{1440}$ Hz. The deterministic component is described only with the first four components (including the constant component) of the Fourier series. The selection of the number of components is explained in section 5.2.2.

The parameters $FC_0^{(h)}$, $FC_k^{(h)}$, $\theta_k^{(h)}$ and $\alpha_{\mathrm{b}}^{(h)}$ for each harmonic order are described with normal distribution functions $\mathcal{N}(N_\mu, N_\sigma)$, with mean N_μ and variance N_σ. The parameter $\sigma_{\mathrm{b}}^{(h)}$ depends on the calculated value of $\alpha_{\mathrm{b}}^{(h)}$ as:

$$\sigma_{\mathrm{b}}^{(h)} = m_{\mathrm{b},1} \cdot \alpha_{\mathrm{b}}^{(h)} + m_{\mathrm{b},2} \tag{5.2}$$

- Normalized unbalanced current magnitudes $\hat{I}^{(h)}_{\mathrm{u1\ norm}}$ and $\hat{I}^{(h)}_{\mathrm{u2\ norm}}$

  The normalized unbalanced current magnitudes are represented with autoregressive models of first order that represent the random variation of both unbalanced currents, including the dependence between successive values. In this case, the autoregressive models have the parameters K_{u}, α_{u} and σ_{u}.

$$\begin{aligned}
I^{(h)}_{\mathrm{u1\ norm}}(t) &= K_{\mathrm{u}} + \alpha_{\mathrm{u}} \cdot I^{(h)}_{\mathrm{u1\ norm}}(t-1) + \mathcal{N}(0, \sigma_{\mathrm{u}}) \\
I^{(h)}_{\mathrm{u2\ norm}}(t) &= K_{\mathrm{u}} + \alpha_{\mathrm{u}} \cdot I^{(h)}_{\mathrm{u2\ norm}}(t-1) + \mathcal{N}(0, \sigma_{\mathrm{u}})
\end{aligned} \tag{5.3}$$

  Parameters K_{u}, α_{u} and σ_{u} have the same expression for all considered harmonic orders. The parameter α_{u} is described with a normal distribution $\mathcal{N}(N_\mu, N_\sigma)$, with mean N_μ and variance N_σ. The parameters K_{u} and σ_{u} depend on the value of α_{u} as:

$$\sigma_{\mathrm{u}} = m_{\mathrm{u},1} \cdot \alpha_{\mathrm{u}} + m_{\mathrm{u},2} \tag{5.4}$$

$$K_{\mathrm{u}} = m_{\mathrm{u},3} \cdot \alpha_{\mathrm{u}} + m_{\mathrm{u},4} \tag{5.5}$$

- Balanced and unbalanced current magnitudes $\hat{I}^{(h)}_{\mathrm{b}}$, $\hat{I}^{(h)}_{\mathrm{u1}}$ and $\hat{I}^{(h)}_{\mathrm{u2}}$

The balanced and unbalanced current magnitudes of a network are obtained by scaling the normalized balanced and unbalanced magnitudes as:

$$\begin{aligned}\hat{I}_{\mathrm{b}}^{(h)}(t) &= s_{\mathrm{b},1}^{(h)} \cdot \hat{I}_{\mathrm{b\ norm}}^{(h)}(t) + s_{\mathrm{b},2}^{(h)} \\ \hat{I}_{\mathrm{u1}}^{(h)}(t) &= s_{\mathrm{u1},1}^{(h)} \cdot \hat{I}_{\mathrm{u1\ norm}}^{(h)}(t) + s_{\mathrm{u1},2}^{(h)} \\ \hat{I}_{\mathrm{u2}}^{(h)}(t) &= s_{\mathrm{u2},1}^{(h)} \cdot \hat{I}_{\mathrm{u2\ norm}}^{(h)}(t) + s_{\mathrm{u2},2}^{(h)}\end{aligned} \tag{5.6}$$

The parameters $s_{\mathrm{X},1}^{(h)}$ and $s_{\mathrm{X},2}^{(h)}$, where X denotes balanced b, first unbalanced $\mathrm{u1}$ and second unbalanced $\mathrm{u2}$ components, depend on the number and type of customers in the network as:

$$s_{\mathrm{X},1}^{(h)} = I_{\mathrm{X,[max\text{-}min]}}^{(h)} \tag{5.7}$$

$$s_{\mathrm{X},2}^{(h)} = I_{\mathrm{X,[max]}}^{(h)} - I_{\mathrm{X,[max\text{-}min]}}^{(h)} \tag{5.8}$$

where:

$$I_{\mathrm{X,[max]}}^{(h)} = p \cdot (n_{\mathrm{u\ TOT}})^{q} \tag{5.9}$$

$$I_{\mathrm{X,[max\text{-}min]}}^{(h)} = v \cdot I_{\mathrm{X,[max]}}^{(h)} \tag{5.10}$$

The values p, q, and v are different for each harmonic order, for the balanced and unbalanced currents, and for the type of customers connected to the network (C1 - SFH or C2 - APT).

Block II - Estimation of harmonic phase angles

The balanced and unbalanced current phase angles ($\hat{\varphi}_{\mathrm{b}}^{(h)}$, $\hat{\varphi}_{\mathrm{u1}}^{(h)}$, $\hat{\varphi}_{\mathrm{u2}}^{(h)}$) are described with a von Mises distribution ($\mathcal{VM}$), which is a circular analogue of the normal distribution (the von Mises distribution is described in appendix B.1):

$$\begin{aligned}\varphi_{\mathrm{b}}^{(h)}(t) &= \mathcal{VM}(\mu_{\mathrm{b}}^{(h)}, \kappa_{\mathrm{b}}^{(h)}) \\ \varphi_{\mathrm{u1}}^{(h)}(t) &= \mathcal{VM}(\mu_{\mathrm{u1}}^{(h)}, \kappa_{\mathrm{u1}}^{(h)}) \\ \varphi_{\mathrm{u2}}^{(h)}(t) &= \mathcal{VM}(\mu_{\mathrm{u2}}^{(h)}, \kappa_{\mathrm{u2}}^{(h)})\end{aligned} \tag{5.11}$$

The parameters μ_X and κ_X represent the mean direction and the dispersion of the phase angles respectively. Each parameter is described with normal distribution functions $\mathcal{N}(N_\mu, N_\sigma)$, with mean N_μ and variance N_σ.

Block III - Transformation to phase currents

The symmetrical current phasors ($\underline{\hat{I}}_{\mathrm{b}}^{(h)}$, $\underline{\hat{I}}_{\mathrm{u1}}^{(h)}$, $\underline{\hat{I}}_{\mathrm{u2}}^{(h)}$) are obtained with the estimated balanced and unbalanced current magnitudes and phase angles:

$$\begin{aligned}\underline{\hat{I}}_{\mathrm{b}}^{(h)}(t) &= \hat{I}_{\mathrm{b}}^{(h)}(t) \angle \hat{\varphi}_{\mathrm{b}}^{(h)}(t) \\ \underline{\hat{I}}_{\mathrm{u1}}^{(h)}(t) &= \hat{I}_{\mathrm{u1}}^{(h)}(t) \angle \hat{\varphi}_{\mathrm{u1}}^{(h)}(t) \\ \underline{\hat{I}}_{\mathrm{u2}}^{(h)}(t) &= \hat{I}_{\mathrm{u2}}^{(h)}(t) \angle \hat{\varphi}_{\mathrm{u2}}^{(h)}(t)\end{aligned} \tag{5.12}$$

Finally, the symmetrical current phasors are transformed to obtain the harmonic current phasors of the three line conductors as:

$$\begin{bmatrix} \hat{\underline{I}}_{\mathrm{A}}^{(h)}(t) \\ \hat{\underline{I}}_{\mathrm{B}}^{(h)}(t) \\ \hat{\underline{I}}_{\mathrm{C}}^{(h)}(t) \end{bmatrix} = \underline{\mathbf{T}}_{120} \cdot \mathbf{P}^{-(h+2)} \cdot \begin{bmatrix} \hat{\underline{I}}_{\mathrm{b}}^{(h)}(t) \\ \hat{\underline{I}}_{\mathrm{u1}}^{(h)}(t) \\ \hat{\underline{I}}_{\mathrm{u2}}^{(h)}(t) \end{bmatrix} \tag{5.13}$$

where the matrix $\underline{\mathbf{T}}_{120}$ is the transformation matrix used to calculate the symmetrical components (Fortescue transformation)[65]. The matrix $\mathbf{P}$ is a permutation matrix that reorganizes the symmetrical current phasors according to the harmonic order, as defined in appendix B.2.

Table 5.1 lists the parameters of the stochastic model. Each of the parameters is estimated with measurements of the low-voltage networks. The following section explains in detail the estimation procedure of each parameter.

Table 5.1.: List of the parameters of the model

		$\hat{\underline{I}}_{\mathrm{b}}$	$\hat{\underline{I}}_{\mathrm{u1}}$	$\hat{\underline{I}}_{\mathrm{u2}}$
Magnitude	Normalized value	$FC_0, FC_1, FC_2, FC_3,$ $\theta_1, \theta_2, \theta_3, \alpha_{\mathrm{b}}, \sigma_{\mathrm{b}}$	$K_{\mathrm{u}}, \alpha_{\mathrm{u}}, \sigma_{\mathrm{u}}$	
	Scaling	$s_{\mathrm{b},1}, s_{\mathrm{b},2}$	$s_{\mathrm{u1},1}, s_{\mathrm{u1},2}$	$s_{\mathrm{u2},1}, s_{\mathrm{u2},2}$
Phase angle		$\mu_{\mathrm{b}}, \kappa_{\mathrm{b}}$	$\mu_{\mathrm{u1}}, \kappa_{\mathrm{u1}}$	$\mu_{\mathrm{u2}}, \kappa_{\mathrm{u2}}$

5.2. Model parametrization

Using the measurements of the different residential networks (sites), the parameters of the stochastic model were estimated. Fig. 5.3 shows the main steps for the parametrization, and the link between the parametrization procedure and the model blocks introduced in the previous section.

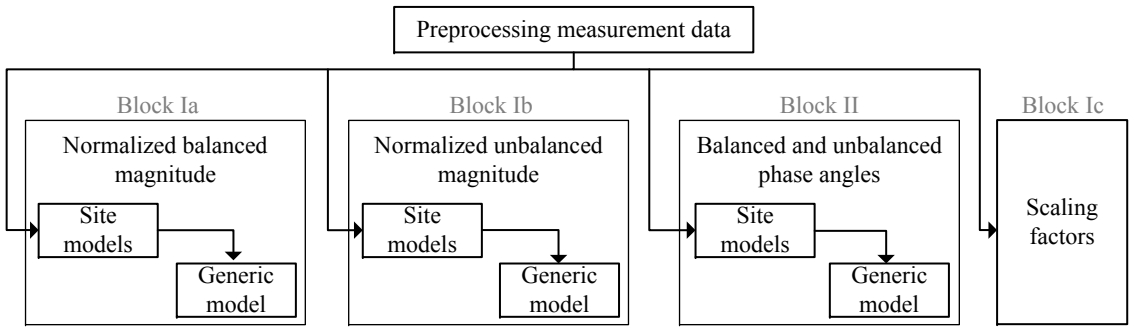

Figure 5.3.: Sumarized procedure for model parametrization

Initially, the measured harmonic magnitudes and phase angles of different residential low-voltage networks are normalized and transformed into symmetrical components (preprocessing). Then, the described model is fitted to each of the sites (site models). The following parameters are obtained for each site i :

- Normalized balanced magnitude: $FC_{0,i},\ FC_{1,i},\ FC_{2,i},\ FC_{3,i},\ \theta_{1,i},\ \theta_{2,i}, \theta_{3,i},\ \alpha_{\mathrm{b},i},\ \sigma_{\mathrm{b},i}$
- Normalized unbalanced magnitudes: $K_{\mathrm{u1},i},\ \alpha_{\mathrm{u1},i},\ \sigma_{\mathrm{u1},i},\ K_{\mathrm{u2},i},\ \alpha_{\mathrm{u2},i},\ \sigma_{\mathrm{u2},i}$
- Balanced and unbalanced phase angles: $\mu_{\mathrm{b},i},\ \kappa_{\mathrm{b},i},\ \mu_{\mathrm{u1},i},\ \kappa_{\mathrm{u1},i},\ \mu_{\mathrm{u2},i},\ \kappa_{\mathrm{u2},i}$

In a third step, the parameters of the generic model are obtained through the comparison of the model parameters of the sites. The following parameters are obtained:

- Normalized balanced magnitude: $FC_0,\ FC_1,\ FC_2,\ FC_3,\ \theta_1,\ \theta_2, \theta_3,\ \alpha_\mathrm{b},\ \sigma_\mathrm{b}$
- Normalized unbalanced magnitudes: $K_\mathrm{u},\ \alpha_\mathrm{u},\ \sigma_\mathrm{u}$
- Balanced and unbalanced phase angles: $\mu_\mathrm{b},\ \kappa_\mathrm{b},\ \mu_\mathrm{u1},\ \kappa_\mathrm{u1},\ \mu_\mathrm{u2},\ \kappa_\mathrm{u2}$

Finally, the relation between the number and type of customers with the balanced and unbalanced current magnitudes is obtained. The relation allows the scaling of the normalized balanced and unbalanced magnitudes of the generic model (Block Ic in Fig. 5.2). The parameters $s_\mathrm{b,1}$, $s_\mathrm{b,2}$, $s_\mathrm{u1,1}$, $s_\mathrm{u1,2}$, $s_\mathrm{u2,1}$ and $s_\mathrm{u2,2}$ are obtained.

The result of the parametrization of the generic model based on the measurements of German low-voltage networks is presented below.

5.2.1. Preprocessing of measurements

The measured harmonic magnitudes and phase angles of each site were preprocessed for the modeling. The preprocessing consists of three steps:

1. The measured harmonic currents of each site are transformed into symmetrical components.
2. The obtained harmonic balanced and unbalanced current magnitudes are normalized based on a min-max normalization (see appendix B.3), in order to adjust all measurements to the range [0,1], and eliminate the scaling produced by the number of customers.
3. The measurements of each site are separated in two parts, one for model fitting (5 days), and other for model verification (3 days).

5.2.2. Normalized balanced magnitude

Parametrization of each residential site

The normalized balanced magnitude comprises two components, a deterministic and a stochastic component (c.f. equation 5.1). The parameters of the deterministic component are obtained with the Fourier transform of the normalized balanced harmonic magnitude of each site. The parameters of the stochastic component are obtained with the residuals between the original values and the calculated deterministic component. Fig. 5.4 shows exemplary the original data (normalized balanced magnitude), the estimated deterministic component $\underline{I}^{(3)}_{\mathrm{b\ norm\ D}}(t)$ and the obtained residuals of the third harmonic of one site. For this example, the obtained deterministic and stochastic components are:

$$\underline{I}^{(3)}_{\mathrm{b\ norm\ D}}(t) = 0.35 + 0.32 \cdot \cos(2\pi \cdot f_\mathrm{D} \cdot t + 67^\circ) + 0.15 \cdot \cos(4\pi \cdot f_\mathrm{D} \cdot t + 86^\circ) + 0.05 \cdot \cos(6\pi \cdot f_\mathrm{D} \cdot t + 110^\circ)$$

$$\underline{I}^{(3)}_{\mathrm{b\ norm\ R}}(t) = 0.95 \cdot \underline{I}^{(3)}_{\mathrm{b\ norm\ R}}(t-1) + \mathcal{N}(0\,,\,0.00029) \tag{5.14}$$

The deterministic component is described with the first four components (including the constant component) of the Fourier series. The number of components was selected based on an iterative procedure, where the number of components was increased step by step until the mean squared error between the original time-series and the deterministic component had a

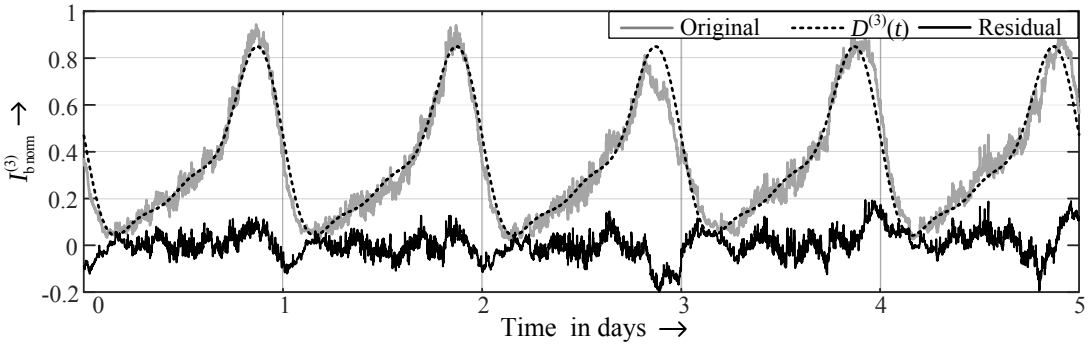

Figure 5.4.: Example model fitting of one site

difference of less than 5%. The iterative procedure was applied to each site and each harmonic order, and the final selected number of components is the number of components that describes most of the sites and most of the harmonic orders appropriately.

The stochastic component is described with an autoregressive model of first order, which is fitted to the residuals of each site using maximum likelihood estimation [23]. The autoregressive model was selected based on the autocorrelation function (ACF) and the partial autocorrelation function (PACF) of the residuals of each site and each harmonic order. Fig. 5.5 shows exemplary the ACF and PACF of the residuals of the example in Fig. 5.4. In this case, the ACF decays exponentially and the PACF has only one statistically significant spike at lag 1, which is the typical behavior of an autoregressive model of first order [110]. Similar graphs were obtained for each harmonic order and each site, and the autoregressive model of first order is selected as it is the best representation in most of the cases. Simple probability distributions are not recommended to describe the residuals, because they are not able to represent the dependence between successive values, a characteristic that should not be neglected with this type of data.

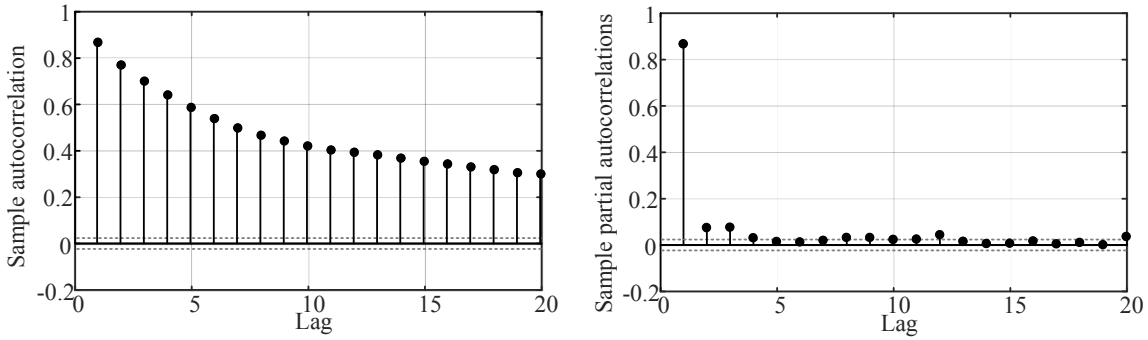

(a) ACF (b) PACF

Figure 5.5.: Autocorrelation function and partial autocorrelation of the residuals of one site

The adequacy of the model to represent the normalized balanced magnitudes of each site is evaluated comparing the time-series and the probability distributions of the measured (dataset for modeling verification) and estimated data (data obtained with the model). The time-series are compared visually using time-series plots and the similarity measures introduced in section 4.4. The probability distributions are compared using Q-Q plots, which compare the quantiles of the original and estimated data sets, and if they come from the same distribution, then the Q-Q plot appears linear. Fig. 5.6 shows the time-series plots and the Q-Q plot of the example in Fig. 5.4. Both graphs show a very good similarity between the original and estimated data. Moreover, the Euclidean distance $DM_{\text{E}} = 5.78$ and Pearson's correlation coefficient

$SM_{\mathrm{P}} = 0.99$ indicate a very good similarity between real and estimated time-series, validating the model for this specific site.

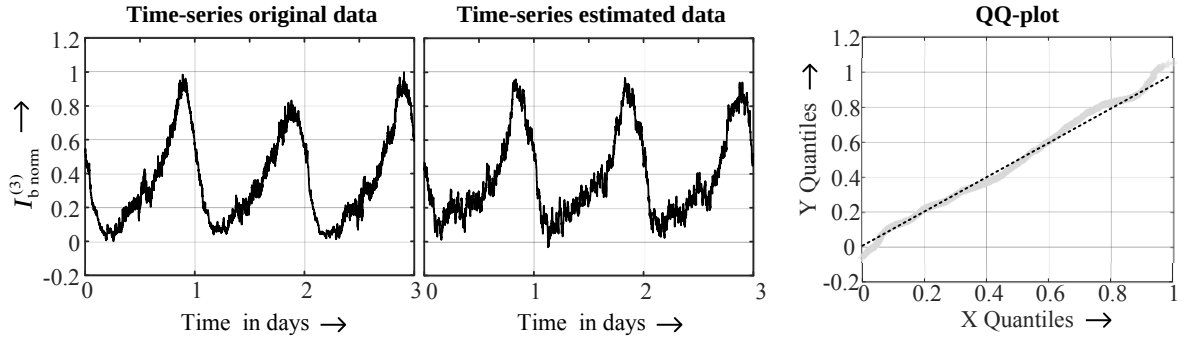

Figure 5.6.: Model evaluation results of one site, third harmonic, balanced component magnitude.

Here it is important to clarify, that the objective is to develop a generic model which is able to represent the behavior of typical residential sites, and not to develop accurate models of each site. In this case, approximate models of the sites are developed, which later can be compared to develop the generic model. For that reason, the number of Fourier coefficients and the order of the autoregressive model were fixed for all site models. Moreover, the models of each site can not be severally evaluated using formal fitting evaluation criteria or probabilistic tests, and the adequacy of the model can only be assessed by visual comparison of the time series and the probability functions.

Table 5.2 indicates the percentage of sites for which the model gives accurate results. The best results are obtained for the third, fifth and ninth harmonics, where more than 70% of the sites were correctly modeled. For the 13$^{\mathrm{th}}$ harmonic, only 19% of the sites could be correctly modeled with the time-series representation. This results are comparable with the time-series characterization presented in section 4.4. Comparing Table 5.2 with Fig. 4.14, it is clear that the model is successful only if the harmonic currents show a clear time-series. In general, the selected model can represent the harmonic behavior of the balanced harmonic magnitude of most residential sites. However, there are sites were there is no time-series, and the model may be not appropriate in those cases. To improve the model, first the characteristics of residential networks that lead to a time-series characteristic in the harmonic currents should be wholly comprehended, in order to define corresponding modeling methodologies for the sites where the time-series approach is not adequate.

Table 5.2.: Percentage of sites for which the time-series representation of $I^{(h)}_{\mathrm{b}}$ is adequate

	Harmonic order						
	3	5	7	9	11	13	15
Percentage of sites	97%	70%	55%	76%	49%	19%	51%

Parametrization of the generic model

The parameters of the models of the sites of the normalized balanced component are compared in order to determine the parameters of the generic model. Fig. 5.7 shows exemplary the comparison of the parameters $FC_{1,i}$ and $\theta_{1,i}$ of each of the sites, where a good similarity between the parameters of the sites is noticeable. For the comparison, only the results of the sites where the time series was successful are considered. Good similarity was also found for the other parameters of the deterministic component, which indicates a similar time-series between the

different sites. This result is also comparable with the time-series characterization made in the previous chapter (c.f. Table 4.1).

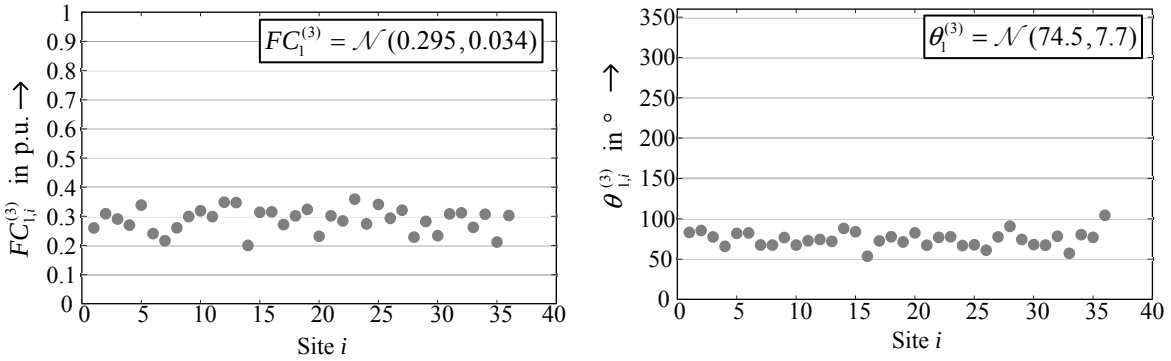

(a) Parameter $FC_1^{(3)}$ (b) Parameter $\theta_1^{(3)}$

Figure 5.7.: Comparison parameters $FC_{1,i}^{(3)}$ and $\theta_{1,i}^{(3)}$ and estimation of the parameters of the generic model

Normal distribution functions are selected to represent the parameters of the generic model, in such a way that the differences between different networks are also considered. For example, the parameter $FC_1^{(3)}$ of the generic model is a normal distribution of mean 0.295 and standard deviation 0.034, and the parameter $\theta_1^{(3)}$ is a normal distribution of mean $74.5°$ and standard deviation $7.7°$, as shown in Fig. 5.7. The mean and standard deviation of the normal distribution of each parameter are obtained by distribution fitting of the results of the different sites.

A correlation analysis between the parameters revealed that the parameters of the stochastic component, i.e. α_b and σ_b, are highly correlated, and the correlation is almost the same for all harmonic orders. Fig. 5.8b shows the correlation between $\sigma_{\mathrm{b}}^{(h)}$ and $\alpha_{\mathrm{b}}^{(h)}$ for all considered harmonic orders ($h = 3, 5, ..., 15$). The correlation between both parameters can be described with a linear regression. In this way, the parameter $\alpha_{\mathrm{b}}^{(h)}$ is described with a normal distribution for each harmonic order, while the parameter $\sigma_{\mathrm{b}}^{(h)}$ is obtained with the regression. Fig. 5.8a shows exemplary the comparison of $\alpha_{\mathrm{b}}^{(3)}$ and its corresponding normal distribution

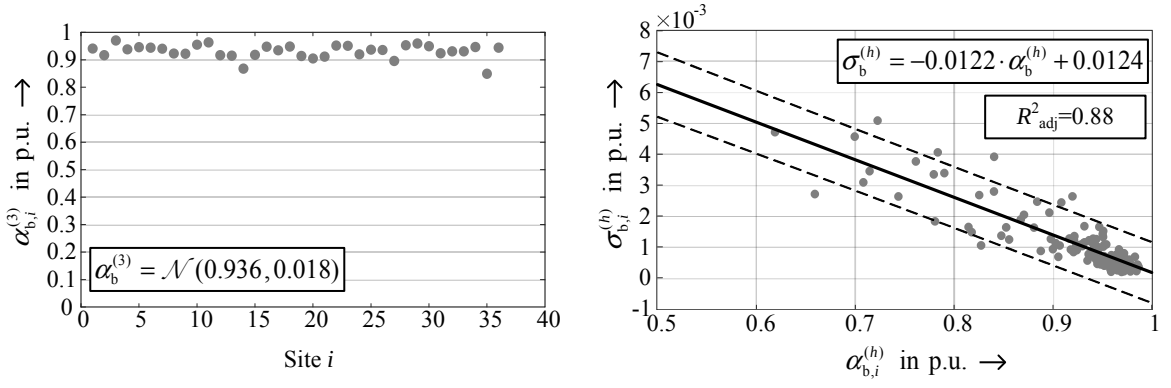

(a) Parameter $\alpha_{\mathrm{b}}^{(3)}$ (b) Correlation $\alpha_{\mathrm{b},i}^{(3)}$ and $\sigma_{\mathrm{b},i}^{(3)}$

Figure 5.8.: Comparison parameters $\alpha_{\mathrm{b},i}^{(3)}$ and $\sigma_{\mathrm{b},i}^{(3)}$ and estimation of the parameters for the generic model

The mean and standard deviation of the normal distribution of each parameter of the generic model, including their confidence intervals, are listed in appendix C.

5.2.3. Normalized unbalanced magnitudes

Parametrization of each residential site

Different modeling techniques were applied to represent the random behavior of the unbalanced magnitudes, including time-series approximation and mixture distribution fitting. However, the final result of the stochastic model, i.e. the resulting phase currents, did not improve considerably with the accuracy in the representation of the unbalanced magnitudes. The reason is that the behavior of the phase currents is mainly determined by the behavior of the balanced component, and the ratio between the balanced and unbalanced components. For this reason, the model of the unbalanced magnitudes was selected in order to have a good approximation of the random behavior of the unbalanced magnitudes, but keeping the model as simple as possible to reduce the amount of parameters of the generic model.

The normalized unbalanced magnitudes are modeled with autoregressive models of first order with three parameters (c.f. equation 5.3). The procedure to select the model and calculate the model parameters of each site is similar as the procedure used for the stochastic component of the normalized balanced magnitude explained before, but in this case, for each site i and each harmonic order, six parameters are obtained: $K^{(h)}_{\mathrm{u1},i}$, $K^{(h)}_{\mathrm{u2},i}$, $\alpha^{(h)}_{\mathrm{u1},i}$, $\alpha^{(h)}_{\mathrm{u2},i}$, $\sigma^{(h)}_{\mathrm{u1},i}$ and $\sigma^{(h)}_{\mathrm{u2},i}$.

Fig. 5.9 compares exemplary the first unbalanced component of the third harmonic of one site during three consecutive days (original data) with the data estimated with its corresponding AR model. The calculated autoregressive model has the parameters $K^{(3)}_{\mathrm{u1},i} = 0.03$, $\alpha^{(3)}_{\mathrm{u1},i} = 0.93$ and $\sigma^{(3)}_{\mathrm{u1},i} = 0.0034$. Comparing the original and estimated data it is clear that the model cannot represent exactly the daily variation of the unbalanced magnitudes, but, as mentioned before, a high detailed representation of the unbalanced magnitudes is not required. The Q-Q-plot of Fig. 5.9 shows that the autoregressive model gives an approximated representation of the unbalanced magnitude.

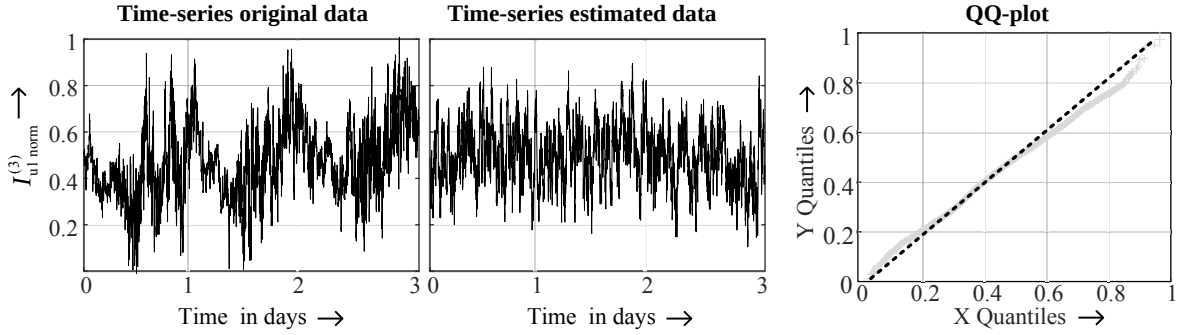

Figure 5.9.: Model evaluation results of one site, third harmonic, first unbalanced component magnitude.

Parametrization of the generic model

The model parameters of the sites are then compared in order to determine the parameters of the generic model. Fig. 5.10 compares the boxplots of the parameters obtained for all sites. As can be seen, the parameters for the first and second unbalanced components and the different harmonic orders have similar values. Therefore, the model of the normalized unbalance magnitudes can be simplified as following:

$$\begin{aligned} I^{(h)}_{\mathrm{u1\ norm}}(t) &= K_{\mathrm{u}} + \alpha_{\mathrm{u}} \cdot I^{(h)}_{\mathrm{u1\ norm}}(t-1) + \mathcal{N}(0, \sigma_{\mathrm{u}}) \\ I^{(h)}_{\mathrm{u2\ norm}}(t) &= K_{\mathrm{u}} + \alpha_{\mathrm{u}} \cdot I^{(h)}_{\mathrm{u2\ norm}}(t-1) + \mathcal{N}(0, \sigma_{\mathrm{u}}) \end{aligned} \tag{5.15}$$

The parameters K_{u}, α_{u} and σ_{u} are the same for all harmonic orders, and for the first and second normalized unbalanced magnitudes. Each of the parameters are estimated with the results of the models of each site, filtering first all outliers, i.e. sites that have a completely different behavior (outliers in the boxplots of Fig. 5.10). The parameter α_{u} is described with the following normal distribution:

$$\alpha_{\mathrm{u}} = \mathcal{N}(0.95, 0.22) \tag{5.16}$$

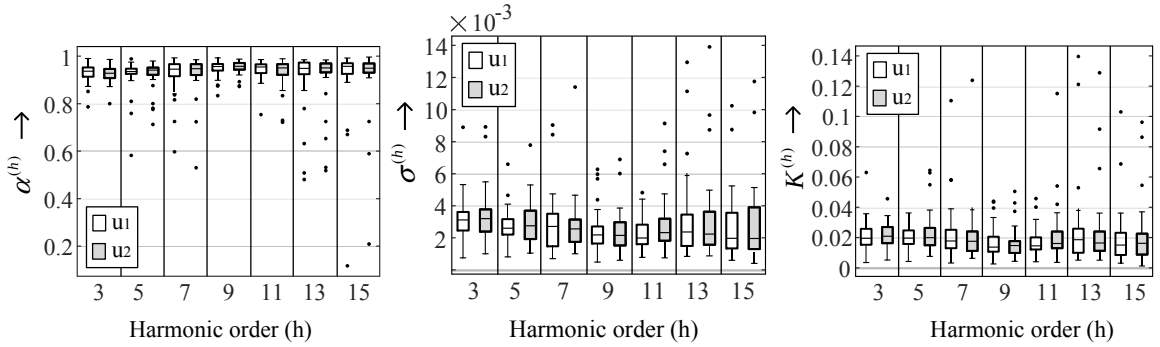

(a) $\alpha_{\mathrm{u1},i}^{(h)}$ and $\alpha_{\mathrm{u2},i}^{(h)}$ (b) $\sigma_{\mathrm{u1},i}^{(h)}$ and $\sigma_{\mathrm{u2},i}^{(h)}$ (c) $K_{\mathrm{u1},i}^{(h)}$ and $K_{\mathrm{u2},i}^{(h)}$

Figure 5.10.: Comparison of the site models parameters for the normalized first (u1) and second unbalanced (u2) magnitudes

The parameters K_{u} and σ_{u} are defined based on their correlation with the parameter α_{u}. Fig. 5.11 shows the correlation between the parameters obtained for all harmonic orders and the first and second unbalanced magnitudes.

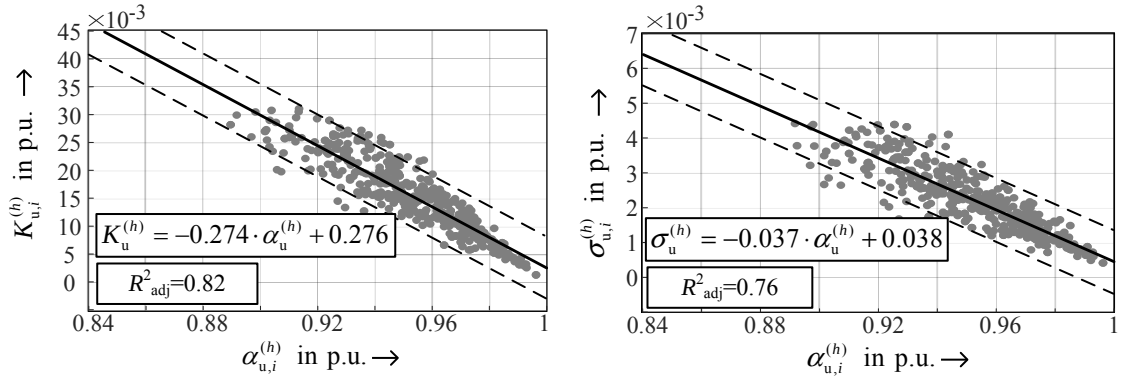

(a) Correlation $\alpha_{\mathrm{u}}^{(h)}$ and $K_{\mathrm{u}}^{(h)}$ (b) Correlation $\alpha_{\mathrm{u}}^{(h)}$ and $\sigma_{\mathrm{u}}^{(h)}$

Figure 5.11.: Correlation between the parameters $\alpha_{\mathrm{u}}^{(h)}$, $\sigma_{\mathrm{u}}^{(h)}$ and $K_{\mathrm{u}}^{(h)}$ of the AR model of the normalized unbalanced magnitudes

5.2.4. Balanced and unbalanced phase angles

Parametrization of each residential site

Balanced and unbalanced harmonic phase angles are represented with the von Mises distribution $\mathcal{VM}(\mu, \kappa)$, which can be considered as the analogue of the normal distribution for circular data. The von Mises distribution is a symmetric unimodal distribution, where μ is the mean direction of the phase angles, and κ indicates the concentration of the phase angles around the mean direction. The lower the value of κ, the more disperse are the phase angles in the complex plane. If $\kappa = 0$, the von Mises distribution resembles a uniform distribution in the interval

$[0°, 360°]$. Appendix B.1 contains more details about this distribution and some examples for different values of μ and κ.

The von Mises distribution is ideal to represent the behavior of both, balanced (high concentrated) and unbalanced (high dispersed) phase angles. Other distribution functions were also tested, but the von Mises distribution had the best fitting, especially in the representation of unbalanced phase angles. As example, Fig. 5.12 compares the PDFs (Q-Q plot) of the balanced and first unbalanced third harmonic phase angles of one exemplary site with two different approximations, one with a *t* location-scale distribution, and the other with a von Mises distribution. Both distributions can represent the balanced phase angles, but for the unbalanced phase angles, only the von Mises distribution gave accurate results. The *t* location-scale distribution, as well as the normal, logistic and other widely used distribution functions, are defined for linear-scaled data; therefore, those distributions are not adequate for the phase angles that are described in a circular scale.

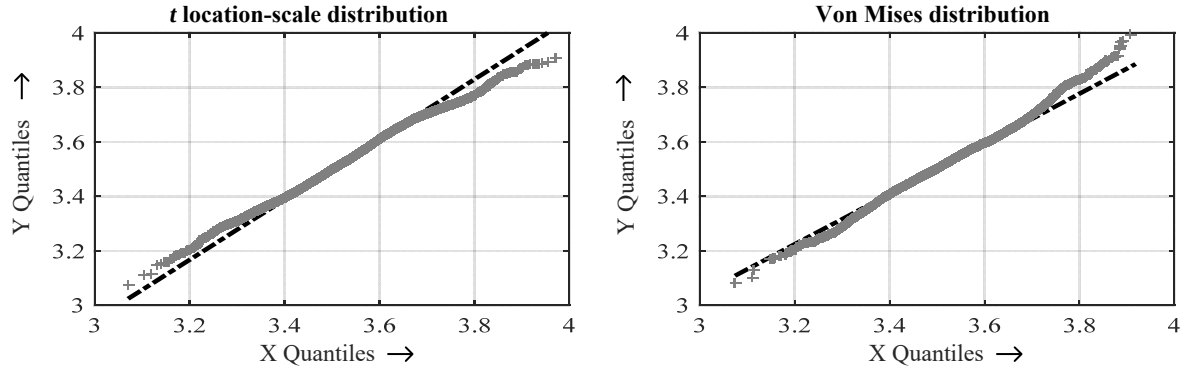

(a) First balanced phase angle $\varphi_{\mathrm{b}}^{(3)}$

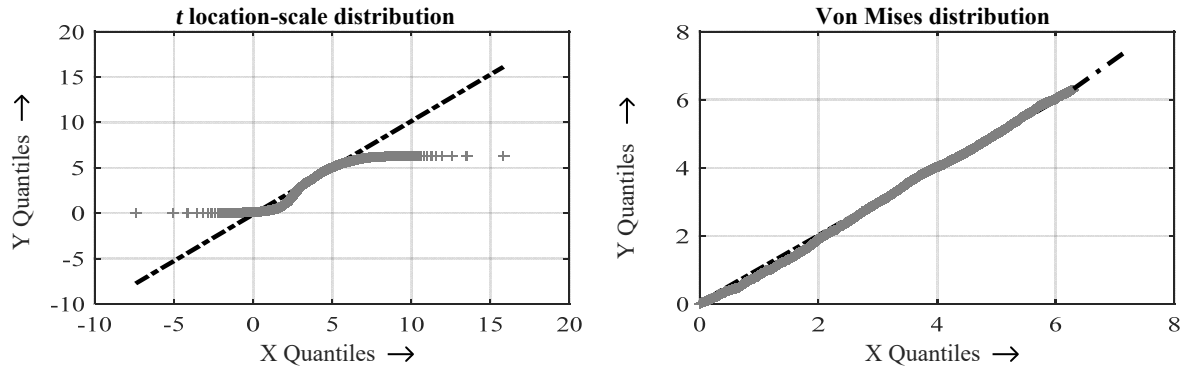

(b) Second unbalanced phase angle $\varphi_{\mathrm{u1}}^{(3)}$

Figure 5.12.: Q-Q plot of the balanced and first unbalanced third harmonic phase angles of one site fitted with a von Mises and t location-scale distribution

Parametrization of the generic model

The parameters of the von Mises distribution obtained of each site are compared to define the parameters for the generic model. Fig. 5.13 compares the values of μ and κ of the third harmonic for the balanced and first unbalanced phase angles. The balanced phase angles of all sites have similar value of $\mu_{\mathrm{b}}^{(3)}$ around 200° and a $\kappa_{\mathrm{b}}^{(3)}$ higher than 20, i.e. the phase angles are concentrated around the mean direction. On the other side, the comparison of $\mu_{\mathrm{u1}}^{(3)}$ and $\kappa_{\mathrm{u1}}^{(3)}$ shows that the unbalanced phase angles are closed to a uniform distribution (κ_{u1} close to zero)

where a common direction of the phase angles cannot be defined. Similar results were obtained for the other harmonic orders.

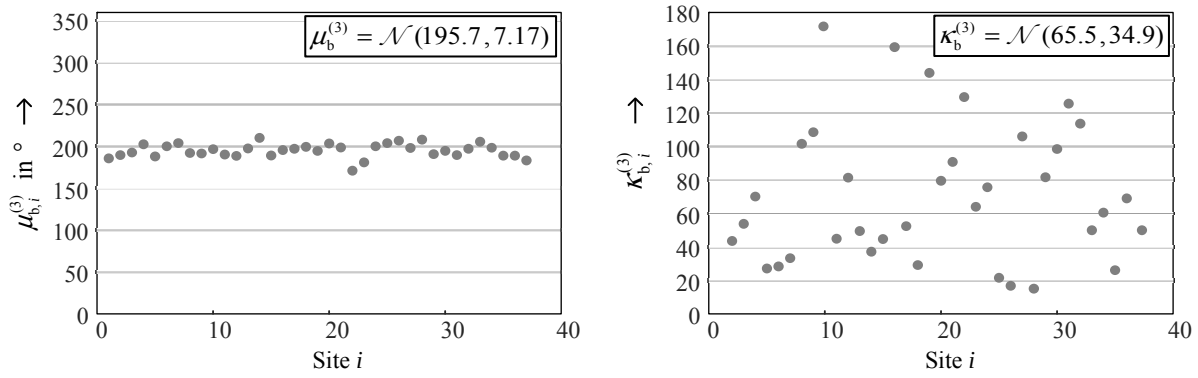

(a) Parameters $\mu_{\mathrm{b}}^{(3)}$ and $\kappa_{\mathrm{b}}^{(3)}$

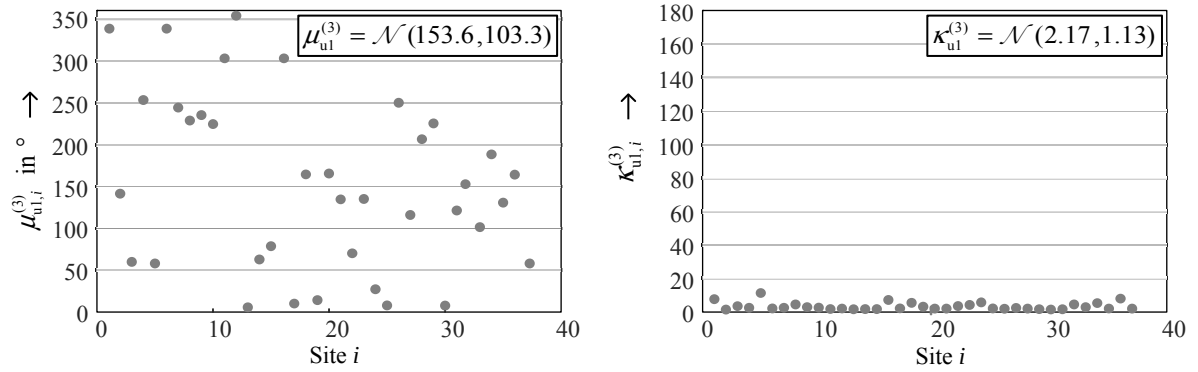

(b) Parameters $\mu_{\mathrm{u1}}^{(3)}$ and $\kappa_{\mathrm{u1}}^{(3)}$

Figure 5.13.: Comparison of the site models parameters for the third harmonic balanced and first unbalanced phase angles and estimation of the parameters for the generic model

The parameters μ and κ for each harmonic order and for the balanced, first unbalanced and second unbalanced phase angles are finally described with normal distribution functions that represent the different values of both parameters in typical residential networks. Fig. 5.13 contains the normal distribution of $\mu_{\mathrm{b}}^{(3)}$, $\kappa_{\mathrm{b}}^{(3)}$, $\mu_{\mathrm{u1}}^{(3)}$ and $\kappa_{\mathrm{u1}}^{(3)}$. Appendix C contains the normal distributions of the balanced and unbalanced phase angles for each harmonic order, including the corresponding confidence intervals.

5.2.5. Scaling

In order to estimate the harmonic currents of a specific network, it is necessary to scale first the normalized balanced and unbalanced harmonic magnitudes according to the number and type of customers in the network (c.f. Fig. 5.2). The scaling is determined with equation 5.6, which is repeated here for convenience:

$$\hat{I}_{\mathrm{b}}^{(h)}(t) = s_{\mathrm{b},1}^{(h)} \cdot \hat{I}_{\mathrm{b\,norm}}^{(h)}(t) + s_{\mathrm{b},2}^{(h)}$$
$$\hat{I}_{\mathrm{u1}}^{(h)}(t) = s_{\mathrm{u1},1}^{(h)} \cdot \hat{I}_{\mathrm{u1\,norm}}^{(h)}(t) + s_{\mathrm{u1},2}^{(h)}$$
$$\hat{I}_{\mathrm{u2}}^{(h)}(t) = s_{\mathrm{u2},1}^{(h)} \cdot \hat{I}_{\mathrm{u2\,norm}}^{(h)}(t) + s_{\mathrm{u2},2}^{(h)}$$

The scaling consists in reversing the initial min-max normalization (c.f. appendix B.3). Therefore, the parameters $s_{\mathrm{X},1}^{(h)}$ and $s_{\mathrm{X},2}^{(h)}$ (X denotes balanced b, first unbalanced $\mathrm{u1}$ and second unbalanced $\mathrm{u2}$ components) are related to the maximum and minimum balanced or unbalanced

currents of a network, which depend on the number and type of customers. Specifically, $s^{(h)}_{\mathrm{X},1}$ indicates the difference between the maximum and minimum balanced or unbalanced harmonic current, while $s^{(h)}_{\mathrm{X},2}$ corresponds to the minimum balanced or unbalanced harmonic current, that is:

$$s^{(h)}_{\mathrm{X},1} = I^{(h)}_{\mathrm{X},[\mathrm{max}]} - I^{(h)}_{\mathrm{X},[\mathrm{min}]} = I^{(h)}_{\mathrm{X},[\mathrm{max\text{-}min}]} \tag{5.17}$$

$$s^{(h)}_{\mathrm{X},2} = I^{(h)}_{\mathrm{X},[\mathrm{min}]} \tag{5.18}$$

In order to estimate the scaling parameters, the relation between the number of customers ($n_{\mathrm{u\ TOT}}$) and the maximum and minimum balanced and unbalanced harmonic magnitudes ($I^{(h)}_{\mathrm{X},[\mathrm{max}]}$, $I^{(h)}_{\mathrm{X},[\mathrm{min}]}$) of the measured low-voltage networks is analyzed. Fig. 5.14-a and 5.14-b show exemplary the relation between the minimum and maximum balanced current magnitude of the third harmonic with the number of customers for networks with SFH (customer configuration C1). There is a clear increasing tendency, which can be represented with a power function. The coefficient of determination R^2_{adj} indicates that the regression with a power function is a good regression in both cases. Moreover, there is also a linear regression among the difference between the maximum and minimum harmonic magnitude $I^{(3)}_{\mathrm{b},[\mathrm{max\text{-}min}]}$ and the maximum harmonic magnitude $I^{(3)}_{\mathrm{b},[\mathrm{max}]}$ as shown in Fig. 5.14-c. These relations coincide with the analysis presented in section 4.2 about the influence of the customer configuration on the harmonic magnitudes.

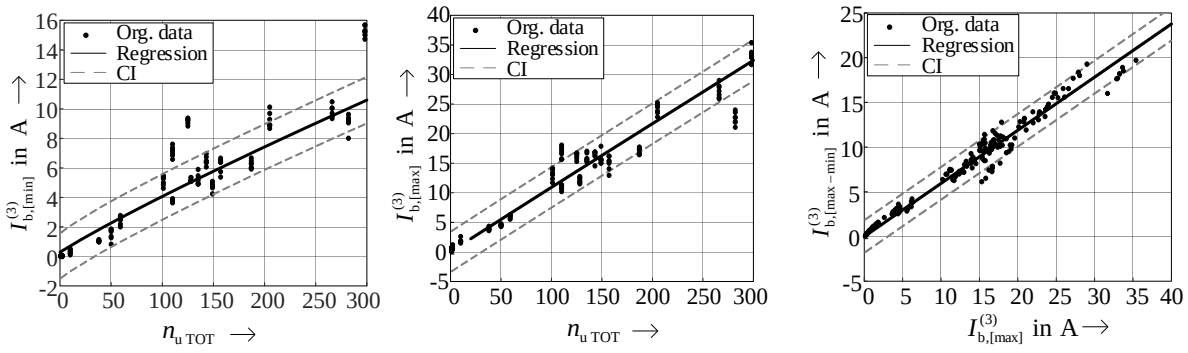

(a) $n_{\mathrm{u\ TOT}}$ and $I^{(3)}_{\mathrm{b},[\mathrm{min}]}$ (b) $n_{\mathrm{u\ TOT}}$ and $I^{(3)}_{\mathrm{b},[\mathrm{max}]}$ (c) $I^{(3)}_{\mathrm{b},[\mathrm{max}]}$ and $I^{(3)}_{\mathrm{b},[\mathrm{max\text{-}min}]}$

Figure 5.14.: Relation between the number of customers ($n_{\mathrm{u\ TOT}}$) and the maximum and minimum balanced harmonic magnitudes. CI: confidence intervals

Besides the data from the low-voltage networks, some measurements of individual customers and a small group of 10 customers were added to the analysis in order to have a better regression (see the original data of Fig. 5.14-a and Fig. 5.14-b for 1 and 10 customers). Those measurements were obtained from different residential customers living in SFH during 2 weeks in winter. The characteristics of those measurements are detailed in chapter 6 and reference [16].

The regression between maximum and minimum balanced and unbalanced harmonic magnitudes with the number of customers was obtained for each harmonic order. However, the regression of $I^{(h)}_{\mathrm{X},[\mathrm{min}]}$ with n_{u} is not accurate for all harmonic orders, especially for the 11$^{\mathrm{th}}$, 13$^{\mathrm{th}}$ and 15$^{\mathrm{th}}$ harmonics where R^2_{adj} was below 0.6. The regressions obtained with $I^{(h)}_{\mathrm{X},[\mathrm{max}]}$ are more accurate in all cases. For this reason, the scaling parameters are obtained based on the

regression with $I^{(h)}_{\mathrm{X},[\mathrm{max}]}$ as following:

$$s^{(h)}_{\mathrm{X},1} = I^{(h)}_{\mathrm{X},[\text{max-min}]} \tag{5.19}$$

$$s^{(h)}_{\mathrm{X},2} = I^{(h)}_{\mathrm{X},[\mathrm{max}]} - I^{(h)}_{\mathrm{X},[\text{max-min}]} \tag{5.20}$$

where:

$$I^{(h)}_{\mathrm{X},[\mathrm{max}]} = p \cdot (n_{\mathrm{u\ TOT}})^q \tag{5.21}$$

$$I^{(h)}_{\mathrm{X},[\text{max-min}]} = r \cdot I^{(h)}_{\mathrm{X},[\mathrm{max}]} \tag{5.22}$$

The values p, q, and r are different for each harmonic order, for the balanced and unbalanced currents, and for the type of customers connected to the network (C1 - SFH or C2 - APT). Those values are obtained with the corresponding correlations of equation 5.21 and 5.22, as illustrated in Fig. 5.14-b and Fig. 5.14-c. Appendix C contains the values of the parameters p. q and r for all cases, including their corresponding confidence intervals and the coefficient of determination R^2_{adj}. The power function of eq. 5.21 was selected for the fitting, as it is the best type of regression that fits all harmonic orders and the balanced and unbalanced components. In some cases a simple linear regression may be sufficient, but in order to have a more general model, the power function is used for all regressions.

Fig. 5.15 shows exemplary the coefficient of determination R^2_{adj} obtained in each regression of equations 5.21 and 5.22 for customers configuration C1 and C2 and for the balanced and first unbalanced currents.

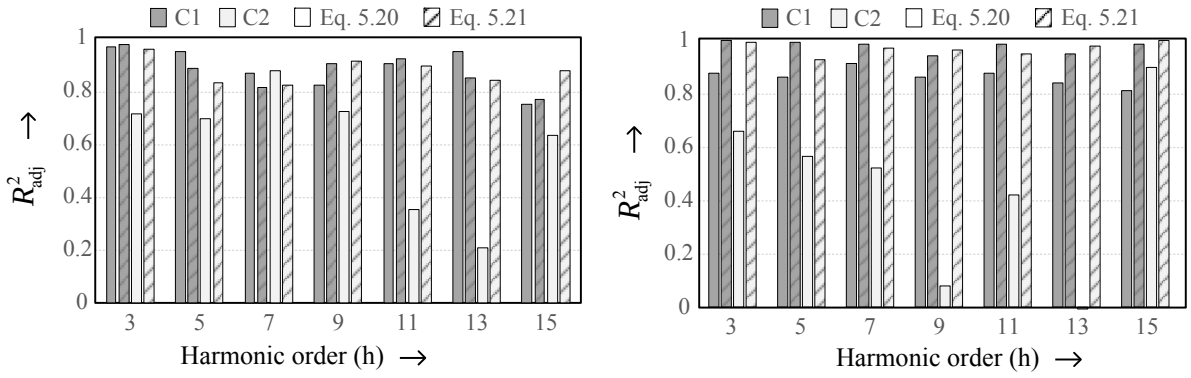

(a) Balanced component

(b) First unbalanced component

Figure 5.15.: Coefficient of determination R^2_{adj} obtained in the fitting of equation equation 5.21 and 5.22

Most regressions have a R^2_{adj} higher than 0.8, indicating a good regression between parameters. However, the regressions obtained for networks with customer configuration C2 are not as accurate as the regression for networks with customer configuration C1, especially for the 9$^{\mathrm{th}}$, 11$^{\mathrm{th}}$ and 13$^{\mathrm{th}}$ harmonics. This is caused by the higher variety of customers living in apartments in comparison with the customers living in SFH. While in SFH most of the customers are families with 3 to 5 members with a similar routine, customers living in apartments are more diverse, with different number of residents and different usage behaviors. Therefore, the measurements obtained in networks type C2 are more diverse than the measurements of networks C1, which results in a high uncertainty in the regression between the number of customers and the harmonic currents. A better regression can be obtained with a bigger database, where a clustering of the networks according to the level of harmonic emission may be applied. This idea was already introduced in [16], and it is recommended here to improve the regression and model of the different types of networks, especially networks with mainly MFH.

5.3. Model validation

The stochastic model of low-voltage residential networks is validated comparing data estimated with the model with measurements of real networks. As the parameters of the model are obtained with normal distribution functions, the output of the stochastic model is not an unique output but a set of possible outcomes, i.e. the possible daily harmonic current magnitudes and phase angles of typical residential networks with certain number and type of customers. Therefore, for the model validation, a set of 100 different harmonic current magnitudes and phase angles are randomly generated for networks with different number and types of customers. Table 5.3 summarizes the different cases created for networks with customer configuration C1 and C2.

Table 5.3.: Simulation cases for model verification

	Customer configuration C1									
Case	1	2	3	4	5	6	7	8	9	10
$n_{\mathrm{u\ TOT}}$	30	60	90	120	150	180	210	240	270	300

	Customer configuration C2									
Case	11	12	13	14	15	16	17	18	19	20
$n_{\mathrm{u\ TOT}}$	120	180	240	300	360	420	480	540	600	660

Fig. 5.16 exemplary shows the comparison of the CDFs of the 100 randomly generated third harmonic currents of case 2 (grey lines) and the CDF of the measured third harmonic currents (black lines, 1 CDF per line conductor) of a residential network with 60 SFH. The measured harmonic magnitudes and phase angles are well represented by the model. As expected, the estimated magnitudes and phase angles vary in a wide range because the stochastic model represents the behavior of different residential networks.

The time-series of the harmonic magnitudes is also well represented by the model. Fig. 5.17 compares the time-series plot of the measured third harmonic of one line conductor, and one of the estimated third harmonic currents of the residential network in case 2. The model is able to represent the daily variation of harmonic magnitudes, where there is a lower emission during the night, and a higher emission during the evenings for the third harmonic. The figure also compares the polar plots of the measured and estimated data, where also a good match of the direction of the data cloud is noticeable.

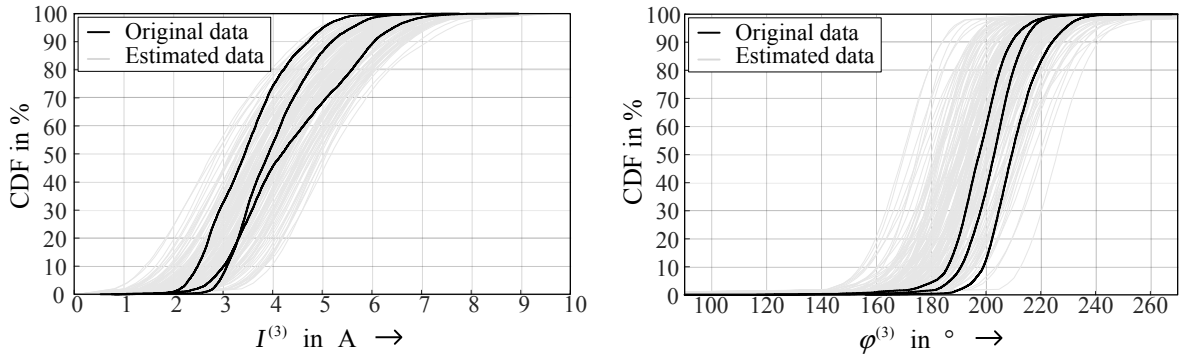

(a) Harmonic magnitude

(b) Harmonic phase angle

Figure 5.16.: CDFs of estimated and measured third harmonic for a network with 60 customers configuration C1.

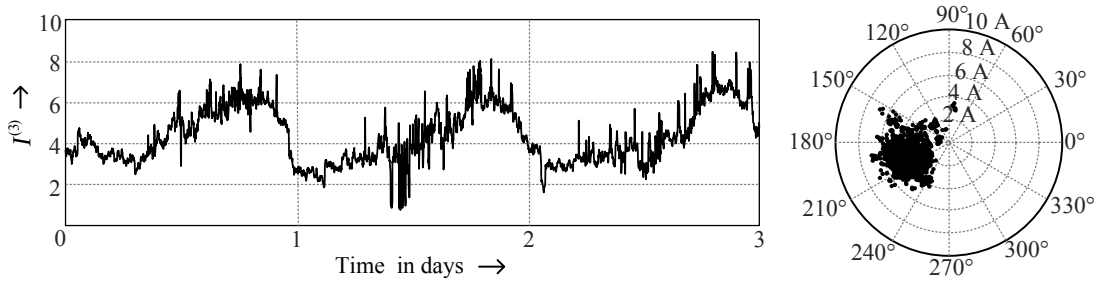

(a) Measured data

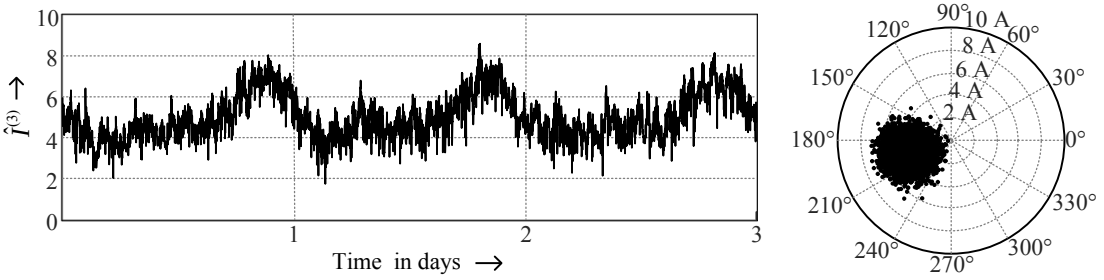

(b) Estimated data

Figure 5.17.: Third harmonic current of a residential site with 60 customers

In order to compare the results of all cases with the measurements of real networks, the statistics of magnitudes and phase angles selected in the previous chapter are used to compare the statistical characteristics of the measured and simulated data. Fig. 5.18 compares the statistics of harmonic magnitudes and phase angles of the third, fifth and seventh harmonics of the measurements (dots) and the simulations (bars) of networks with customer configuration C1. The bars represent the variation of the respective statistic for the 100 simulations of each case. The results of the other cases and other harmonic orders are included in appendix C. According to the results, the model is able to represent the statistical behavior of harmonic magnitudes and phase angles of most networks. The central tendency and variation of the simulated harmonic magnitudes increase with the number of customers as in real networks, and the simulated phase angles have a similar direction and dispersion as the measured data. There are some real networks that are not properly represented by the model because those networks have a significantly different harmonic emission in comparison with other networks. Those differences may be caused by seasonal effects that are not included in the model, the presence of other non-residential customers, or specific networks characteristics, as the presence of resonances.

Looking at the results of the model verification of all harmonics, it is noticed that the model hat more inaccuracies in the modeling of the 13$^{\text{th}}$ and 15$^{\text{th}}$ harmonics. As discussed before, the randomness of harmonic magnitudes and phase angles increases with the harmonic order, and there are higher differences in the behavior of the 13$^{\text{th}}$ and 15$^{\text{th}}$ harmonics between residential networks, which makes the developing of a generic model more difficult. However, the presented model gives a good approximation of the magnitudes and phase angles of the 13$^{\text{th}}$ and 15$^{\text{th}}$ harmonics present in most networks.

Finally, the unbalance of harmonic currents of the proposed model is also compared with the real harmonic unbalance of low-voltage networks. For this verification, the 95$^{\text{th}}$ percentile of the aggregate harmonic unbalance factor ($AHU^{(h)}$) of the estimated and measured data are compared. Fig. 5.19 shows the comparison for the third, fifth and seventh harmonics, and appendix C contains the comparison for the other harmonic orders. In all cases, the model shows very good response, indicating that the proposed method is also able to represent the harmonic unbalance of residential networks.

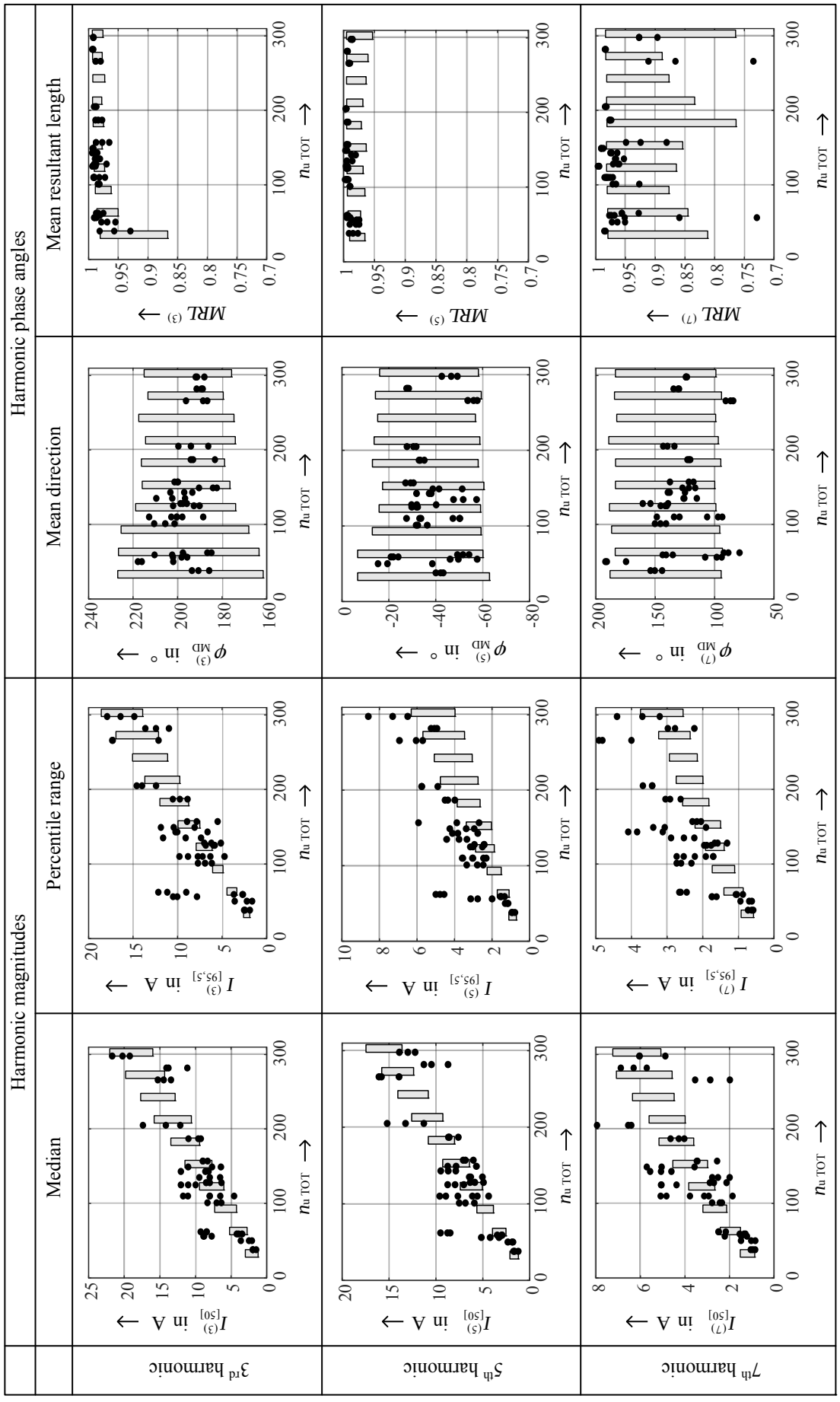

Figure 5.18.: Comparison of the different statistics of harmonic magnitudes and phase angles obtained with measurements of residential networks (points) and estimated data (grey bar)

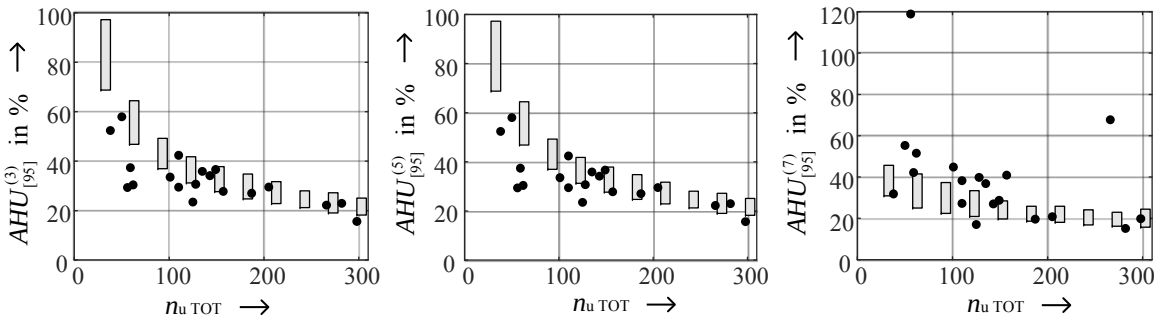

(a) Third harmonic (b) Fifth harmonic (c) Seventh harmonic

Figure 5.19.: Comparison of the 95$^{\text{th}}$ percentile of the AHU factors obtained with measurements of residential networks (points) and estimated data (grey bar)

5.4. Chapter summary

A stochastic model of residential low-voltage networks was developed using a measurement based approach. Different to other approaches, this model is based on the representation of the symmetrical components of the harmonic currents, which allows the representation of not only the behavior of harmonic magnitudes and phase angles, but also the harmonic unbalance, which is of great importance for accurate simulation of medium-voltage networks.

The model is summarized in Fig. 5.2, where three estimation blocks are identified: estimation of balanced and unbalanced harmonic magnitudes (Block I), estimation of balanced and unbalanced harmonic phase angles (Block II), and transformation to phase currents (Block III). The balanced current magnitude is represented with a stochastic time-series model, while the normalized unbalanced magnitudes are described with autoregressive models. The balanced and unbalanced phase angles are represented with von Mises distributions. Once the symmetrical components are estimated, the harmonic phase currents are calculated applying the Fortescue transform. The model takes into account the differences between harmonic orders and the scaling of harmonic magnitudes with the number and type of customers in the network.

The parameters of the model were estimated using the measurements of German residential low-voltage networks, but the parametrization procedure can be applied to get the parameters of the model for other regions with different electrical and non-electrical environment.

The stochastic model was finally validated comparing the output of the model with several measurements of real low-voltage networks. The model gave satisfactory results, where the variation of harmonic magnitudes and phase angles and the harmonic unbalanced of residential networks is properly represented.

6. Model of aggregate residential customers

Models of small number of customers (feeder, feeder section) that represent also the daily variation of harmonic magnitudes and phase angles are required for different kinds of analyses of low-voltage networks (c.f. Table 2.1). There are different ways to obtain models of aggregate residential customers, being the component-based approach the most applied modeling method, as discussed in chapter 3. However, it may be possible to obtain a model of aggregate customers based on a top-down approach, where the measurements of low-voltage networks are used as base for the modeling (c.f. Fig. 3.5). In this chapter, the top-down approach is applied to extend the stochastic model of low-voltage residential networks presented in the previous chapter in order to represent small groups of customers that can be used in simulations of low-voltage networks.

The model of low-voltage residential networks was developed on the basis that the harmonic current magnitudes have a clear daily pattern that can be modeled with time series techniques, and that the phase angles have a quasi-stationary behavior (no significant statistical changes in time) that can be modeled with uni-variate distribution functions. However, it is expected that the statistical characteristics of harmonic magnitudes and phase angles change for small aggregates of customers. For that reason, the first section of this chapter compares the harmonic emission of single customers and groups of customers and shows, how the variation of harmonic magnitudes and phase angles changes with the number of customers. Based on the characteristics of the harmonic current aggregation, the limitations of the time-series stochastic model are recognized and the limit of the amount of aggregate customers that can be modeled with the time-series stochastic model is defined.

The second section explains in detail how the top-down approach was applied to obtain the model of aggregate residential customers. Finally, the extended model is verified with measurements of real networks.

6.1. Aggregation process

Harmonic current emission of single residential customers is highly time-variant due to the continuous changes in load conditions (e.g. type and number of connected devices) and system parameters (e.g. voltage magnitude and voltage distortion). Fig. 6.1-a shows exemplary the third harmonic current emission of a family with four members living in a single family house for two consecutive days. The time series plot shows many sharp "needle peaks" of different size that appear when the family members connect different electric appliances or when the devices change their operation state. There are some appliances that are used during short periods of time, while others remain connected for several minutes or hours. Some devices have approximately constant harmonic emission, but many others have time-variable harmonic emission, e.g. due to their changing power consumption like computers and laptops. The devices are randomly distributed to the three phases, which results in a significant harmonic current unbalance at this point in the network. The polar plot shows that the high variation affects not only the harmonic magnitude, but also the harmonic phase angle. As expected, both days behave different with more activity during the evenings than in the mornings for this specific customer.

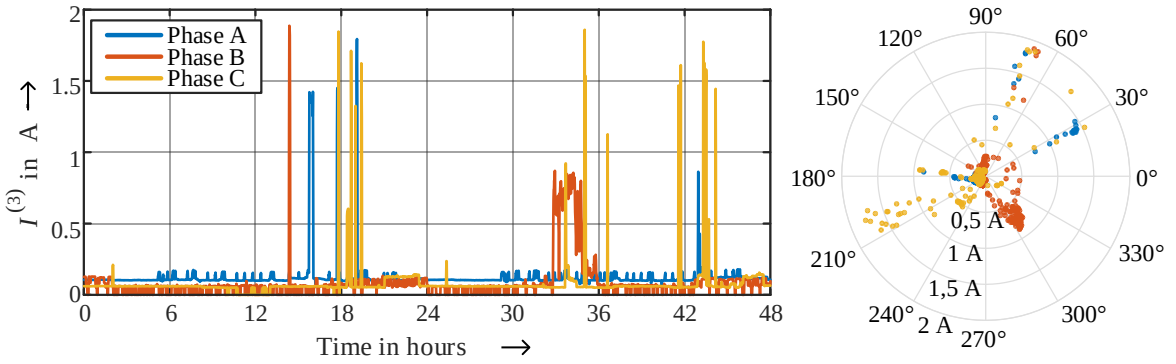

(a) Single customer

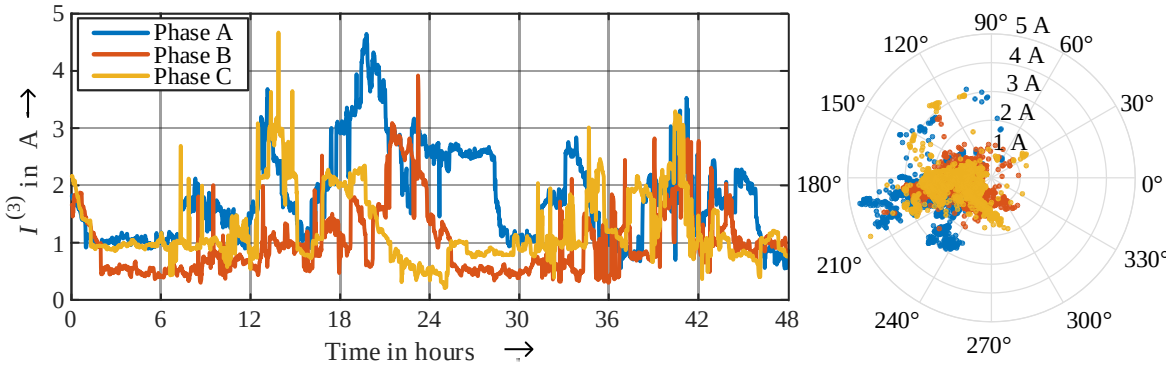

(b) 10 aggregate customers

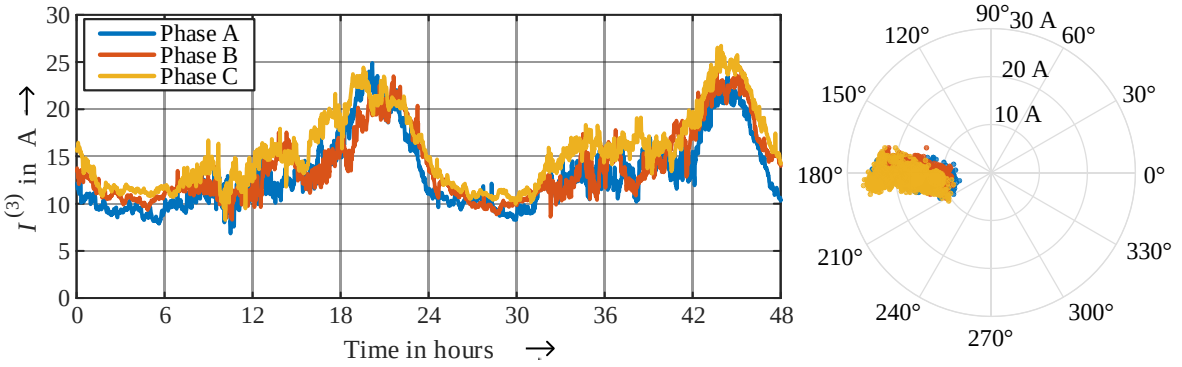

(c) 300 aggregate customers

Figure 6.1.: Third harmonic current emission of different amount of aggregate residential customers

Residential low-voltage distribution networks are composed by several customers, each with different number of electric devices and usage behavior, which results in different harmonic emission characteristics [16]. The harmonic current emission of the network is finally the result of the aggregation (phasor sum) of the erratic harmonic current emission of the customers connected thereto. Fig. 6.1-b and Fig. 6.1-c show the total third harmonic current emission of 10 and 320 aggregate customers respectively. Comparing the curves, it is clear that with the increase of customers the daily curve of the harmonic magnitudes becomes "smoother" and the harmonic phase angle reduces its diversity and concentrates more and more in one direction.

In order to understand better the aggregation process as well as the transition from virtually random behavior of single customers to the less varying, prevailing emission of multiple customers, an iterative simulation based on the measurements of single customers is developed. This simulation includes the identification of the minimum number of customers for which a "smooth" daily curve of harmonic magnitudes and a prevailing direction of harmonic phase

angles can be assumed, i.e. the minimum number of customers for which the stochastic model presented in the previous chapter is valid. Below is a summary of the most important results of the simulation, but the complete description of the simulation framework and results is available in [13].

6.1.1. Simulation framework

The simulation is based on the measurements of third and fifth harmonic currents of 16 different SFH. The details about the measurement procedure and measurement accuracy can be found in [16]. In total 450 different daily curves of harmonic magnitudes and phase angles during wintertime were selected (measurement during 150 days, 3 phases, 1 minute interval). Due to the accuracy of the measured currents, only the third and fifth harmonics are simulated.

Twelve cases were defined with different number of customers (N) as shown in Table 6.1. For each case, N different daily curves were selected randomly from the database and the total harmonic current emitted by the N customers was calculated using the phasor sum of the individual harmonic currents at each time instant. Line conductors are treated individually. Next, the statistics that represent the central tendency and variation of harmonic magnitudes and phase angles were calculated. The procedure was repeated 1000 times for each case and each line conductor. Fig. 6.2 presents a detailed flow chart of the procedure.

Table 6.1.: Simulation cases

Simulation case	1	2	3	4	5	6	7	8	9	10	11	12
Number of customers N	3	5	8	10	15	20	30	40	50	60	80	100

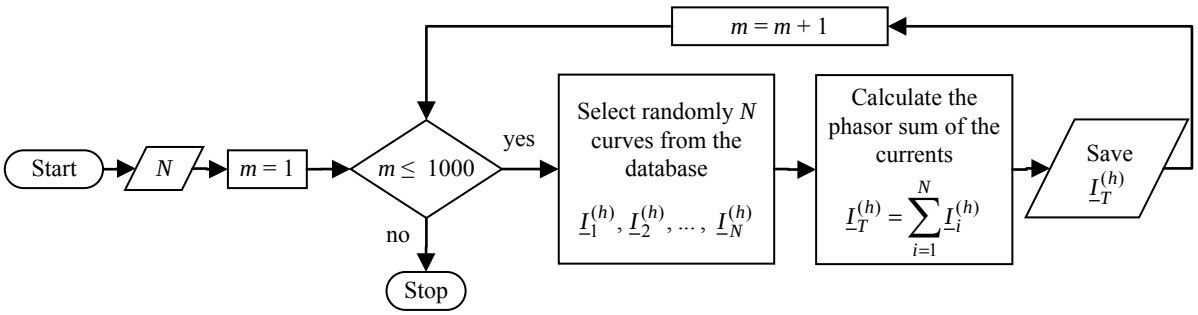

Figure 6.2.: Flow-chart of the implemented iterative simulation

The calculated statistics are the same as the ones used in the previous chapters to characterize harmonic magnitudes and phase angles, i.e. the median ($I_{[50]}^{(h)}$) and the percentile range ($I_{[95,5]}^{(h)}$) for harmonic magnitudes, and the mean direction ($\varphi_{\mathrm{MD}}^{(h)}$) and the mean resultant length ($MRL^{(h)}$) for harmonic phase angles. Moreover, the $AHU^{(h)}$ factors are calculated for each case to assess the change in the unbalance of harmonic currents depending on the amount of aggregate customers.

6.1.2. Simulation results

Fig. 6.3 shows the boxplots of the obtained statistics for each case and each line conductor for the third harmonic magnitudes and phase angles. As expected, the median and percentile range of the harmonic magnitudes increase with the number of customers, while the phase

angles show a lower dispersion an a more concentrate direction with the increase in the number of aggregate customers. From case 7 (30 customers and more) the mean resultant length is higher than 0.8, indicating a low variation of the harmonic phase angles. The analysis of the fifth harmonic gave similar results (c.f. [13]).

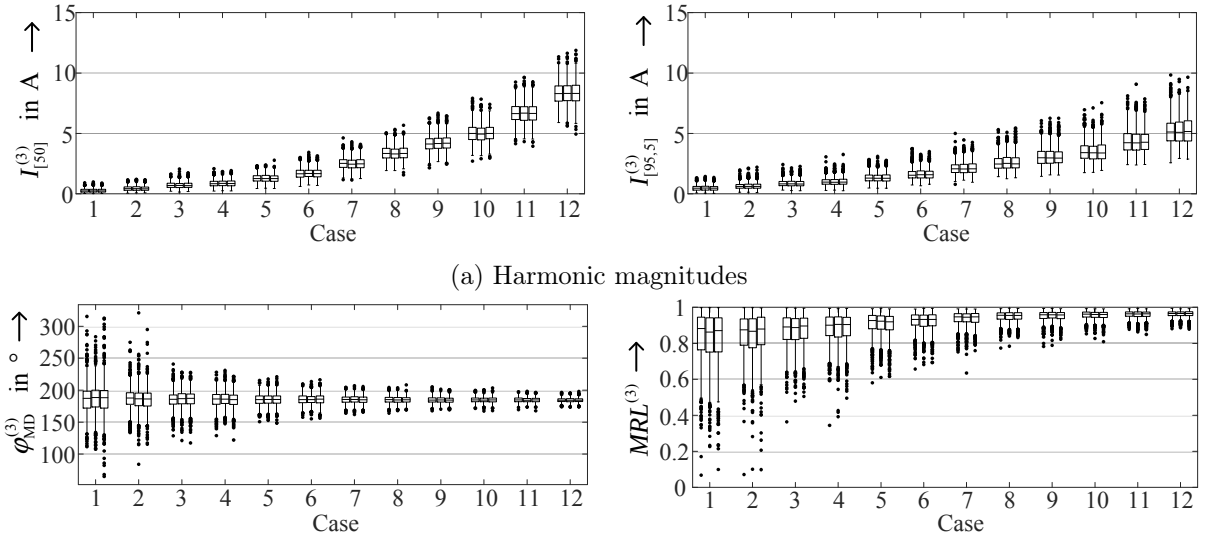

(a) Harmonic magnitudes

(b) Harmonic phase angles

Figure 6.3.: Boxplot of the statistics of the simulated third harmonic currents

The harmonic unbalance decreases with the amount of aggregate customers. Fig. 6.4 shows the boxplots of the AHU factors of the third harmonic obtained for each case. As expected, the unbalance is extremely high for low amount of customers, and in some cases, it can reach values higher than 100%. Those high unbalances are the result of the random distribution of the household appliances to the line conductors, which operate at different times. With the increase of customers, the unbalance decreases, but it does not become negligible.

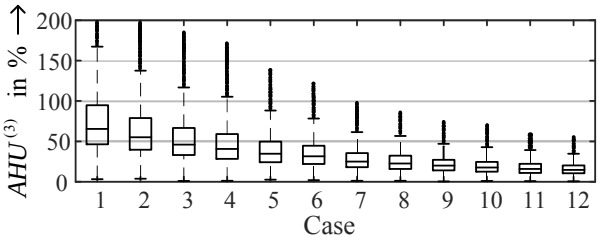

Figure 6.4.: AHU factors of the simulated third harmonic currents

A visual comparison of the simulated daily characteristic of harmonic currents indicates a significantly "smooth" behavior for groups of also 30 customers or more. Therefore, in case of aggregates with more than 30 customers, smooth time-series of the harmonic magnitudes and a prevailing direction of harmonic phase angles can be clearly identified. Consequently, the time series stochastic model can be applied to represent aggregate customer with minimum 30 customers.

6.2. Top-down approach

Fig. 6.5 shows a general representation of a low-voltage network, where the residential customers were grouped in m_{cg} number of groups, each with n_{cg} number of customers ($n_{\mathrm{u\ TOT}} =$

$m_{\mathrm{cg}} \cdot n_{\mathrm{cg}}$). Assuming that there are no additional harmonic impedances that may affect the flow of harmonic currents, the phasor sum of the harmonic currents emitted by the groups of customers should be equal to the total harmonic current at the low-voltage side of the distribution transformer (total harmonic current emitted by the low-voltage network), as described in equation 6.1:

$$\underline{I}_{\mathrm{TOT}}^{(h)} = \sum_{i=1}^{m_{\mathrm{cg}}} \underline{I}_{i}^{(h)} \tag{6.1}$$

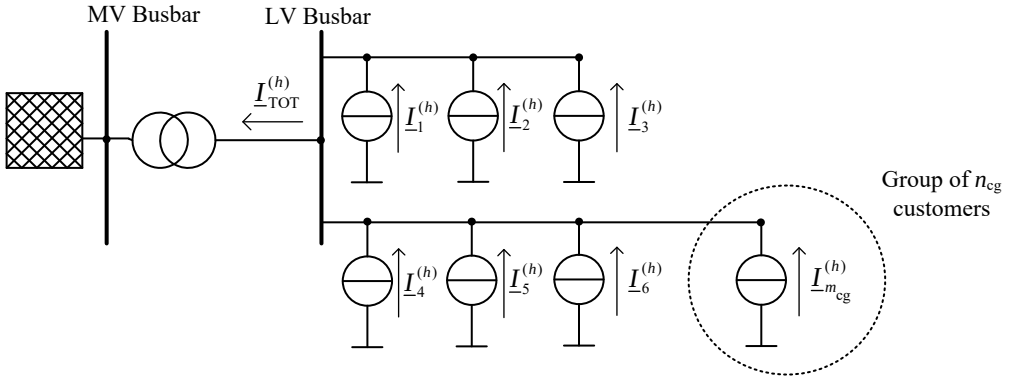

Figure 6.5.: General representation of a residential low-voltage network

The time-series stochastic model presented in the previous chapter estimates the total current emitted by a residential low-voltage network (estimation of current $\underline{I}_{\mathrm{TOT}}^{(h)}$ in Fig. 6.5, i.e $\hat{\underline{I}}_{\mathrm{TOT}}^{(h)}$). For simulations of low-voltage networks, it is required to estimate the harmonic currents emitted by small groups of customers, in such a way that the phasor sum of those currents is approximately the same as the current $\hat{\underline{I}}_{\mathrm{TOT}}^{(h)}$. Using the same stochastic model, the harmonic current emitted by groups of minimum 30 customers can be estimated, but an additional factor is introduced in order to match the phasor sum of the harmonic currents of the groups of customers with the total current $\hat{\underline{I}}_{\mathrm{TOT}}^{(h)}$, that is:

$$\hat{\underline{I}}_{\mathrm{TOT}}^{(h)} = CAF^{(h)} \cdot \sum_{i=1}^{m_{\mathrm{cg}}} \hat{\underline{I}}_{\mathrm{i}}^{(h)} \tag{6.2}$$

where $CAF^{(h)}$ is the Customers Aggregation Factor. As discussed in section 4.2.1, the harmonic currents in low-voltage networks do not increase linearly with the number of aggregate customers, and there are clear differences in the aggregation characteristic for networks with customer configuration C1 or C2. Therefore, the $CAF^{(h)}$ is a factor that represents the non-linear characteristic of the aggregation of harmonic currents in residential networks, and it is different depending on the customer configuration of the network.

The $CAF^{(h)}$ factor only takes into account the aggregation characteristic of harmonic magnitudes. As discussed in section 4.2.1, the phase angles (mean direction and mean resultant length) do not change considerably with the amount and type of customers of networks with more than 30 aggregate customers. For this reason, the aggregation factor $CAF^{(h)}$ only concerns the variation of harmonic magnitudes with the number of aggregate customers.

In order to calculate the $CAF^{(h)}$ factor, the difference between the estimated total current of the complete network ($\hat{\underline{I}}_{\mathrm{TOT}}^{(h)}$), and the sum of the harmonic currents from the groups of customers ($\sum_{i=1}^{m_{\mathrm{cg}}} \hat{\underline{I}}_{\mathrm{i}}^{(h)}$) has to be estimated. The following procedure was applied to calculate the $CAF^{(h)}$ factor:

1. Several cases with different amount of groups of customers m_{cg} and different number of customers in a group n_{cg} were defined. The cases represent networks with different total number of customers ($n_{\mathrm{u\ TOT}}$), which are disaggregated in different number of groups. Table 6.2 lists exemplary the first 10 cases defined for customer configuration C1. Appendix D includes all cases defined for both customer categories.

   For each case:

2. Estimate the total harmonic current of the network $\hat{\underline{I}}^{(h)}_{\mathrm{TOT}}$ with $n_{\mathrm{u\ TOT}}$ number of customers using the stochastic model. Calculate the CDF of the magnitude of $\hat{\underline{I}}^{(h)}_{\mathrm{TOT}}$.
3. Estimate the harmonic currents ($\hat{\underline{I}}^{(h)}_{\mathrm{i}}$) of m_{cg} groups of customers, each with n_{cg} aggregate customers, using the stochastic model.
4. Calculate the phasor sum of the harmonic currents of the m_{cg} groups of customers as:

$$\hat{\underline{I}}^{(h)}_{\mathrm{PHS}} = \sum_{i=1}^{m_{\mathrm{cg}}} \hat{\underline{I}}^{(h)}_{\mathrm{i}} \tag{6.3}$$

   Calculate the CDF of the magnitude of $\hat{\underline{I}}^{(h)}_{\mathrm{PHS}}$.
5. Repeat 100 times the steps 2 to 4, in order to cover different outputs from the stochastic model.
6. Calculate a mean CDF of the CDFs of the currents $\hat{\underline{I}}^{(h)}_{\mathrm{TOT}}$.
7. Calculate a mean CDF of the CDFs of the currents $\hat{\underline{I}}^{(h)}_{\mathrm{PHS}}$.
8. Calculate the $CAF^{(h)}$ factor as the mean value of the ratio between the CDFs obtained in steps 6 and 7
9. Repeat steps 2 to 8 and get the $CAF^{(h)}$ factor for each case.

Table 6.2.: First 10 cases to estimate the $CAF^{(h)}$ factor for customer topology C1

	Case									
	1	2	3	4	5	6	7	8	9	10
n_{cg}	30	30	30	30	30	30	30	30	30	40
m_{cg}	4	6	8	10	2	3	5	7	8	2
$n_{\mathrm{u\ TOT}}$	120	180	240	300	60	90	150	210	240	80

In order to illustrate better the estimation process, Fig. 6.6 shows the calculation of the $CAF^{(7)}$ factor for case 2 of customer configuration C1. The grey curves correspond to the 100 CDFs of the currents $\hat{\underline{I}}^{(7)}_{\mathrm{TOT}}$ and the 100 CDFs of the currents $\hat{\underline{I}}^{(7)}_{\mathrm{PHS}}$ calculated in steps 2 to 5. In steps 6 and 7, using each group of CDFs, a mean CDF is calculated in order to represent approximately the behavior of the currents $\hat{\underline{I}}^{(7)}_{\mathrm{TOT}}$ (blue CDF) and $\hat{\underline{I}}^{(7)}_{\mathrm{PHS}}$ (red CDF). The $CAF^{(7)}$ is obtained with the mean value of the ratio between the mean CDFs, which in this case gives a value of 0.66 (step 8). The black CDF in the figure corresponds to the mean CDF of $\hat{\underline{I}}^{(7)}_{\mathrm{PHS}}$ multiplied by the estimated factor $CAF^{(7)}$.

The correlation between the obtained $CAF^{(h)}$ factors with the input parameters n_{cg} and m_{cg} are initially evaluated using scatter plots. This analysis revealed that the $CAF^{(h)}$ factor has a good correlation with the number of groups m_{cg}, and a weak correlation with the number of customers in a group n_{cg}, which is explained by the similar values of n_{cg} used in the different cases ($30 \leq n_{\mathrm{cg}} \leq 60$). Fig. 6.7 shows the scatter plots between the $CAF^{(h)}$ factors of the

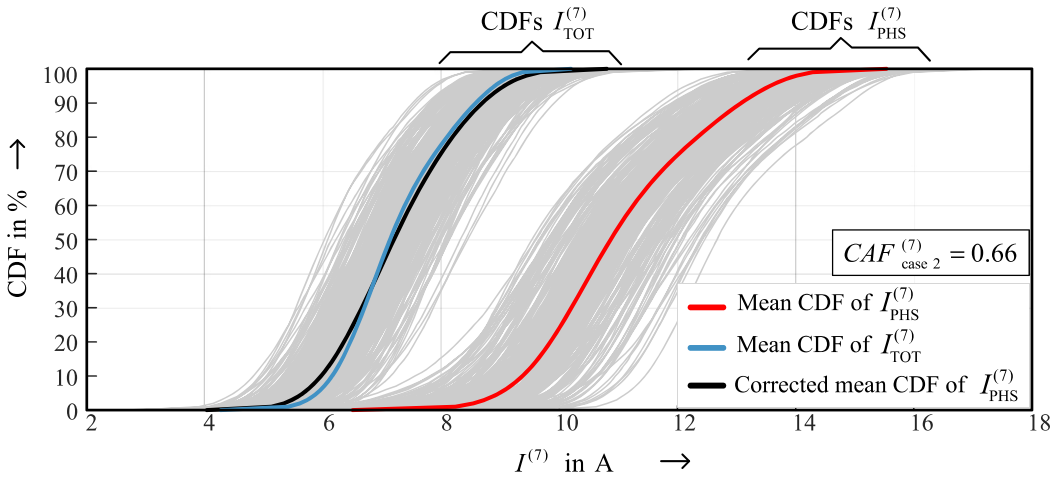

Figure 6.6.: Calculation of the $CAF^{(h)}$ of the sevent harmonic for case 2

3th, 7th and 13th harmonics for customer configuration C1 with the number of groups m_{cg}. For the third harmonic, the $CAF^{(h)}$ factor is almost 1 for all cases, which indicates that for this harmonic order no additional factor $CAF^{(h)}$ is required for simulations of low-voltage networks. However, for the other harmonic orders the $CAF^{(h)}$ factor clearly changes with m_{cg}. For the seventh harmonic the factor is always below one, which indicates that the factor $CAF^{(h)}$ reduces the phasor sum of the harmonic currents of the groups of customers (c.f. eq. 6.2). For the 13th harmonic, the $CAF^{(h)}$ is above one, which indicates that the sum of harmonic currents is too low, and its value needs to be increased to match the total harmonic current of the network.

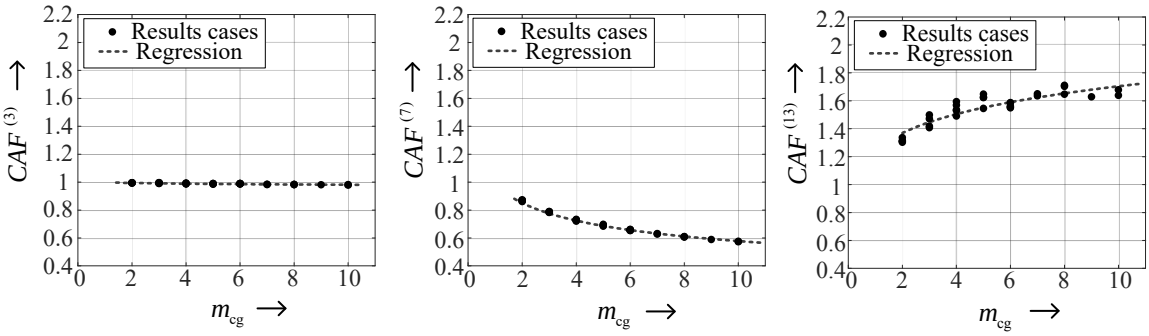

(a) 3th harmonic (b) 7th harmonic (c) 13th harmonic

Figure 6.7.: Regression characteristic between the $CAF^{(h)}$ factors and the number of groups m_{cg} for customer configuration C1

The correlation between the $CAF^{(h)}$ factor and m_{cg} is described with a power function. Fig. 6.7 shows the regression of the 3th, 7th and 13th harmonics for customer configuration C1 and the corresponding coefficient of determination R^2_{adj} that indicates a very good appropriateness of the power function for the regression. Appendix D contains the regression obtained for all harmonic orders and for customer configuration C1 and C2. In all cases, a coefficient of determination higher than 0.7 was obtained, indicating a good regression between the $CAF^{(h)}$ factor and m_{cg}.

With the obtained regressions of the $CAF^{(h)}$ factor, the stochastic model can now be used to simulate the harmonic emission of aggregate customers for simulations of low-voltage networks. Fig. 6.8 shows the extension of the original stochastic model (Model of residential low-voltage networks) to obtain the harmonic currents of aggregate customers (c.f. Fig. 5.1). The input parameters are the total amount of customers in the network ($n_{\mathrm{u\ TOT}}$), the amount of groups of customers (m_{cg}), the harmonic order and the type of customers in the network. With $n_{\mathrm{u\ TOT}}$ and m_{cg} the number of customers in a group n_{cg} can be calculated , and with it the stochastic model is applied as explained in the previous chapter (referring to Fig. 5.1, $n_{\mathrm{u}} = n_{\mathrm{cg}}$). The number of customers in a group should be between 30 and 60 customers. The $CAF^{(h)}$ factor is calculated and finally used to correct the magnitude of the harmonic currents obtained with the stochastic model. The output is the harmonic magnitudes and phase angles of n_{cg} aggregate customers that are connected to a low-voltage network with a total of $n_{\mathrm{u\ TOT}}$ residential customers.

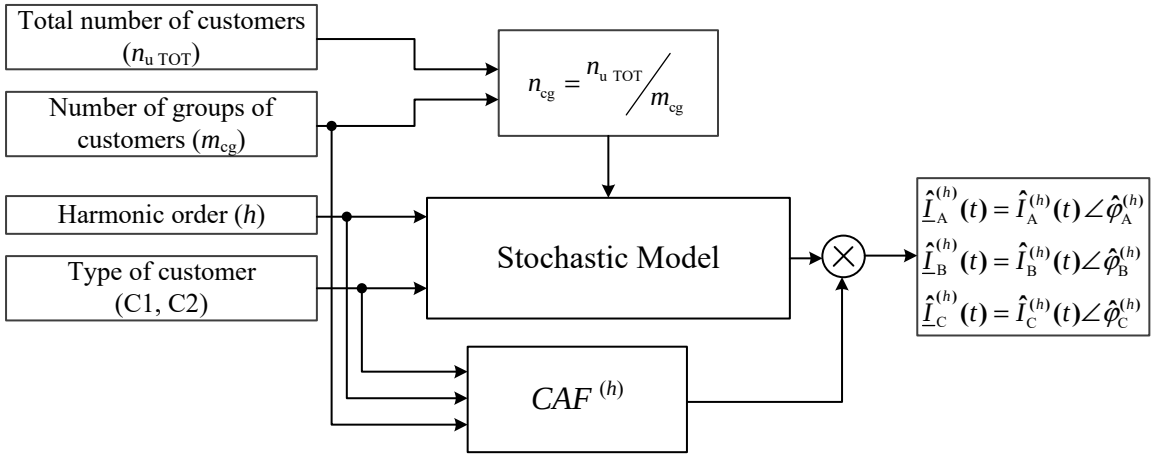

Figure 6.8.: Model of aggregate customers for the analysis of low-voltage networks

6.3. Model validation

The model of aggregate customers is validated in a similar way as the model of residential low-voltage networks explained in the previous chapter. Using the same cases defined in Table 5.3, and assuming $n_{\mathrm{cg}} = 30$, the number of groups m_{cg} is obtained and the stochastic model is applied to obtain the harmonic currents of the m_{cg} groups of aggregate customers for each case. Then, the phasor sum of the harmonic currents of the m_{cg} groups of customers is calculated ($\hat{\underline{I}}_{\mathrm{TOT}}^{(h)}$ in eq. 6.2), and compared with real measurements of low-voltage networks. The process is repeated 100 times to cover the different outputs of the stochastic model.

Fig. 6.9 compares the statistics of harmonic magnitudes and phase angles of the measured (dots) and simulated (bars) data for the third, fifth and seventh harmonics for customer configuration C1 (figures of the other harmonic orders in appendix D). The bars represent the variation of the respective statistics for the 100 simulations of each case. The central tendency of magnitudes and phase angles are good represented, but the dispersion of both variables is slightly lower. Comparing Fig. 6.9 with Fig. 5.18, it is clear that the extended stochastic model results in a lower variation of harmonic magnitudes and phase angles, which is caused by some level of cancellation of harmonics currents from the aggregate customers in the phasor sum. However, the statistical characteristics of the harmonic magnitudes and phase angles are still very close to the statistical characteristics of real networks, and the model of aggregate

Figure 6.9.: Comparison of the measurements of residential networks (points) and estimated data with the model of aggregate residential customers (grey bar)

customers can be applied for analysis of low-voltage networks.

In this case, the model also has more inaccuracies in the representation of the 13th and 15th harmonics, especially in their phase angles. As discussed before, this is the result of the higher variation of harmonic magnitudes and phase angles that can not be accurately represented with the selected time-series stochastic model. However, the model can give a good approximation of the magnitudes and phase angles of the 13th and 15th harmonics that can be useful for approximate analysis in low-voltage networks.

The unbalance of the simulated harmonic currents is also compared with the real harmonic unbalance of low-voltage networks. Fig. 6.10 shows the comparison for the 95th percentile of the aggregate harmonic unbalance factor ($AHU^{(h)}$) of the third, fifth and seventh harmonics. In all cases, the model shows very good response, indicating that the model of aggregate residential customers represents accurately the harmonic unbalance of residential networks.

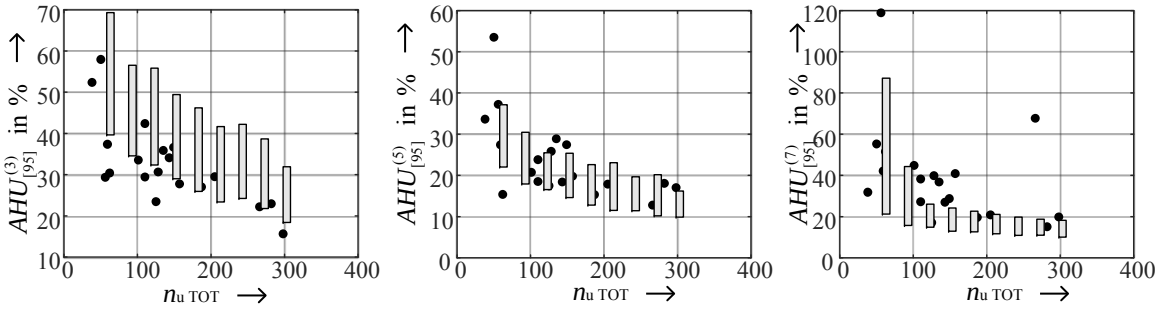

(a) Third harmonic (b) Fifth harmonic (c) Seventh harmonic

Figure 6.10.: Comparison of the 95th percentile of the AHU factors obtained with measurements of residential networks (points) and estimated data (grey bar)

6.4. Chapter summary

The characteristics of the magnitudes and phase angles of aggregate residential customers depend strongly on the amount of customers. Single customers show a random variation of harmonic magnitudes and phase angles where no daily pattern of harmonic magnitudes or prevailing direction of harmonic phase angles can be defined. As the amount of aggregate customers increases, the harmonic magnitudes begin to show a smooth time-series characteristic and the harmonic phase angle reduces its diversity and concentrates more and more in one direction. In case of aggregates with more than 30 customers, smooth time-series of the harmonic magnitudes and a prevailing direction of harmonic phase angles can be clearly identified. Consequently, the time series stochastic model presented in chapter 5 can be correctly applied for the representation of minimum 30 aggregate customers.

A top-down approach was applied in order to extend the original stochastic model to represent groups of minimum 30 customers (feeder, feeder section) that can be used in simulations of low-voltage networks. The applied top-down approach does not change the parameters of the original stochastic model, but introduces a new variable, the *Customers aggregation factor* CAF, that modifies the harmonic magnitudes in order to include the complex aggregation characteristic of harmonic currents in low-voltage networks. The extended model is verified using measurement of real networks, given satisfactory results.

The model of aggregate customers is useful for the simulations of low-voltage networks, where the residential customers can be aggregated in several groups. The extended model has the limitation that only groups of minimum 30 customers can be simulated. For some analyses,

the model of single customers or smaller number of aggregate customers are required, and for those analyses the presented model is not suitable. For those cases, a different modeling methodology is recommended, where the high random variation of harmonic magnitudes and phase angles of single customers is better represented.

7. Application example

The stochastic model of residential low-voltage networks is used in a simulation of a medium-voltage network in order to show its applicability and its advantages for a more reliable analysis. In this case, the impact of the massive use of electric vehicles on the medium-voltage networks is studied.

The chapter is divided in two main parts. The first part explains the simulation framework, including the characteristics of the simulated network, and the representation of the electric vehicles and residential customers. The second part shows the results of the simulations and discusses the impact of the increasing number of electric vehicles on the low-voltage and medium-voltage networks.

7.1. Simulation framework

Real medium-voltage networks are very diverse, with different configurations (meshed or radial), components (cables, overhead lines, transformers, etc), and type and number of connected customers (residential, commercial and industrial customers). The electric characteristics of the network lead to different behavior in terms of harmonic propagation, due to different characteristics of the harmonic impedances and harmonic sources. Therefore, the following analysis is made on a synthetic network instead of a real network configuration, where complete control of the parameters and characteristics of the network is possible. The use of a synthetic network allows a better understanding of the interaction between the harmonic emission of residential customers and the harmonic emission of electric vehicles.

Different cases with different penetration percentages of electric vehicles were defined. Table 7.1 details each of the simulation cases, including the resulting number of electric vehicles in each low-voltage network. It is important to clarify, that the number of electric vehicles of the table corresponds to the total amount of devices that can be connected during the day, i.e. the amount of customers that own an electric vehicle. This has to be differentiated from the number of electric vehicles that are connected to the network at some time instant. The number of electric vehicles connected to the network is obtained based on a stochastic scheme, which will be explained in detail below.

Table 7.1.: Simulation cases for the application example

Simulation case	Percentage of EVs in the network	Total number of EVs in the MV network	Total number of EVs in each LV network
Sim 1	0%	0	0
Sim 2	10%	1000	20
Sim 3	30%	3000	60
Sim 4	50%	5000	100
Sim 5	70%	7000	140

The simulation cases were selected in order to analyze step-by-step the influence of the increasing number of electric vehicles in medium-voltage networks. However, the cases may not

represent real future scenarios, especially cases Sim 4 and Sim 5 which consider a very high amount of electric vehicles in the network that may not be seen in the future. The analysis is limited to the third, fifth and seventh harmonics.

The complete characteristics of the synthetic network, and the modeling characteristics of the aggregate residential customers and the electric vehicles are described in the following subsections.

7.1.1. Synthetic medium-voltage network characteristics

Fig 7.1a shows the synthetic medium-voltage network, which consists of ten feeders, each with five low-voltage networks. Each of the low-voltage networks (LV1 ... LV50) has 200 residential customers, which were represented with a Norton equivalent. Besides, the aggregate electric vehicles (sum of all electric vehicles in a low-voltage network) were also represented with a Norton equivalent (c.f. Fig. 7.1b).

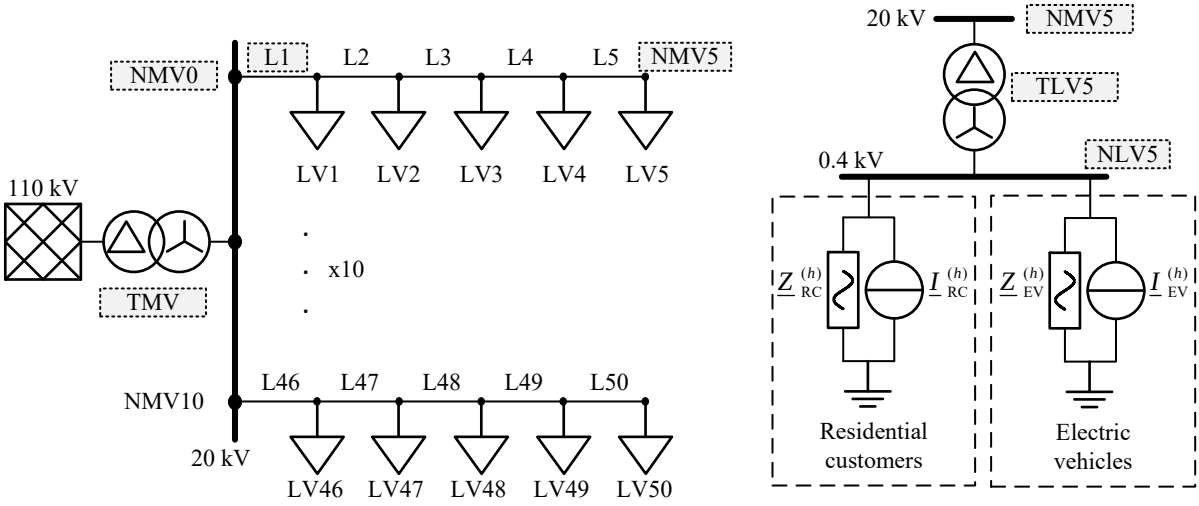

(a) MV network (b) LV network

Figure 7.1.: Simulated medium-voltage network

The distribution of the low-voltage networks on the feeders and the characteristics of the lines and transformers were selected in order to have a symmetric network, where the harmonic propagation can be easily comprehended. Therefore, each feeder has the same length, the low-voltage networks are equally distributed along the feeder and all MV/LV transformers are of the same type and size. The selected types of lines and transformers correspond to the most common type of both elements in European distribution networks, according to information provided by several network operators and references [29, 43, 106]. The electric characteristics of the lines and transformers are detailed in Tables 7.2 and 7.3.

7.1.2. Model of Residential customers

The harmonic currents $\underline{I}_{\mathrm{RC}}^{(h)}$ of the corresponding Norton equivalent were generated with the stochastic model presented in chapter 5. The total number of customers (n_{u}) is fixed to 200, while the type of customers (C1 or C2) were selected randomly for each low-voltage network (c.f. Fig. 5.1). The magnitude and phase angle of the third, fifth and seventh harmonics during one day were generated separately for each low-voltage network, i.e. the model was applied 50 times to generate the harmonic emission of all low-voltage networks.

Table 7.2.: Underground cable characteristics

Lines	Length [m]	Type of cable	Cross-sectional area [mm^2]	R_{AC} (20°C) [Ω / km]	X [Ω/km]	Rated current [A]
L1 ... L50	500	NA2XS2Y	120	0.343	0.275	320

Table 7.3.: Transformers characteristics

Transformer	Rated power [MVA]	Rated voltage [kV]	Vector group	Short-circuit voltage [%]	Cooper losses [kW]
TMV	25	110 / 20	Dyn1	12	25
TLV1 ... TLV50	0.63	20 / 0.4	Dyn5	6	6.9

In order to have a more realistic propagation of harmonic currents in the network and a better estimation of the harmonic voltages, an equivalent harmonic impedance of the residential customers $\underline{Z}_{\mathrm{RC}}^{(h)}$ is also included. This impedance is a RL‖RC circuit as shown in Fig. 7.2, which values were estimated based on the equivalent impedance of individual residential curstomers presented in [95]. In this case, the equivalent impedance $\underline{Z}_{\mathrm{RC}}^{(h)}$ of the aggregate customers corresponds to the parallel connection of the impedance of 100 individual residential customers, which represents approximately the average value of the total impedance of the 200 aggregate residential customers. It is clear that the equivalent impedance of aggregate residential customers varies during the day and it depends on the type of customers (C1 or C2) and the characteristics of the low-voltage network (e.g. types of lines, length of the lines, transformer size, etc.), but as this information is not available, only an average impedance can be implemented. As mention in [95, 123] more detailed studies about the behavior of network harmonic impedance and the equivalent impedance of aggregate customers are required, especially because the increase of electronic equipment has an increasing impact on the network harmonic impedance, and consequently, an impact on the level of the harmonic voltages and harmonic currents in distribution networks (more details in [28]).

Fig. 7.2b and Fig. 7.2c show the frequency response of the impedance $\underline{Z}_{\mathrm{RC}}^{(h)}$. The impedance shows a small resonance at 200 Hz (4$^{\mathrm{th}}$ harmonic) and a capacitive nature due to the high amount of electronic household appliances [95].

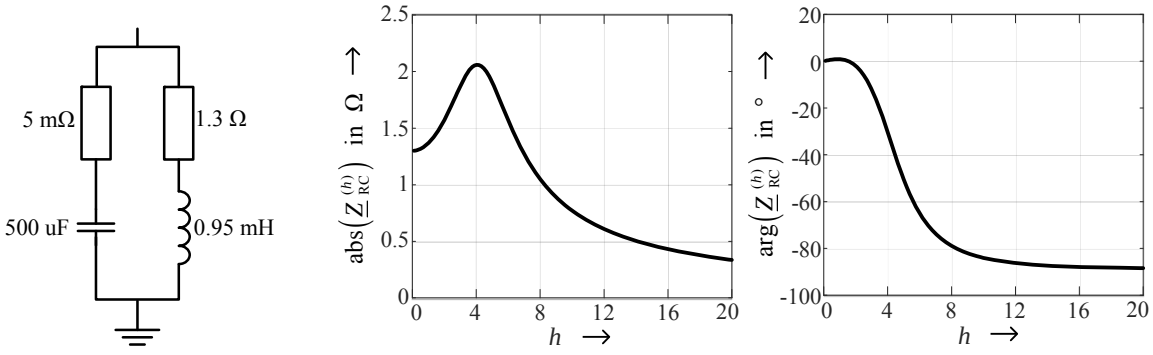

(a) RL‖RC equivalent (b) Magnitude $\underline{Z}_{\mathrm{RC}}^{(h)}$ (c) Phase angle $\underline{Z}_{\mathrm{RC}}^{(h)}$

Figure 7.2.: Equivalent impedance of 200 aggregate residential customers

7.1.3. Model of aggregate electric vehicles

The current $\underline{I}_{\mathrm{EV}}^{(h)}$ and the impedance $\underline{Z}_{\mathrm{EV}}^{(h)}$ of the Norton equivalent of the aggregate electric vehicles are estimated based on the harmonic emission of real electric vehicles, and a stochastic scheme that simulates the amount of electric vehicles connected during the day. The following section shows the results of different laboratory measurements, which were used to characterize the harmonic emission and the input impedance of different single-phase electric vehicles. Next, the estimation of the Norton equivalent of the aggregate electric vehicles is explained in detail.

Measurement results of single-phase electric vehicles

The harmonic emission and harmonic impedance of five single-phase electric vehicles from different manufacturers were measured in the laboratory, where the magnitude and distortion of the supplied voltage can be easily controlled. The measurement system is not only able to measure with high accuracy the continuous harmonic emission of the electric vehicles during their complete charging cycle, but also their harmonic impedance. The characteristics of the measurement system are detailed in [28, 99].

Fig. 7.3 shows the average harmonic current magnitudes and phase angles of the electric vehicles during the charging-state. The electric vehicles were measured with a flat-top voltage waveform (c.f. section 2.2.1), in order to characterize the harmonic emission of electric vehicles in typical low-voltage networks. There are significant differences in the harmonic current magnitudes of the five electric vehicles, which result from the different electric circuits of the charging boxes implemented by each manufacturer. However, all devices have an active PFC topology, with a THD_{I} below 10% and a power factor higher than 0.98. All harmonic currents have a magnitude below 5% of the fundamental current (fundamental currents range between 11 A and 16 A). There are also significant differences in the harmonic phase angles, except for the third and fifth harmonics. The low diversity of phase angles of the third and fifth harmonics can result in a lower cancellation effect between electric vehicles (c.f. section 2.2.2).

The frequency dependent input impedance of each electric vehicle is shown in Fig. 7.4. The impedance is also different for each electric vehicle, but all show a capacitive behavior. To simulate the impedance in DigSilent, the RL||RC equivalent circuit of Fig. 7.4a was obtained. The values of the different elements of the RL||RC equivalent circuit can be adjusted to get a better representation of the real input impedance of each electric vehicle, but in order to simplify the simulation, an equivalent input impedance that represents approximately the behavior of all selected electric vehicles was used (black line in Fig. 7.4b and Fig. 7.4c).

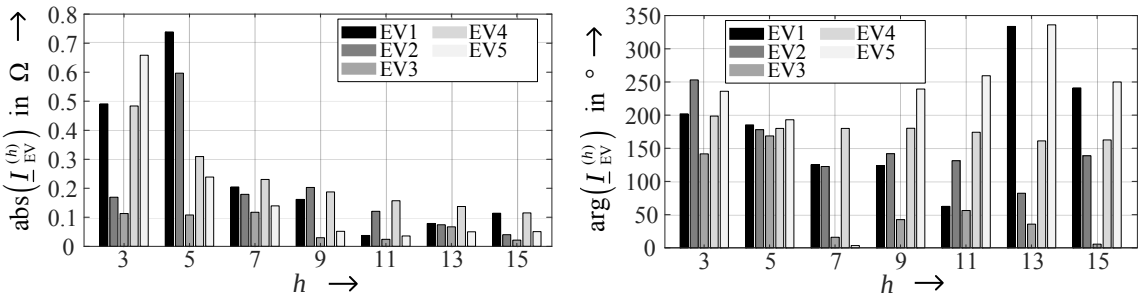

(a) Magnitudes (b) Phase Angles

Figure 7.3.: Harmonic currents of five electric vehicles under flat-top voltage waveform

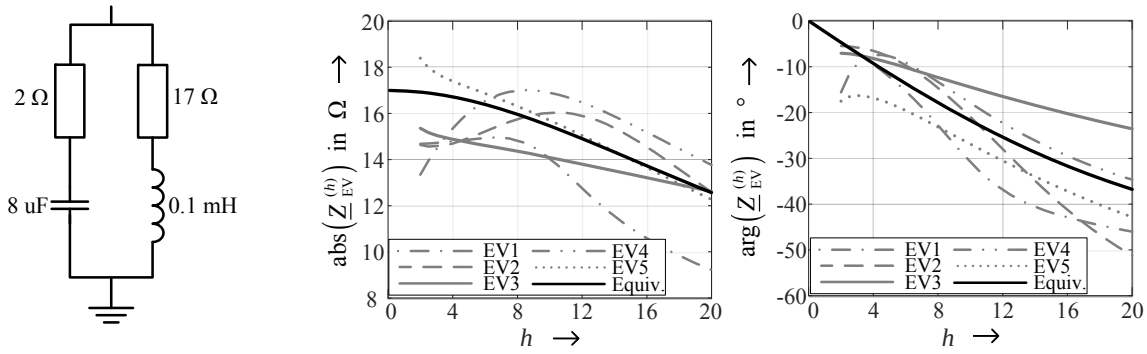

(a) RL‖RC equivalent (b) Magnitude $\underline{Z}_{\mathrm{EV}}^{(h)}$ (c) Phase angle $\underline{Z}_{\mathrm{EV}}^{(h)}$

Figure 7.4.: Equivalent impedance of single EVs

Estimation of the Norton equivalent

According to the number of charging electric vehicles connected to the network (n_{EV}), the parameters of the Norton equivalent change. The value of the aggregate current $\underline{I}_{\mathrm{EV}}^{(h)}$ is obtained with the phasor sum of the harmonic currents of the n_{EV} electric vehicles, while the impedance $\underline{Z}_{\mathrm{EV}}^{(h)}$ is the result of the parallel connection of n_{EV} equivalent impedances. The value of n_{EV} is obtained based on a stochastic scheme, that seeks to represent the random connection of the electric vehicles in the network during a typical day. The following criteria was used to estimate n_{EV}:

- The connection time (time at which an electric vehicle is connected to the network) of each electric vehicle is obtained with the probability distribution of Fig. 7.5a provided by [54]. According to it, the electric vehicles are mostly connected during the evening.
- The charging time of each electric vehicle depends on the charging state of the batteries which is linked to the speed and the distance driven by the customer during the day. To simplify the problem, the charging time is obtained randomly from a uniform distribution between 0 and 6 hours.
- It is assumed that each electric vehicle is charged only once per day.
- The line conductor at which each electric vehicle is connected is selected randomly with a discrete uniform distribution.

Fig. 7.5b shows exemplary the number of connected electric vehicles (n_{EV}) in one low-voltage network during one day for case Sim 2. The electric vehicles are connected at different times after midday, and it is after 6 p.m. (usual time when most of the people return home) when most electric vehicles are connected to the network. The number of connected electric vehicles is also different between the line conductors. In this case, most of the electric vehicles are connected to line conductors A and B.

Based on the amount of connected electric vehicles, the current $\underline{I}_{\mathrm{EV}}^{(h)}$ and the impedance $\underline{Z}_{\mathrm{EV}}^{(h)}$ of each Norton equivalent are estimated. The type of electric vehicle that each customer ownes is assigned randomly from the set of the five electric vehicles available. Fig. 7.6 shows the corresponding variation of the seventh harmonic current magnitudes and phase angles of the example in Fig. 7.5b. The random connection of the electric vehicles, results in a high variation of the harmonic magnitudes and phase angles during the day. In a similar way, the values of RL‖RC equivalent that compose the impedance $\underline{Z}_{\mathrm{EV}}^{(h)}$ are obtained. The values of the Norton equivalent of the aggregate electric vehicles are obtained separately for each low-voltage network and each simulation case.

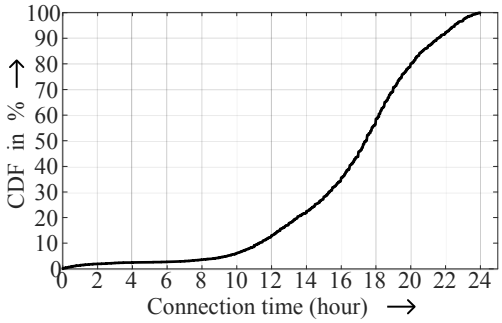

(a) Connection time of electric vehicles

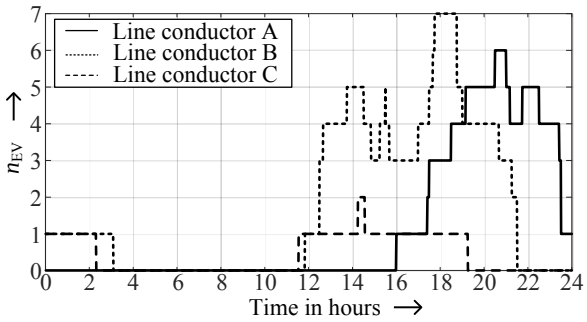

(b) Example case Sim 2

Figure 7.5.: CDF of the connection time of electric vehicles during the day obtained from [54] and example of the number of connected electric vehicles in one network for case Sim 2

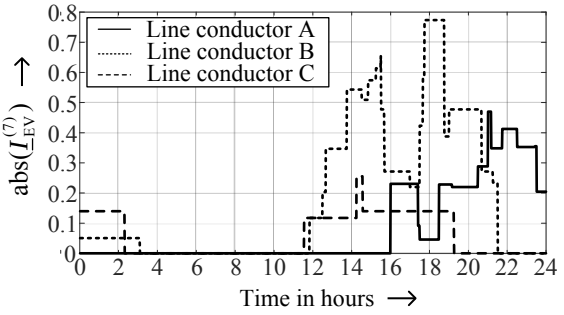

(a) Harmonic magnitude

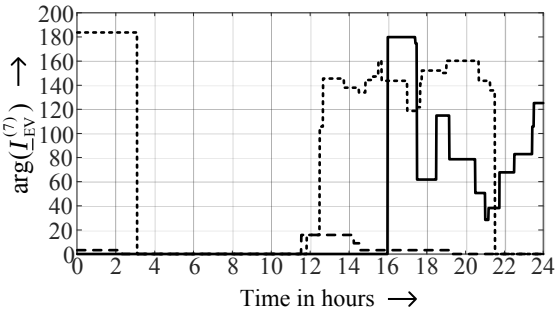

(b) Harmonic phase angle

Figure 7.6.: Example of the harmonic emission of the electric vehicles connected to one LV network for case Sim 2

7.2. Simulation results

The medium-voltage network under the different simulation cases was simulated in DigSilent. The simulation initiates with the calculation of the load flow, which is used to verify that the voltage at all busbars are inside the $\pm 10\%$ band of the nominal voltage, and the transformers are not overloaded. Next, the harmonic load flow is calculated, and with it all harmonic voltages and harmonic currents at the different network elements are estimated. Finally, the network harmonic impedance at the main busbar (NMV0) is obtained with a frequency-sweep.

As the emission of the residential customers and electric vehicles are changing in time, the simulation has to be repeated in order to calculate the harmonic load flow and frequency sweep at each time instant. A python script was implemented in order to run the simulation for each minute. In each iteration, the elements of the Norton equivalents are updated, and the results of the simulation are saved.

The harmonic voltages and currents at some elements in the network are selected for the analysis. Specifically, the elements marked in a grey boxes in Fig. 7.1 were selected (the busbars NMV0, NMV5 and NLV5, the transformers TLV5 and TMV, and the line L1). As the synthetic network is completely symmetric, the results of the other elements are similar.

Harmonic currents

Fig. 7.7 shows the variation of the third, fifth and seventh harmonic magnitudes (upper graphs) and the polar plot of the harmonic currents on the line L1 obtained for each simulation case during the evening (6pm and 10pm). The increase of electric vehicles causes a significant positive change in the fifth harmonic currents, and a slightly increase in the seventh and third harmonic currents, especially during the evening when more electric vehicles are connected. The electric vehicles also cause a significant change in the phase angles of the fifth and seventh harmonics.

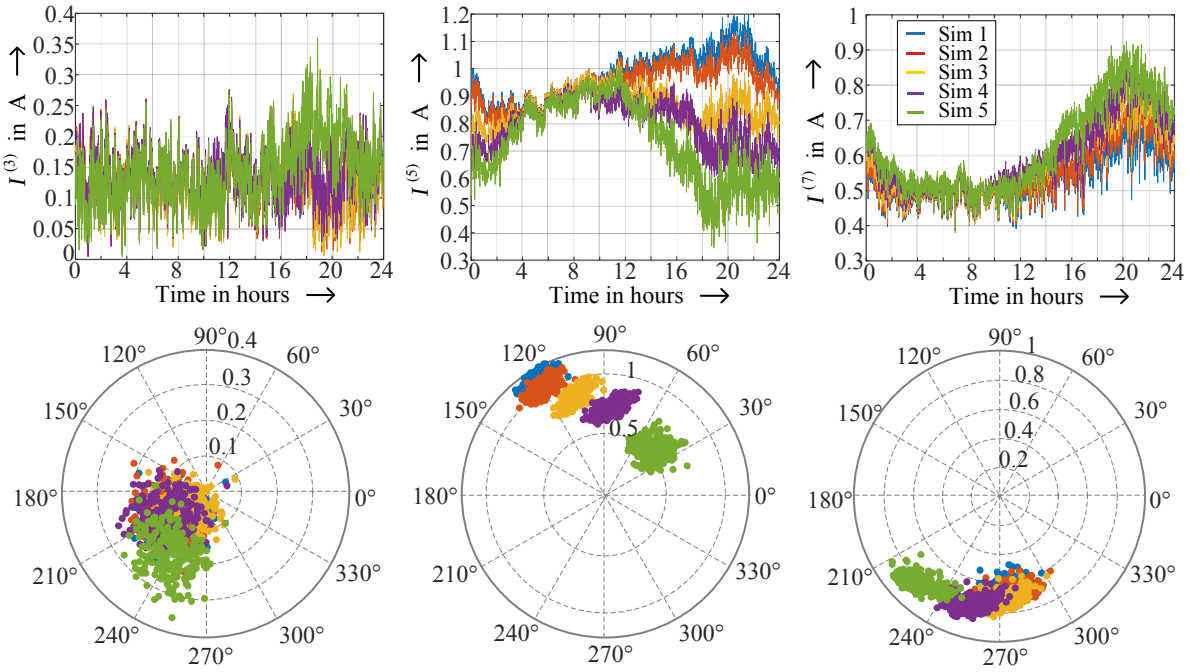

(a) Third harmonic (b) Fifth harmonic (c) Seventh harmonic

Figure 7.7.: Harmonic current at line L1, line conductor A. Time series of the harmonic magnitudes (upper graphs) and polar plot of harmonic currents between 6pm and 10pm

The impact of the electric vehicles is the result of the summation of the harmonic currents from the electric vehicles and the residential customers. To illustrate this point, Fig. 7.8 shows the harmonic currents at the low-voltage side of the transformer TLV5 during the evening for simulation cases Sim 1 (blue) and Sim 5 (green), and the direction of the harmonic currents of the electric vehicles (grey areas) according to the characterization presented in Fig. 7.3. When there are no electric vehicles connected, the simulated harmonic currents show the phase angle direction of aggregate residential customers, i.e. around 200° for the third harmonic, 330° for the fifth harmonic and 120° for the seventh harmonic. With the increase of electric vehicles, the third harmonic increases because the electric vehicles have a similar direction of the harmonic phase angles as the residential customers, resulting in a low cancellation between both harmonic currents. On the other side, the fifth harmonic magnitude decreases, because the phase angle of the electric vehicles is about 150° shifted with respect to the residential customers, which results in some cancellation between both currents. Moreover, the phase angles of the fifth harmonic shifts in direction of the electric vehicles. The seventh harmonic has a low variation because the electric vehicles have different phase angle directions, which results in a low cancellation with the seventh harmonic currents from the residential customers.

As expected, most of the third harmonic currents do not propagate to the medium-voltage network due to the use of delta-wye transformers. However, as the harmonic currents are unbalanced, there is a part of the triple harmonics that propagate to the medium-voltage networks,

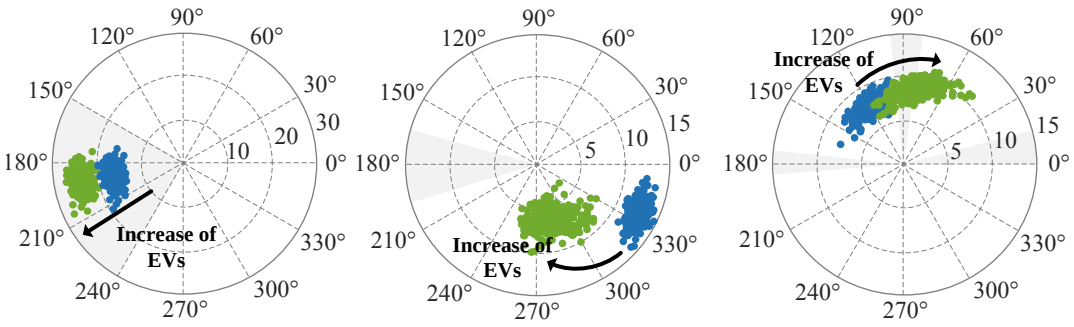

(a) third harmonic (b) fifth harmonic (c) Seventh harmonic

Figure 7.8.: Change of the harmonic currents at the low-voltage side of the transformer TLV5. Blue: Sim 1, Green: Sim 2

which can not be neglected. The amount of triple harmonics that propagate to the medium-voltage network depends on the balanced connection of the electric vehicles and other electronic devices on the three line conductors. This aspect is of high importance, especially in the planning of the network in the near future.

Harmonic voltages

With the increase of electric vehicles, the voltage distortion in the distribution network is also affected. Fig. 7.9 show the 95$^{\text{th}}$ percentile of the THD_{U} and the third, fifth and seventh voltage harmonics on two busbars at the low-voltage and medium-voltage side (busbars NLV5 and NMV0). In both busbars, a clear decrease in the total harmonic distortion is observed. The third harmonic increases clearly on the low-voltage network, but this increase is not significant on the medium-voltage network. The fifth harmonic decreases, while the seventh harmonic increases on both busbars. However, the results from cases Sim 4 and Sim 5 are very similar, which indicates some kind of saturation which is reached when the harmonic emission in the network is mainly caused by the electric vehicles. Nevertheless, the case when more than 30% of the customers own an electric vehicle is not expected in the near future.

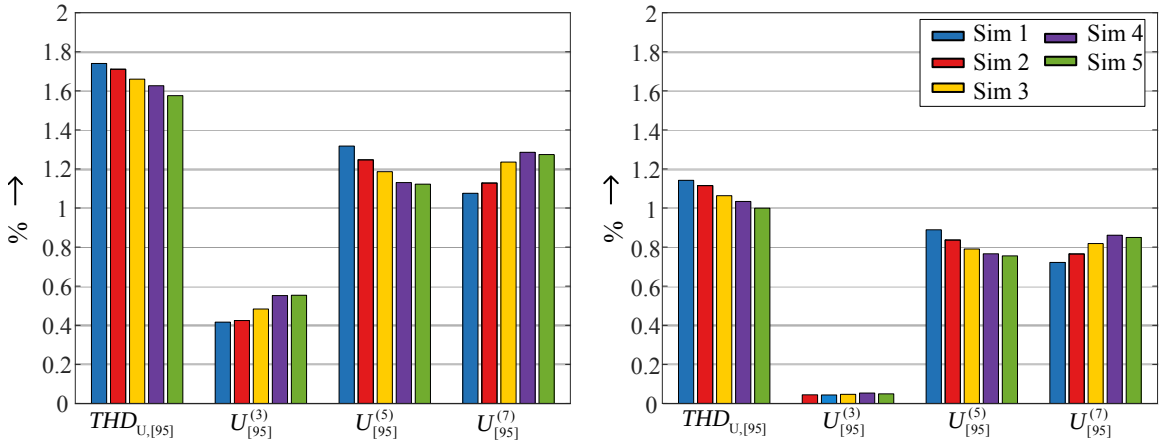

(a) Busbar NLV5 (b) Busbar NMV0

Figure 7.9.: 95$^{\text{th}}$ percentile of the THD_U and the voltage harmonics at busbars NLV5 and NMV0

Network harmonic impedance

Fig. 7.10 shows the variation of the network harmonic impedance at the main busbar (busbar NMV0) with the increasing penetration of electric vehicles. The figure on the left shows the variation of the network impedance at 10 a.m., when there are few electric vehicles connected; and the figure on the right shows the network impedance at 8 p.m., when the amount of electric vehicles is high. The figures show clearly that the electric vehicles have a positive impact on the network impedance, reducing the high resonance at approximately 550 Hz (11$^{\text{th}}$ harmonic). For case Sim 2, a change of more than 50 Ω at the resonance frequency is obtained, which indicates that with a small penetration of electric vehicles, a considerable change in the network impedance has to be expected.

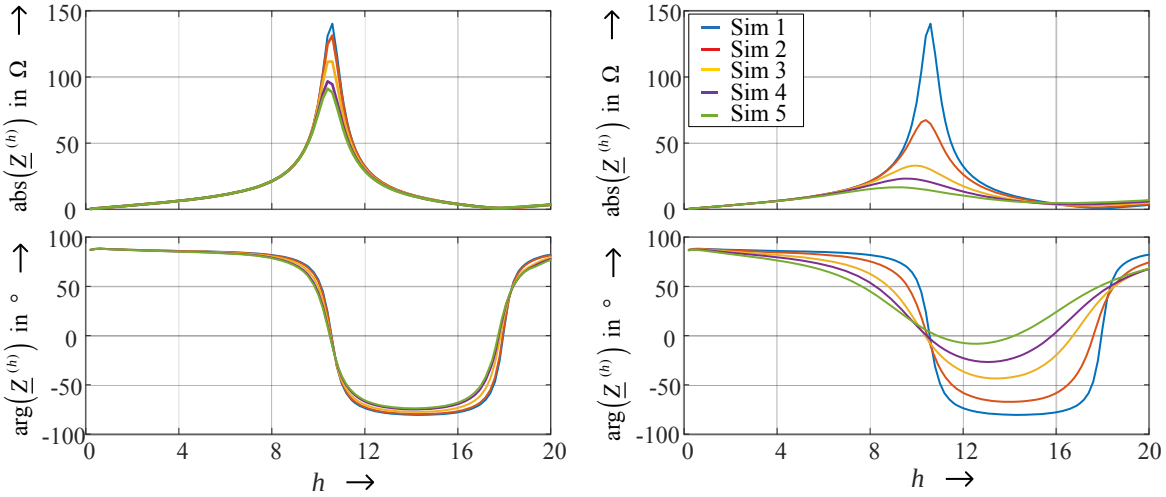

(a) Impedance at 10 a.m.

(b) Impedance at 8 p.m.

Figure 7.10.: Network harmonic impedance at node NMV0

The extremely high magnitude of the network harmonic impedance at the resonance frequency in the synthetic network may be not realistic. However, resonances of the network impedance in the range between 400 Hz and 1000 Hz have also been seen in measurements of real medium-voltage networks [75]. Therefore, it is expected that the massive use of the electric vehicles will have a positive impact, which will be reflected on the levels of the 11$^{\text{th}}$, 13$^{\text{th}}$ and 15$^{\text{th}}$ harmonics.

7.3. Chapter summary

The stochastic model presented in this thesis was used in an application example, where the impact of increasing number of electric vehicles on a synthetic distribution network was analyzed. The stochastic model provided an accurate representation of the daily variation of harmonic magnitudes and phase angles of the harmonic emission of residential customers, which allowed a more detailed analysis of the impact of the electric vehicles during the day.

The results of the application example showed a positive impact of the electric vehicles on the fifth harmonic currents and voltages, and a slightly negative impact on the seventh harmonics, which coincides with the results obtained with recent measurements of a real low-voltage network presented in [100]. However, it is recommended to analyze the impact of electric vehicles on other network configurations with more detailed models of the impedances of the residential customers, in order to explore other scenarios and get more reliable conclusions.

8. Conclusions and further work

Harmonic propagation studies of public distribution networks require accurate models of aggregate residential customers (groups of customers) that simulate the harmonic emission of the multitude of household appliances in the network. Most of the present models were developed with the component-based approach, where models of individual household appliances are combined to build the model of multiple customers. This approach requires high amount of input data, like models of individual household appliances and detailed information of customer behavior and device composition, which is usually not easy to acquire. However, with the increasing number of PQ-analyzers in the networks, the measurement-based approach is now more and more considered for the modeling of aggregate customers. The measurement-based approach uses measurements of the network in combination with top-down methodologies to obtain models of the aggregate customers. Compared to the component-based approach it has several advantages, like inherent consideration of the real operating changes of the individual household appliances, variation of customer behavior, effect of line impedances, cancellation and attenuation effects, etc.

This thesis presents the development of a time-series stochastic model of the low-order harmonic emission of aggregate residential customers based on a top-down measurement-based approach. The model represents the daily variation of the harmonic magnitudes and phase angles. Besides, the model includes the representation of the harmonic unbalances, which is of great importance for the proper analysis of harmonic propagation in medium-voltage networks. The model is parametrized for German networks, but the methodology can be applied to find the models of other regions or countries. The main findings of the thesis are summarized below.

Characteristics of the harmonic currents in residential low-voltage networks:

- The characteristics of the magnitudes and phase angles of aggregate residential customers depend strongly on the amount of customers. Single customers show a random variation of harmonic magnitudes and phase angles where no daily pattern of harmonic magnitudes or prevailing direction of harmonic phase angles can be observed. As the amount of aggregate customers increases, the harmonic magnitudes begin to show a distinct daily pattern and the harmonic phase angle reduces its diversity and concentrates more and more in one direction.
- In case of aggregate customers with more than 30 customers, a clear daily pattern of the harmonic magnitudes and a prevailing direction of harmonic phase angles can be clearly identified for the first 15 odd harmonics in most residential networks. The daily pattern of harmonic magnitudes is linked to the daily activities of residential customers.
- The increase of harmonic magnitude with the number of aggregate customers has a nonlinear characteristic due to the complex (phasor) aggregation of harmonic currents and the variety of residential customers.
- The magnitude of harmonic currents depends also on the type of customers connected to the network. Networks with mainly single-family houses have higher harmonic current

magnitudes than networks with mainly multi-family houses.

- Residential sites show a similar direction of harmonic phase angles, especially for the fundamental, third, fifth, seventh, and ninth harmonic orders. For higher harmonic orders, the variation of phase angles is higher for each site, and there are more differences between sites. There is no clear relation between the type and number of customers with the harmonic phase angles. Moreover, harmonic phase angles do not show a clear daily pattern.
- Harmonic current unbalances are mostly higher than 10% and increase considerably with the harmonic order. Furthermore, harmonic current unbalance is usually not linked to fundamental current unbalance and can be high even if the fundamental current unbalance is low. It is strongly recommended to include harmonic unbalance in harmonic studies of low-voltage networks in order to obtain more accurate and realistic results, especially if the propagation of harmonic currents to the upstream medium-voltage network is of interest.
- Climatic conditions (seasonal variations) and social environment have an influence on the harmonic emission of residential customers, due to their effect on the customers behavior and energy consumption. In Germany, the social environment does not show a clear influence on the harmonic emission characteristics. Different results may be obtained with measurements from other countries.

Stochastic harmonic emission model of aggregate residential customers

- Using the measurement-based approach, a generic stochastic model that represents the typical harmonic emission of the residential low-voltage networks was developed. The model represents the random variations of the first 15 odd harmonic magnitudes and phase angles, considering the daily variations of harmonic magnitudes and the harmonic unbalances. This model is useful for the simulation of medium-voltage networks, where the harmonic emission of the complete residential networks is required.
- Accurate representation of the harmonic unbalance was achieved modeling the symmetrical components (balanced and unbalanced harmonic currents), instead of the phase currents.
  - The balanced current magnitude was described with a stochastic time-series model, which consists of two main parts: a deterministic component (Fourier series) that describes the daily variations of harmonic magnitudes, and a stochastic component (autoregressive model of first order) that represents the random variations around the deterministic component.
  - The unbalanced current magnitudes are represented by autoregressive models of first order that represent the random variation of both unbalanced currents, but including the dependence between successive values.
  - The balanced and unbalanced current phase angles are described with a von Mises distribution, which is a circular analogue of the normal distribution.
- A top-down approach was applied to extend the stochastic model of low-voltage residential networks to represent small groups of customers (feeder or feeder section) that can be used in simulations of low-voltage networks. The applied top-down approach does not change the parameters of the original stochastic model, but introduces a new variable, Customers aggregation factor, that modifies the harmonic magnitudes in order to include the complex aggregation characteristic of harmonic currents in low-voltage networks.

Future work

- The Current source model can be used to represent the harmonic emission of aggregate customers only if the network does not have resonances, and the ratio between the network and the customer impedance is high. However, measurements of low-voltage and medium-voltage networks have shown that these conditions are not always satisfied for all harmonic orders. For those cases, Norton models that include the harmonic impedance of the customers are recommended.

  Comprehensive research projects are required to estimate the harmonic impedance of the aggregate customers. One of the main challenges is the correct measurement of the harmonic impedances in the network, which usually requires specialized measurement systems. Once the measurements of the impedance at several networks are collected, a model of the impedance can be obtained, allowing a better representation of the aggregate customers.

- The stochastic model can be extended to include the seasonal variations and trends of the harmonics, caused by the change in the usage behavior and load composition over the years. This extension requires continuous monitoring of different networks. However, the storage of the data becomes a mayor issue. Methods to analyze and extract the main information of the measurements (data mining) are required, in order to reduce the amount of information that should be stored.

  A possible way to reduce the amount of needed storage is to apply the model presented in this thesis, to extract the main characteristics of the harmonic magnitudes and phase angles. In concrete, the model can be applied to each week of measurements and each measurement site. The obtained parameters are stored, and they can be later applied to recreate the behavior of the original data, monitor the changes in the harmonic magnitudes and phase angles during time, and compare the behavior on different networks. The memory space required to store the parameters of the model will be considerably smaller than the memory required to store the original measurement data.

- The low-voltage networks are comprised of other types of customers and loads, like commercial customers, offices, hospitals, photovoltaic systems, night storage systems, etc. Models that represent those customers or loads are also required for complete and accurate simulations of distribution networks. The modeling methodology presented in this thesis may be also useful for the modeling of other customers.

9. Bibliography

[1] S. Abdelkader, M. Abdel-Rahman, and M. Osman. "A Norton equivalent model for non-linear loads." In: *Large Engineering Systems Conference on Power Engineering*. Halifax, Canada: IEEE, 2001, pp. 63–67. ISBN: 0-7803-7107-0.

[2] E. Ahmed, W. Xu, and G. Zhang. "Analyzing systems with distributed harmonic sources including the attenuation and diversity effects." In: *IEEE Transactions on Power Delivery* vol. 20. no. 4 (2005), pp. 2602–2612. ISSN: 0885-8977.

[3] C. F. M. Almeida and N. Kagan. "Harmonic coupled Norton equivalent model for modeling harmonic-producing loads." In: *14th International Conference on Harmonics and Quality of Power - ICHQP*. Bergamo, Italy: IEEE, Sept. 2010, pp. 1–9. ISBN: 978-1-4244-7244-4.

[4] C. F. M. Almeida and N. Kagan. "A novel technique for modeling aggregated harmonic-producing loads." In: *21st International Conference on Electricity Distribution - CIRED*. Frankfurt, Germany: IEEE, 2011, pp. 1–4.

[5] J. Arrillaga and N. R. Watson. *Power System Harmonics*. Chichester, UK: John Wiley & Sons, Ltd, Sept. 2003. ISBN: 0470851295.

[6] M. T. Au and J. V. Milanovic. "Stochastic assessment of harmonic distortion level of medium voltage radial distribution network." In: *International Conference on Probabilistic Methods Applied to Power Systems*. Stockholm, Sweden: IEEE, June 2006, pp. 1–6. ISBN: 978-91-7178-585-5.

[7] M. T. Au and J. V. Milanovic. "Development of stochastic aggregate harmonic load model based on field measurements." In: *IEEE Transactions on Power Delivery* vol. 22. no. 1 (Jan. 2007), pp. 323–330. ISSN: 0885-8977.

[8] M. T. Au and J. V. Milanovic. "Establishing harmonic distortion level of distribution network based on stochastic aggregate harmonic load models." In: *IEEE Transactions on Power Delivery* vol. 22. no. 2 (Apr. 2007), pp. 1086–1092. ISSN: 0885-8977.

[9] Y. Baghzouz and O. T. Tan. "Probabilistic modeling of power system harmonics." In: *IEEE Transactions on Industry Applications* vol. IA-23. no. 1 (Jan. 1987), pp. 173–180. ISSN: 0093-9994.

[10] Y. Baghzouz et al. "Time-varying harmonics: Part I - Characterizing measured data." In: *IEEE Transactions on Power Delivery* vol. 13. no. 3 (July 1998), pp. 938–944. ISSN: 08858977.

[11] P. Berens. "CircStat: A Matlab toolbox for circular statistics." In: *Journal of Statistical Software* vol. 31. no. 10 (2009), pp. 1–21. ISSN: 19395108.

[12] S. Bhattacharyya, J. F. G. Cobben, and W. L. Kling. "Harmonic current pollution in a low voltage network." In: *IEEE Power and Energy Society General Meeting*. Providence, USA: IEEE, July 2010, pp. 1–8. ISBN: 978-1-4244-6549-1.

[13] A. M. Blanco, J. Meyer, and P. Schegner. "Aggregation characteristic of low-order harmonic currents in residential low-voltage networks." In: *PowerTech*. Manchester, UK: IEEE, 2017.

[14] A. M. Blanco, R. Stiegler, and J. Meyer. "Power quality disturbances caused by modern lighting equipment (CFL and LED)." In: *Powertech*. Grenoble, France: IEEE, June 2013, pp. 1–6. ISBN: 978-1-4673-5669-5.

[15] A. M. Blanco et al. “Impact of supply voltage distortion on the harmonic emission of electronic household equipment.” In: *VII Simposio Internacional sobre Calidad de la Energía Eléctrica - SICEL*. Medellin, Colombia, 2013, pp. 1–8.

[16] A. M. Blanco et al. “Stochastic harmonic load model of residential users based on measurements.” In: *PowerTech*. Eindhoven, Netherlands: IEEE, June 2015, pp. 1–6. ISBN: 978-1-4799-7693-5.

[17] A. M. Blanco et al. “Impact of supply voltage distortion on the current harmonic emission of non-linear loads.” In: *Dyna* vol. 82. no. 192 (2015), pp. 150–159. ISSN: 2346-2183.

[18] A. M. Blanco et al. “Implementation of harmonic phase angle measurement for power quality instruments.” In: *IEEE International Workshop on Applied Measurements for Power Systems - AMPS*. Aachen, Germany: IEEE, 2016, pp. 1–6. ISBN: 978-1-5090-2373-8.

[19] A. M. Blanco et al. “Survey of harmonic current unbalance in public low voltage networks.” In: *17th International Conference on Harmonics and Quality of Power - ICHQP*. Belo Horizonte, Brazil: IEEE, 2016, pp. 289–294. ISBN: 978-1-5090-3792-6.

[20] M. Bollen and I. Gu. *Signal porcessing of power quality disturbances*. John Wiley & Sons, Ltd, 2006.

[21] M. Bollen et al. “Standards for supraharmonics (2 to 150 kHz).” In: *IEEE Electromagnetic Compatibility Magazine* vol. 3. no. 1 (2014), pp. 114–119. ISSN: 2162-2264.

[22] A. Bosovic et al. “Validation of aggregated harmonic current source models based on different customer type configurations.” In: *Electric Power Quality and Supply Reliability*. Tallinn, Estonia: IEEE, Aug. 2016, pp. 77–84. ISBN: 978-1-5090-1562-7.

[23] G. E. Box, G. M. Jenkins, and G. C. Reinsel. *Time series analysis. Forecasting and control*. 4th editio. Hoboken, New Jersey: John Wiley & Sons, Inc., 2008.

[24] G. Brauner and P. Kaluza. “New method for stochastic power quality simulation.” In: *Quality of Power Supply*. Ed. by VDE-Verlag GMBH. Munich, Germany: VDE-Verlag GMBH, 1997, pp. 49–54.

[25] A. Capasso, R. Lamedica, and A. Prudenzi. “Estimation of net harmonic currents due to dispersed nonlinear loads within residential areas.” In: *8th International Conference on Harmonics and Quality of Power - ICHQP*. Vol. 2. Athens, Greece: IEEE, 1998, pp. 700–705. ISBN: 0-7803-5105-3.

[26] A. Cavallini and G. Montanari. “A deterministic/stochastic framework for power system harmonics modeling.” In: *IEEE Transactions on Power Systems* vol. 12. no. 1 (1997), pp. 407–415.

[27] A. Cavallini et al. “Gaussian modeling of harmonic vectors in power systems.” In: *8th International Conference on Harmonics and Quality of Power - ICHQP*. Athens, Greece: IEEE, 1998, pp. 1010–1017. ISBN: 0-7803-5105-3.

[28] D. Chakravorty et al. “Impact of modern electronic equipment on the assessment of network harmonic impedance.” In: *IEEE Transactions on Smart Grid* vol. 8. no. 1 (2017), pp. 382–390. ISSN: 19493053.

[29] CIGRÉ Task Force C6.04.02. *Technical brochure 575 - Benchmark systems for network integration of renewable and distributed energy resources*. Tech. rep. CIGRÉ, 2014.

[30] S. Cobben, W. Kling, and J. Myrzik. “The making and purpose of harmonic fingerprints.” In: *19th International Conference on Electricity Distribution - CIRED*. Viena, Austria: CIRED, 2007, pp. 1–4.

[31] A. Collin et al. “Component-based aggregate load models for combined power flow and harmonic analysis.” In: *7th Mediterranean Conference and Exhibition on Power Generation, Transmission, Distribution and Energy Conversion - MedPower*. Agia Napa, Cyprus: IET, 2010, pp. 352–361. ISBN: 978 1 84919 319 1.

[32] A. Collin et al. “An 11 kV steady state residential aggregate load model. Part 1: Aggregation methodology.” In: *PowerTech*. Trondheim, Norway: IEEE, June 2011, pp. 1–8. ISBN: 978-1-4244-8418-8.

[33] A. Collin et al. “Simulating the time-varying harmonics of the residential load sector.” In: *16th International Conference on Harmonics and Quality of Power - ICHQP*. Bucharest, Romania: IEEE, May 2014, pp. 768–772. ISBN: 978-1-4673-6487-4.

[34] C. Cresswell. “Steady state load models for power system analysis.” Doctoral thesis. The University of Edinburgh, 2009.

[35] J. Crucq and A. Robert. “Statistical approach for harmonics measurements and calculations.” In: *10th International Conference on Electricity Distribution - CIRED*. Brighton, UK: CIRED, 1989, pp. 91–96.

[36] J. Cunill-Sola and M. Salichs. “Study and characterization of waveforms from low-watt compact fluorescent lamps with electronic ballast.” In: *IEEE Transactions on Power Delivery* vol. 22. no. 4 (2007), pp. 2305–2311.

[37] L. S. Czarnecki. “Comments on active power flow and energy accounts in electrical systems with nonsinusoidal waveforms and asymmetry.” In: *IEEE Transactions on Power Delivery* vol. 11. no. 3 (1996), pp. 1244–1250. ISSN: 08858977.

[38] J. Das. *Power system analysis: short-circuit load flow and harmonics*. New York, USA: Marcel Dekker, 2002.

[39] F. C. De la Rosa. *Harmonics and Power Systems*. Boca Raton, USA: CRC Press, 2006. ISBN: 9780849330162.

[40] T. Deflandre et al. *Modeling distribution networks for simulation of harmonics on HV systems*. 1996.

[41] Deutsche Wetterdienst. *Climate Data Center*. URL: `http://www.dwd.de/DE/klimaumwelt/cdc/cdc%7B%5C_%7Dnode.html` (visited on 02/08/2014).

[42] J. Dickert. “Synthese von Zeitreihen elektrischer Lasten basierend auf technischen und sozialen Kennzahlen. Grundlage für Planung, Betrieb und Simulation von aktiven Verteilungsnetzen.” Doctoral thesis. Technische Universität Dresden, 2015.

[43] J. Dickert, M. Domagk, and P. Schegner. “Benchmark low voltage distribution networks based on cluster analysis of actual grid properties.” In: *PowerTech*. Grenoble, France: IEEE, June 2013, pp. 1–6. ISBN: 978-1-4673-5669-5.

[44] M. Domagk. “Identifikation und Quantifizierung korrelativer Zusammenhänge zwischen elektrischer sowie klimatischer Umgebung und Elektroenergiequalität.” Doctoral thesis. Technische Universität Dresden, 2015.

[45] M. Domagk, J. Meyer, and P. Schegner. “Characterization of public low voltage grids by clustering time series of power quality parameters.” In: *12th International Conference on Probabilistic Methods Applied to Power Systems*. Istambul, Turkey: PMAPS, 2012, pp. 558–563.

[46] M. Domagk, J. Meyer, and P. Schegner. “Seasonal variations in long-term measurements of power quality parameters.” In: *PowerTech*. Eindhoven, Netherlands: IEEE, 2015, pp. 1–6.

[47] M. Domagk et al. “Trend identification in power quality measurements.” In: *Australasian Universities Power Engineering Conference - AUPEC*. Wollongong, Australia: IEEE, 2015, pp. 1–6.

[48] R. C. Dugan et al. *Electrical power systems quality. 3rd edition.* 3rd editio. McGraw Hill, 2012. ISBN: 9780071761550.

[49] M. El Arini. “A time domain load modelling technique and harmonics analysis.” In: *8th International Conference on Harmonics and Quality of Power - ICHQP*. Athens, Greece: IEEE, 1998, pp. 930–938. ISBN: 0-7803-5105-3.

[50] A. Elmoudi, M. Lehtonen, and H. Nordman. “Effect of harmonics on transformers loss of life.” In: *IEEE International Symposium on Electrical Insulation*. Vol. 2. IEEE, 1995, pp. 408–411. ISBN: 1-4244-0333-2.

[51] M. Fauri. “Harmonic modelling of non-linear load by means of crossed frequency admittance matrix.” In: *IEEE Transactions on Power Systems* vol. 12. no. 4 (1997), pp. 1632–1638. ISSN: 08858950.

[52] L. Feola, R. Langella, and A. Testa. “On the effects of unbalances, harmonics and interharmonics on PLL systems.” In: *IEEE Transactions on Instrumentation and Measurement* vol. 62. no. 9 (2013), pp. 2399–2409. ISSN: 00189456.

[53] N. Fisher. *Statistical analysis of circular data*. New York, USA: Cambridge University Press, 1993. ISBN: 9780511564345.

[54] R. Follmer et al. *Mobilität in Deutschland 2008. Ergebnisbericht. Struktur - Aufkommen - Emissionen - Trends*. Tech. rep. Bonn and Berlin, Germany, 2010. URL: `http://www.mobilitaet-in-deutschland.de/mid2008-publikationen.html`.

[55] S. Frank et al. “Reevaluation of induction motor loss models for conventional and harmonic power flow.” In: *North American Power Symposium - NAPS*. Champaign, USA: IEEE, Sept. 2012, pp. 1–6. ISBN: 978-1-4673-2308-6.

[56] E. F. Fuchs and M. A. Masoum. *Power Quality in Power Systems and Electrical Machines*. Academic Press, 2008.

[57] T. Goeke and W. Wellssow. “A statistical approach to the calculation of harmonics in MV systems caused by dispersed LV customers.” In: *IEEE Transactions on Power Systems* vol. 11. no. 1 (1996), pp. 325–331. ISSN: 08858950.

[58] T. Gönen. *Electric power distribution engineering*. 3rd edition. Boca Raton, USA: CRC Press, 2014. ISBN: 9781482207002.

[59] O. Gul and J. Milanovic. “Sensitivity of harmonic load model parameters to voltage and current waveforms.” In: *9th International Conference on Harmonics and Quality of Power - ICHQP*. Orlando, USA: IEEE, 2000, pp. 1041–1046. ISBN: 0-7803-6499-6.

[60] J. Han, M. Kamber, and J. Pei. *Data Mining Concepts and Techniques*. 3rd editio. Morgan Kaufmann Publishers, 2012. ISBN: 978-0123814791.

[61] S. Hansen, P. Nielsen, and F. Blaabjerg. “Harmonic cancellation by mixing nonlinear single-phase and three-phase loads.” In: *IEEE Transactions on Industry Applications* vol. 36. no. 1 (2000), pp. 152–159.

[62] IEC International Electrotechnical Comission. *IEC/TR 61000-1-1. Electromagnetic compatibility (EMC) - Part 1: General - Section 1: Application and interpretation of fundamental definitions and terms*. 1992.

[63] IEC International Electrotechnical Comission. *IEC 61000-2-2:2002. Electromagnetic Compatibility (EMC) - Pat 2-2: Environment - Compatibility levels for low-frequency conducted disturbances and signaling in public low-voltage power supply systems*. 2003.

[64] IEC International Electrotechnical Comission. *IEC 61000-3-6 TR Ed.2 Assessment of emission limits for the connection of distorting installations to MV, HV and EHV power systems*. 2007.

[65] IEC International Electrotechnical Comission. *IEC 62428:2008 Electric power engineering - Modal components in three-phase A.C. systems - Quantities and transformations*. 2008.

[66] IEC International Electrotechnical Comission. *IEC 61000-4-7:2002+A1:2008. Electromagnetic compatibility (EMC) - Part 4-7: Testing and measurement techniques - General guide on harmonics and interharmonics measurements and instrumentation, for power supply systems and equipment conected thereto*. 2009.

[67] IEC International Electrotechnical Comission. *IEC 61000-3-12:2011 Electromagnetic compatibility (EMC) - Part 3-12: Limits - Limits for harmonic currents produced by equipment connected to public low-voltage systems with input current >16 A and ≤75 A per phase*. 2011.

[68] IEC International Electrotechnical Comission. *Standard IEC 61000-4-30 - Testing and measurement techniques - Power quality measurement methods*. 2012.

[69] IEC International Electrotechnical Comission. *IEC 61000-3-2:2014. Electromagnetic compatibility (EMC) - Part 3-2: Limits - Limits for harmonic current emissions (equipment input current 16 A per phase)*. 2014.

[70] IEEE Power & Energy Society. *IEEE Std 1459 Standard Definitions for the measurement of electric power quantities under sinusoidal, nonsinusoidal, balanced, or unbalanced conditions*. New York, USA, 2010.

[71] V. Ignatova et al. "Statistical matrix representation of time-varying electrical signals. reconstruction and prediction applications." In: *9th International Conference on Probabilistic Methods Applied to Power Systems - PMAPS*. Stockholm, Sweden: IEEE, 2006, pp. 1–6. ISBN: 9171783520.

[72] Institut für Elektrische Energieversorgung und Hochspannungstechnik. *Equipment Harmonic Database - PANDA*. 2012. URL: `http://panda.et.tu-dresden.de/`.

[73] G. J. Janacek, a. J. Bagnall, and M. Powell. "A likelihood ratio distance measure for the similarity between the Fourier transform of time series." In: *9th Pacific-Asia Conference on Advances in Knowledge Discovery and Data Mining*. Hanoi, Vietnam, 2005, pp. 737–743. ISBN: 3-540-26076-5, 978-3-540-26076-9.

[74] C. Jiang et al. "Assessing the collective harmonic impact of modern residential loads - part II: Applications." In: *IEEE Transactions on Power Delivery* vol. 27. no. 4 (2012), pp. 1947–1955. ISSN: 0885-8977.

[75] M. Jordan. "Untersuchung von Methoden zur Identifikation der zeit- und frequenzabhängigen Netzimpedanz (Investigation of methods for the identification of time and frequency-dependent network impedances)." Doctoral dissertation. Helmut Schmidt Universität, 2016.

[76] E. Kazibwe, T. Ortmeyer, and M. Hammam. "Summation of probabilistic harmonic vectors." In: *IEEE Transactions on Power Delivery* vol. 4. no. 1 (1989), pp. 621–628. ISSN: 08858977.

[77] A. S. Koch et al. "Harmonic measurement and modeling for mass implementation of nonlinear appliances." In: *IEEE Power and Energy Society General Meeting*. San Diego, USA: IEEE, 2012, pp. 1–6. ISBN: 9781467327275.

[78] A. S. Koch et al. "Evaluation and validation of Norton approaches for nonlinear harmonic models." In: *PowerTech*. Grenoble, France: IEEE, 2013, p. 6.

[79] P. Korovesis et al. “Influence of large-scale installation of energy saving lamps on the line voltage distortion of a weak network supplied by photovoltaic station.” In: *IEEE Transactions on Power Delivery* vol. 19. no. 4 (2004), pp. 1787–1793. ISSN: 0885-8977.

[80] M. Kumar, N. R. Patel, and J. Woo. “Clustering seasonality patterns in the presence of errors.” In: *8th International conference on knowledge discovery and data mining*. Alberta, Canada, 2002, pp. 557–563. ISBN: 158113567X.

[81] L. Kutt et al. “Harmonic load of residential distribution network - Case study monitoring results.” In: *Electric Power Quality and Supply Reliability Conference*. IEEE, June 2014, pp. 93–98. ISBN: 978-1-4799-5022-5.

[82] J. Lachaume, T. Deflandre, and M. Meunier. “Harmonics in MV and LV distribution systems: present and future levels.” In: *12th International Conference on Electricity Distribution -CIRED*. Birmingham, UK: CIRED, 1993, pp. 1–5.

[83] C. Y. Lee, Y. J. Lin, and C. R. Chen. “The effect of harmonic phase angle on the operation performance of a three-phase induction motor.” In: *Power Engineering Society Summer Meeting*. Seattle, USA: IEEE, 2000, pp. 2499–2505. ISBN: 0780364201.

[84] E. Makram and S. Varadan. “A generalized load modeling technique using actual recorded data and its use in a harmonic load flow program.” In: *Electric Power Systems Research* vol. 27 (1993), pp. 203–208.

[85] J. Maletic and A. Marcus. “Data cleansing: A prelude to knowledge discovery.” In: *Data Mining and Knowledge Discovery Handbook*. Ed. by O. Maimon and L. Rokach. Boston, MA: Springer US, 2010. Chap. 2. ISBN: 978-0-387-09822-7.

[86] A. Mansoor et al. “An investigation of harmonics attenuation and diversity among distributed single-phase power electronic loads.” In: *IEEE Transactions on Power Delivery* vol. 10. no. 1 (1995), pp. 467–473.

[87] A. Mansoor et al. “Effect of supply voltage harmonics on the input current of single-phase diode bridge rectifier loads.” In: *IEEE Transactions on Power Delivery* vol. 10. no. 3 (July 1995), pp. 1416–1422. ISSN: 08858977.

[88] A. Mansoor et al. “Predicting the net harmonic currents produced by large numbers of distributed single-phase computer loads.” In: *IEEE Transactions on Power Delivery* vol. 10. no. 4 (1995), pp. 2001–2006. ISSN: 08858977.

[89] K. V. Mardia and P. E. Jupp. *Directional Statistics*. Wiley Series in Probability and Statistics. Hoboken, NJ, USA: John Wiley & Sons, Inc., 1999. ISBN: 9780470316979. URL: http://doi.wiley.com/10.1002/9780470316979.

[90] H. E. Mazin et al. “A study on the harmonic contributions of residential loads.” In: *IEEE Transactions on Power Delivery* vol. 26. no. 3 (July 2011), pp. 1592–1599. ISSN: 0885-8977.

[91] A. Medina et al. “Harmonic analysis in frequency and time domain.” In: *IEEE Transactions on Power Delivery* vol. 28. no. 3 (2013), pp. 1813–1821. ISSN: 08858977.

[92] J. Meyer and J. Kilter. “Case studies for power quality monitoring in public distribution grids – some results of working group CIGRE / CIRED C4 .112.” In: *Electric Power Quality and Supply Reliability Conference*. Rakvere, Estonia: IEEE, 2014. ISBN: 9781479950225.

[93] J. Meyer and P. Schegner. “Characterization of power quality in low voltage networks based on modeling by mixture distributions.” In: *International Conference on Probabilistic Methods Applied to Power Systems*. Stockholm, Sweden: IEEE, June 2006, pp. 1–6. ISBN: 978-91-7178-585-5.

[94] J. Meyer et al. “Accuracy of harmonic voltage measurements in the frequency range up to 5 kHz using conventional instrument transformers.” In: *21st International Conference on Electricity Distribution - CIRED*. Frankfurt, Germany: CIRED, 2011, pp. 1–4.

[95] J. Meyer et al. “Harmonic resonances in residential low voltage networks caused by customer electronics.” In: *24th International Conference on Electricity Distribution - CIRED*. Gasgow, UK: CIRED, 2017, pp. 1–5.

[96] J. Meyer et al. “Assessment of prevailing harmonic current emission in public low-voltage networks.” In: *IEEE Transactions on Power Delivery* vol. 32. no. 2 (Apr. 2017), pp. 962–970. ISSN: 0885-8977.

[97] L. Miegeville and P. Guerin. “Identification of the time-varying pattern of periodic harmonics.” In: *IEEE Transactions on Power Delivery* vol. 21. no. 2 (Apr. 2006), pp. 845–851. ISSN: 0885-8977.

[98] L. Miegeville, P. Guerin, and R. Le Doeuff. “Identification of the harmonic currents drawn by an institutional building: application of a stochastic approach.” In: *9th International Conference on Harmonics and Quality of Power - ICHQP*. Orlando, USA: IEEE, 2000, pp. 595–601. ISBN: 0-7803-6499-6.

[99] F. Möller, J. Meyer, and P. Schegner. “Load model of electric vehicles chargers for load flow and unbalance studies.” In: *Electric Power Quality and Supply Reliability Conference*. Rakvere, Estonia: IEEE, 2014. ISBN: 9781479950225.

[100] F. Möller et al. “Impact of Electric Vehicle Charging on Unbalance and Harmonic Distortion – Field Study in an Urban Residential Area.” In: *23rd International Conference on Electricity Distribution (CIRED)*. Lyon, France, 2015.

[101] S. Müller et al. “Impact of a high penetration of electric vehicles and photovoltaic inverters on power quality in an urban residential grid part II – Harmonic distortion key words.” In: *International Conference on Renewable Energies and Power Quality - ICREPQ*. Madrid, Spain, 2016.

[102] A. Nassif and W. Xu. “Characterizing the harmonic attenuation effect of compact fluorescent lamps.” In: *IEEE Transactions on Power Delivery* vol. 24. no. 3 (July 2009), pp. 1748–1749. ISSN: 0885-8977.

[103] A. Nassif, J. Yong, and W. Xu. “Measurement-based approach for constructing harmonic models of electronic home appliances.” In: *IET Generation, Transmission & Distribution* vol. 4. no. 3 (2010), pp. 363–375. ISSN: 17518687.

[104] A. B. Nassif and J. Acharya. “An investigation on the harmonic attenuation effect of modern compact fluorescent lamps.” In: *13th International Conference on Harmonics and Quality of Power - ICHQP*. Wollongong, Australia: IEEE, 2008, pp. 1–6. ISBN: 9781424417704.

[105] E. E. Nino and W. Xu. “Measurement of Harmonic Sources in Three-Wire Single-Phase Supply Systems.” In: *IEEE Transactions on Power Delivery* vol. 22. no. 4 (2007), pp. 2527–2533. ISSN: 0885-8977.

[106] D. Oeding and B. R. Oswald. *Elektrische Kraftwerke und Netze*. Berlin, Heidelberg: Springer, 2011. ISBN: 978-3-642-19245-6.

[107] E. Palmer and G. F. Ledwich. “Three phase harmonic modelling of power system loads.” In: *IEE Generation, Transmission and Distribution* vol. 140. no. 3 (1993), pp. 206–212.

[108] L. Pierce. “Transformer design and application considerations for nonsinusoidal load currents.” In: *IEEE Transactions on Industry Applications* vol. 32. no. 3 (1996), pp. 633–645. ISSN: 00939994.

[109] D. Rafiei. “Fourier-transform based techniques in efficient retrieval of similar time sequences.” Doctoral thesis. University of Toronto, 1999.

[110] T. A. Reddy. *Applied Data Analysis and Modeling for Energy Engineers and Scientists*. Boston, USA: Springer US, 2011. ISBN: 978-1-4419-9612-1.

[111] A. A. Romero et al. "A novel fuzzy number based method to model aggregate loads for harmonic load-flow calculation." In: *Transmission and Distribution Conference and Exposition: Latin America*. Bogota, Colombia: IEEE, Aug. 2008, pp. 1–8. ISBN: 978-1-4244-2217-3.

[112] S. Rönnberg, M. Bollen, and A. Larsson. "Grid impact from PV-installations in Northern Scandinavia." In: *22th International Conference on Electricity Distribution - CIRED*. Stockholm, Sweden: CIRED, 2013.

[113] D. Salles et al. "Assessing the collective harmonic impact of modern residential loads—Part I: Methodology." In: *IEEE Transactions on Power Delivery* vol. 27. no. 4 (2012), pp. 1937–1946. ISSN: 0885-8977.

[114] W. G. Sherman. "Summation of harmonics with random phase angles." In: *Proceedings of the Institution of Electrical Engineers* vol. 119. no. 11 (1972), pp. 1643–1648.

[115] J. Smith et al. *Power quality aspects of solar power*. Tech. rep. CIGRE, 2016.

[116] S. A. Soliman, N. Abbasy, and M. El-Hawary. "Frequency domain modelling and identification of nonlinear loads using a least error squares algorithm." In: *Electric Power Systems Research* vol. 40. no. 1 (Jan. 1997), pp. 1–6. ISSN: 03787796.

[117] S. A. Soliman, A. M. Al-Kandari, and M. E. El-Hawary. "Time domain estimation techniques for harmonic load models." In: *Electric Machines & Power Systems* vol. 25. no. 8 (Sept. 1997), pp. 885–896. ISSN: 0731-356X.

[118] S. Soliman and R. Alammari. "Harmonic modeling of linear and nonlinear loads based on Kalman filtering algorithm." In: *Electric Power Systems Research* vol. 72. no. 2 (2004), pp. 147–155. ISSN: 03787796.

[119] A. M. Stankovic and E. a. Marengo. "A dynamic characterization of power system harmonics using markov chains." In: *IEEE Transactions on Power Systems* vol. 13. no. 2 (1998), pp. 442–448. ISSN: 08858950.

[120] Statista. *Anzahl der Elektroautos in Deutschland von 2006 bis 2017*. 2017. URL: `https://de.statista.com/statistik/daten/studie/265995/umfrage/anzahl-der-elektroautos-in-deutschland/`.

[121] Statistisches Bundesamt Deutschland. *Laufende Wirtschaftsrechnungen Ausstattung privater Haushalte mit ausgewählten Gebrauchsgütern. Fachserie 15 Reihe 2*. Tech. rep. Wiesbaden, germany, 2016.

[122] Statistisches Bundesamt Deutschland. *Regionaldatenbank Deutschland*. URL: `https://www.regionalstatistik.de/genesis/online` (visited on 02/08/2014).

[123] R. Stiegler et al. "Measurement of network harmonic impedance in presence of electronic equipment." In: *International Workshop on Applied Measurements for Power Systems - AMPS*. Aac: IEEE, 2015. ISBN: 9781479999989.

[124] Task Force on Harmonics Modeling and Simulation. "Characteristics and modeling of harmonic sources - power electronic devices." In: *IEEE Transactions on Power Delivery* vol. 16. no. 4 (2001), pp. 791–800. ISSN: 08858977.

[125] Task Force on Harmonics Modeling and Simulation. "Modeling devices with nonlinear voltage-current characteristics for harmonic studies." In: *IEEE Transactions on Power Delivery* vol. 19. no. 4 (Oct. 2004), pp. 1802–1811. ISSN: 0885-8977. URL: `http://ieeexplore.ieee.org/lpdocs/epic03/wrapper.htm?arnumber=1339349`.

[126] S. Theodoridis and K. Koutroumbas. *Pattern Recognition, 4th edition*. Elsevier Inc., 2009.

[127] E. Thunberg. "On the Benefit of Harmonic Measurements in Power Systems." Doctoral Thesis. Royal Institute of Technology, 2001.

[128] E. Thunberg and L. Soder. "A Norton approach to distribution network modeling for harmonic studies." In: *IEEE Transactions on Power Delivery* vol. 14. no. 1 (1999), pp. 272–277. ISSN: 08858977.

[129] VEÖ et al. *D-A-CH-CZ Technical rules for the assessment of network disturbances*. 2007.

[130] L. Wagmann and Z. Beničić. "Stochastic deterministic method of Monte Carlo simulation of harmonic currents at MV/LV transformer stations." In: *Engineering Review* vol. 30. no. 1 (2010), pp. 23–34.

[131] G. Wakileh. *Power System Harmonics. Fundamentals, analysis and filter design*. Springer, 2001.

[132] T. Warren Liao. "Clustering of time series data - A survey." In: *Pattern Recognition* vol. 38. no. 11 (2005), pp. 1857–1874. ISSN: 00313203.

[133] N. Watson, T. Scott, and S. Hirsch. "Implications for Distribution Networks of High Penetration of Compact Fluorescent Lamps." In: *IEEE Transactions on Power Delivery* vol. 24. no. 3 (July 2009), pp. 1521–1528. ISSN: 0885-8977.

[134] Z. Wei, N. Watson, and L. Frater. "Modelling of compact fluorescent lamps." In: *13th International Conference on Harmonics and Quality of Power - ICHQP*. Wollongong, Australia: IEEE, 2008, pp. 1–6. ISBN: 978-1-4244-1771-1.

[135] G. Ye et al. "Stochastic residential harmonic source modeling for grid impact studies." In: *Energies* vol. 10. no. 3 (Mar. 2017), p. 372. ISSN: 1996-1073.

[136] J. Yong, A. Nassif, and W. Xu. "Effect of voltage crest shape on the harmonic amplification and attenuation of diode-bridge converter-based loads." In: *IET Generation, Transmission & Distribution* vol. 5. no. 10 (2011), p. 1033. ISSN: 17518687.

[137] X. Zhang et al. "A novel clustering method on time series data." In: *Expert Systems with Applications* vol. 38. no. 9 (2011), pp. 11891–11900. ISSN: 09574174.

List of Figures

List of Tables

Appendices

A. Measurement campaign

A.1. Measurement campaign

Measurements of several low-voltage networks were carried out in different cities and towns in Germany with the collaboration of 32 network operators. The measurements were made at the low-voltage side of the distribution transformer, either at the whole substation or at one of its feeders. The RMS voltage and RMS current, the harmonic voltages and harmonic currents up to 50^{th} order, the active, and apparent power and the total voltage and current distortion (THD) were recorded. Additionally, information about the electrical characteristics of the network or feeder, the social environment, and the climate conditions during the measurements were also available. The electrical characteristics were provided by the network operators, while the information about the social environment and the climate conditions were obtained from the Federal Statistical Office of Germany [122] and the German Meteorological Service [41], respectively. Fig. 4.1 shows all the available parameters that describe the electrical and non-electrical characteristics of each of the measured sites.

Each site was measured with a single type of power quality analyzer, which complies with IEC 61000-4-30 class A [68]. The measurement period was between 1 to 4 weeks with an aggregation interval of 1 minute. Harmonic magnitudes were aggregated according to the IEC 61000-4-30 (RMS value), while the harmonic phase angles were aggregated based on the phasor sum of the 10-period harmonic phasors measurements in the considered aggregation interval, as explained in [18, 96]. The reference of the harmonic phase angles of each line conductor is the zero-crossing of the voltage fundamental of the respective line conductor, i.e. the "absolute" phase angles as defined in the standard IEC 61000-3-12 [67] were obtained. In this thesis only the magnitude and phase angle of the harmonic currents were further processed.

The measurement campaign was carried out during winter, when the emission levels in Germany are in general slightly higher compared to the summer months [44]. Moreover, the measurements were made during the same year and during the same season in order to reduce the influence of seasonal variations and trends.

Moreover, networks with a high number of photovoltaic systems were also not considered. The impact of photovoltaic systems on the harmonic levels of low-voltage networks has been studied over the last decades, and several dedicated measurements have corroborated that the level of harmonic currents in the network change when photovoltaic systems are introduced (e.g. [101, 112, 115]). Therefore, only sites with no or a very small penetration of distributed generation were selected (penetration of distributed generation is measured with the ratio of the rated power of the distributed generators $P_{\mathrm{G\ TOT}}$ and the rated power of the distribution transformer $S_{\mathrm{r\ T}}$. Low penetration: $P_{\mathrm{G\ TOT}} \leq 0.1 \cdot S_{\mathrm{r\ T}}$ [96]).

The sample contains 76 sites located in different regions in Germany and from different types of settlements. Fig. A.1 shows the percentage of networks from different types of settlements which were defined according to the population density ρ_{pop} as follow:

- Rural settlement: $\rho_{\mathrm{pop}} \leq 100\ \mathrm{habitants/km}^2$
- Suburban: $100 < \rho_{\mathrm{pop}} \leq 1000\ \mathrm{habitants/km}^2$

- Urban: $1000 < \rho_{\mathrm{pop}} \leq 2000$ habitants/km^2
- Highly urban: $\rho_{\mathrm{pop}} > 2000$ habitants/km^2

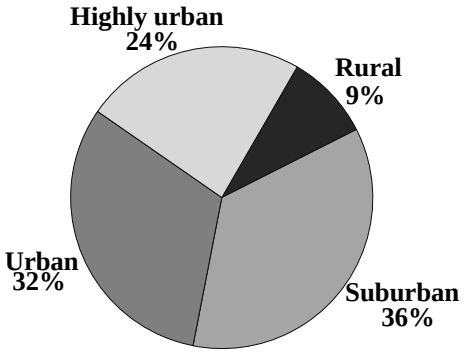

Figure A.1.: Distribution of the low-voltage networks according to the type of settlement.

The sites also have different consumer and network topologies (c.f. Fig. 4.1). In order to facilitate the classification of the measured sites according to their electrical characteristics, the following categories were defined:

- Customer topology: Indicates the type of housing of the customers. This category is subdivided into the following subcategories:
  - C1 - Residential sites where the number of customers living in single-family houses represents at least 80% of the total number of customers: $n_{\mathrm{u\ SFH}} \geq 0.8 \cdot n_{\mathrm{u\ TOT}}$.
  - C2 - Residential sites where the number of customers living in apartments represents at least 80% of the total number of customers: $n_{\mathrm{u\ APT}} \geq 0.8 \cdot n_{\mathrm{u\ TOT}}$.
  - M1 - Residential sites where the number of customers living in single-family houses predominates: $0.5 \cdot n_{\mathrm{u\ TOT}} \leq n_{\mathrm{u\ SFH}} < 0.8 \cdot n_{\mathrm{u\ TOT}}$.
  - M2 - Residential sites where the number of customers living in apartments predominates: $0.5 \cdot n_{\mathrm{u\ TOT}} \leq n_{\mathrm{u\ APT}} < 0.8 \cdot n_{\mathrm{u\ TOT}}$.
- Network configuration: The network configuration is mainly determined with the short-circuit power of the distribution transformer ($S_{\mathrm{k\ T}}$) and the total length of the lines in the network or feeder (ℓ_{TOT}):
  - T1 - Low short-circuit level: $S_{\mathrm{k\ T}} \leq 8$ kVA
  - T2 - Medium short-circuit level: 8 kVA $< S_{\mathrm{k\ T}} \leq 13$ kVA
  - T3 - High short-circuit level: $S_{\mathrm{k\ T}} > 13$ kVA
  - N1 – Small-sized network: $\ell_{\mathrm{TOT}} \leq 1000$ m
  - N2 – Medium-sized network: 1000 m $< \ell_{\mathrm{TOT}} \leq 3000$ m
  - N3 – Large-sized network: 3000 m $< \ell_{\mathrm{TOT}} \leq 6000$ m
  - N4 – Large-sized network: $\ell_{\mathrm{TOT}} > 6000$ m

Fig. A.2 shows the percentage of sites with different electrical characteristics organized according to the type of settlement. As expected, single-family houses are more common in rural and suburban areas, while urban and highly urban areas have more multi-family houses or larger buildings with several apartments. On the other side, the network configuration seems to be similar in all types of settlements, i.e. the type of transformer and the length of the lines depend

on the amount and type of customers and the physical distribution of the customers, and is not linked to the type of settlement.

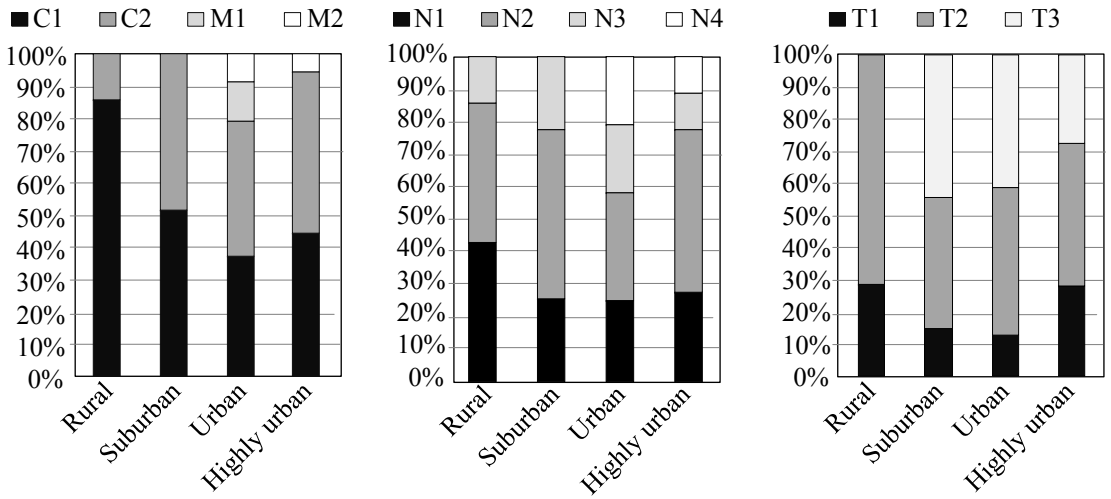

(a) Customer (b) Lines (c) Transformer

Figure A.2.: Percentage of measured residential sites according to their electrical characteristics and the type of settlement

In summary, the sample contains measurements of several residential low-voltage distribution networks with different electrical characteristics. The sample contains data from residential customers of different regions in Germany living in different types of settlements, which guarantees the inclusion of customers from different social environments. The sample was made during the same year and during the same season (winter) in order to reduce the influence of seasonal variations and trends.

A.2. Measurement procedure

A.3. Data cleaning

Data cleaning (also known as data cleansing or data screening) is the process of identifying and correcting corrupt or inaccurate records from a data set [85]. This process detects not only missing or inaccurate data, but also measurements that depart from the assumptions on which the analysis is based. This process can be divided into different tests in order to detect the erroneous data under different conditions.

In order to clean the measured current and voltage harmonic magnitudes and phase angles, the cleaning process is divided into two steps. The first step consists of an accuracy test which identifies missing data and data that is below the accuracy threshold of the measurement device, i.e. data that was not accurately obtained. The second step is a plausibility test where different graphical representations are used to determine if the data seems reasonable. Only the first 15 odd harmonics are analyzed, in accordance with the objective of this thesis.

A.3.1. Accuracy test

Inaccurate and missing measurements are determined using the following criteria:

1. Measurements below the threshold of the measurement instrument or above the range of the measurement probes (Table A.1) are considered inaccurate.
2. Harmonic magnitudes with a value of exactly 0.0 are considered as missing values. Also all measurements declared as "NaN" (not a number) or "Inf" (infinite) by the measurement device are consider as missing values.
3. It is assumed that harmonic magnitudes and phase angles are measured accurately simultaneously. If a harmonic magnitude (or harmonic phase angle) is inaccurate or is missing, it is assumed that the corresponding harmonic phase angle (or harmonic magnitude) is inaccurate too.

Table A.1.: Threshold of the measurement instrument

Variable	Range (RMS values)	Threshold harmonics	Error harmonic	
			magnitude	phase angle
Voltage	0 - 830 V	0.1 V	$< 10\%$	$< 5°$
Current	1 - 3000 A	0.1 A	$< 10\%$	$< 5°$

The range of the measurement probes was obtained from the handbook of the measurement device. The accuracy threshold of the measurement instrument was obtained by laboratory testing using a high precision measurement system capable to generate three-phase balanced voltages and currents with different harmonic content (harmonics of different order with different magnitudes and phase angles). The verification was made by setting a voltage of 230 V and a current of 20 A. Then, harmonic voltages and currents were added to the main signals using discrete steps and the error between the real harmonic voltages and currents (the programmed values) and the values measured with the measurement instrument was calculated. The threshold is selected as the value of the harmonic voltage and harmonic current magnitudes with a maximum error of 10% and 5° for harmonic phase angles. An example of the procedure applied for voltage harmonics can be found in [92].

A site was only included in the further analysis if more than 95% of the data was still available after the accuracy test for the first 15 odd harmonics. From the test, 5 sites were excluded from the analysis. That reduces the initial dataset to 71 sites.

A.3.2. Plausibility test

Different types of graphs were used in order to characterize and compare the harmonic emission of the available residential sites and identify measurements that are conspicuously different from the others. Initially, time series plots were used to verify that the fundamental current and the third and fifth harmonic current magnitudes had a clear daily behavior over all measured days. The time-series plots allowed an easy identification of atypical sites where the daily variation of harmonic magnitudes was clearly different from the typical daily behavior. As an example, Fig. A.3 shows the time series plots of two residential sites, one with a typical behavior (Site A) and another with an atypical behavior (Site B). Site B has a different daily pattern with a high power consumption during the night, which is not usual in pure residential networks. Site B has mainly residential customers, but it also has a considerable number of storage heaters that clearly affect the magnitude of the fundamental current and some harmonic currents.

Storage heaters are three-phase linear loads that are turned on during different time periods of the day, but mainly during the night when the energy cost is low. These loads increase the consumed active power and consequently the fundamental current which can be easily identified

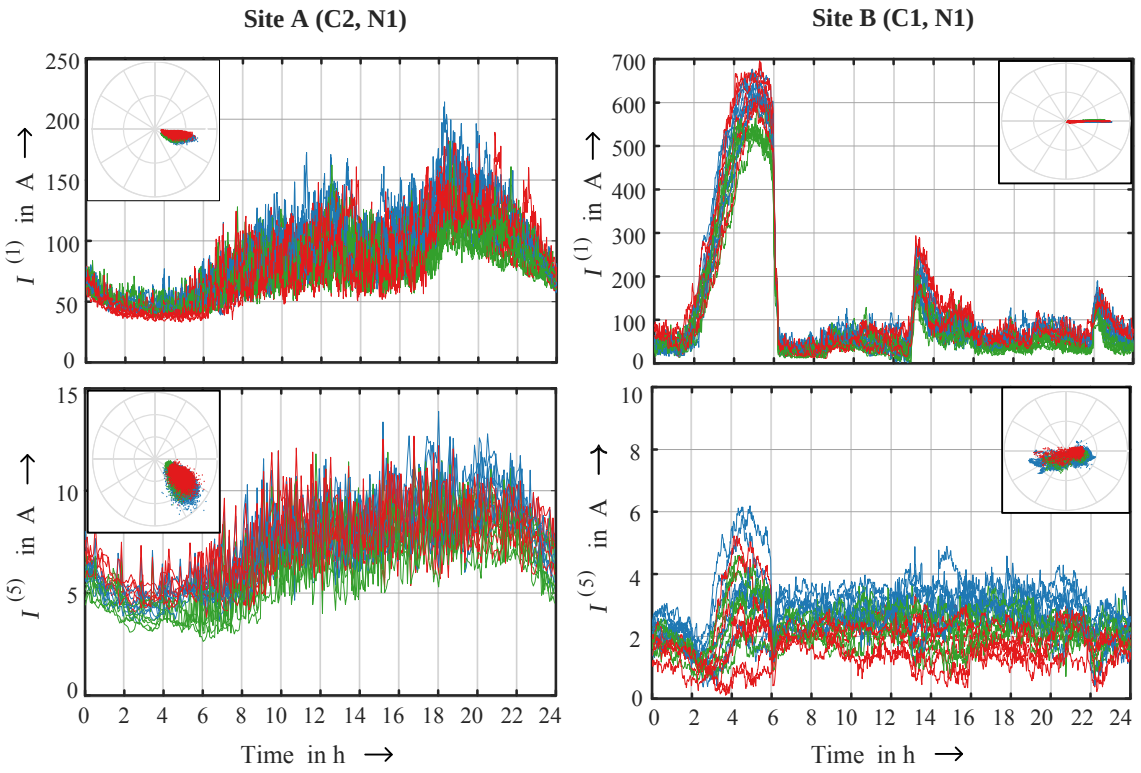

Figure A.3.: Time-series and polar plot of the fundamental current and fifth harmonics for two residential sites. blue: line conductor A; green: line conductor B; red: line conductor C

with the time-series plot. In some cases the connection of the storage heaters also increased the harmonic currents, as in site B for the fifth harmonic between 2 am and 6 am. This response is caused by the considerable decrease of the impedance, which causes the increase of not only the fundamental current but also all positive and negative sequence harmonics produced due to the already distorted voltage. However, the impact depends on the power consumption of the storage heaters in relation to the power consumed by the residential customers. Comparing all time-series plots, it was identified that 14 sites have storage heaters.

Using the same methodology, it was recognized that some sites with shopping centers, construction zones, and institutions (schools, medical centers, etc.) also presented a different behavior. The impact of other types of customers on the behavior of the feeder or network depends on the power consumption of such customers in relation to the power consumed by the residential customers. As this information is not known, the time-series plots were an effective tool to identify measurements that reveals the behavior of residential customers.

Besides time-series plots, polar plots were also used to identify sites with atypical behavior. Harmonic phase angles do not show a clear daily pattern as harmonic magnitudes, but their variation range is similar between different sites. Comparing the polar plots of all the sites and the first 15 odd harmonics (see e.g. the top left graphs of Fig. A.3), one recognizes that the direction of the "data cloud" is similar and the phase angles vary in a close interval for most sites and for most harmonics. For example, the phase angle of the fundamental current is usually between -30° and 10°, while the fifth harmonic is between 300° and 360°, as with site A in Fig. A.3. The variation of harmonic phase angles increases with the harmonic order, and the presence of other non-residential loads can affect the direction of the cloud considerably. For example, most of the sites with storage heaters presented more disperse data clouds, as with site B in Fig. A.3 for the fifth harmonic.

The time-series and polar plots allowed for the identification of atypical sites where the variation of harmonic magnitudes and/or phase angles was clearly different from most sites. Since the objective of this thesis is to analyze and model the harmonic emission of typical residential customers, only sites that represent the harmonic emission of residential customers were exclusively considered. Therefore, sites with storage heaters (14), sites with other important non-residential customers (15), and sites with strange behavior (4) were excluded from the analysis. The final data set consist of 37 measurements.

B. Mathematical background

B.1. Directional statistics

Data that is defined on an angular scale cannot be analyzed or modeled with standard statistical measures and distributions, like median, mean, percentiles, normal distribution, etc., because those measures and distributions are defined exclusively for data on a linear scale. On the angular scale, there is no designated zero, and the designation of high and low values are arbitrary. Directional statistics are special statistics that take into account the circular nature of the data. Below is a summary of the different measures for circular data used in this text. References [53, 89] contain a more detailed description of these measures and many other measures suitable for circular data. The implementation of each of these measures in Matlab was possible through the toolbox CircStat [11].

B.1.1. Mean direction

The mean direction is a measure of the location (central tendency) of a set of angles. Given n angles $\theta_1 ... \theta_n$, the mean direction θ_{MD} is calculated by:

$$\theta_{\mathrm{MD}} = tan^{-1}\left(\frac{\frac{1}{n}\sum_{i=1}^{n}\cos(\theta_i)}{\frac{1}{n}\sum_{i=1}^{n}\sin(\theta_i)}\right) \tag{B.1}$$

B.1.2. Mean resultant length

The mean resultant length is a measure of concentration of the data around the mean direction. The mean resultant length MRL of n angles $\theta_1 ... \theta_n$ is computed by:

$$MRL = \sqrt{\left(\frac{1}{n}\sum_{i=1}^{n}\cos(\theta_i)\right)^2 + \left(\frac{1}{n}\sum_{i=1}^{n}\sin(\theta_i)\right)^2} \tag{B.2}$$

MRL varies in the interval $[0, 1]$, and the closer it is to 1, the more concentrated the data is around the mean direction. To determine suitable value ranges for the interpretation of MRL, simulations based on different groups of synthetic angles were performed. Angles were simulated using a von Mises distribution (see next subsection) with fixed mean direction $\theta_{\mathrm{MD}} = 180°$ and κ values from 0 to 30. Fig. B.1a exemplary shows the distribution of the generated data for $\kappa = 0$, $\kappa = 3$ and $\kappa = 10$ using circular histograms. Fig. B.1b shows the non-linear increase of MRL with the increase of κ, i.e. with the decrease in the dispersion of the angles. Analyzing the distribution of the data and the corresponding values of MRL, the following categories are defined:

- Very low dispersion ($MRL \geq 0.95$). The angles have almost the same value.
- Low dispersion ($0.89 \leq MRL < 0.95$). The angles have a good similarity and all point to a similar direction.

- Medium dispersion ($0.8 \leq MRL < 0.89$). The angles are more disperse, but still a general direction can be identified.
- High dispersion ($MRL < 0.8$). The angles are wide disperse and a common direction cannot be identified. The use of a mean direction may be misleading.

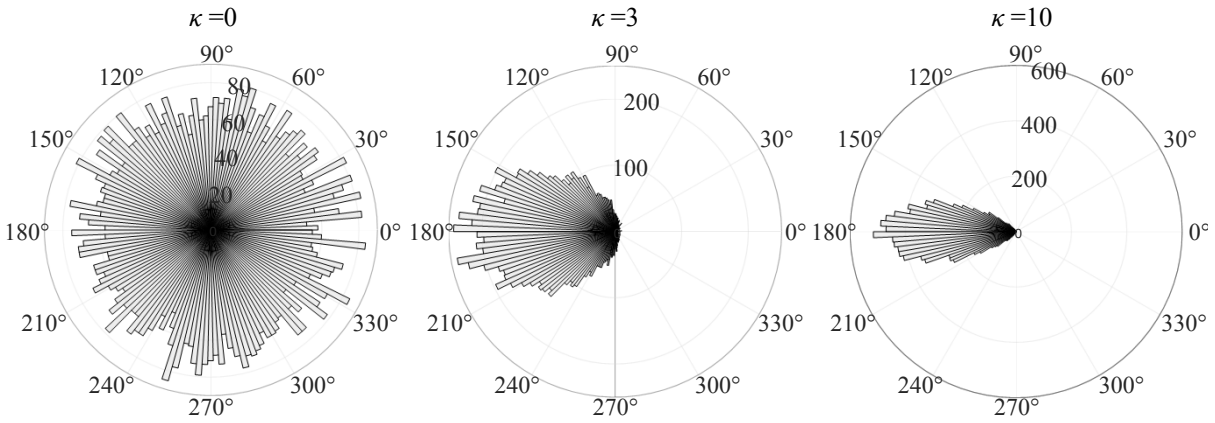

(a) Examples of synthetic data

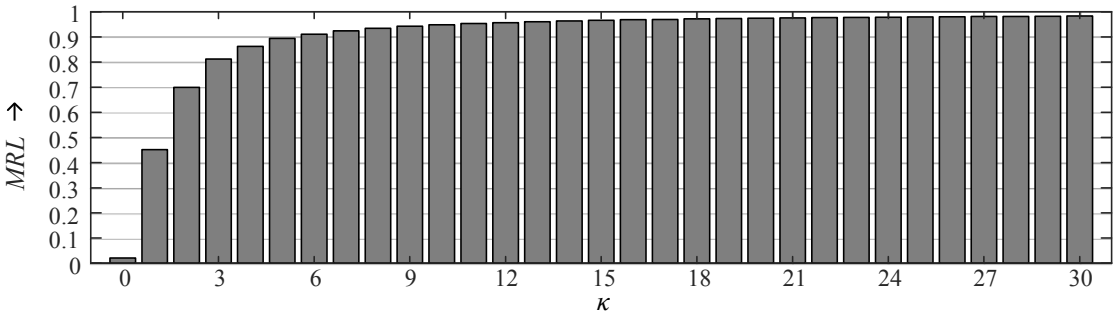

(b) Results

Figure B.1.: MRL values for synthetic data

B.1.3. The von Mises distribution

This is a symmetric unimodal distribution which is the most common model for unimodal circular data because it is considered a circular analogue of the normal distribution. The probability density function is given by [89]:

$$\mathcal{VM}(\theta;\mu,\kappa) = \frac{1}{2\pi I_0(\kappa)} e^{\kappa \cdot cos(\theta-\mu)} \tag{B.3}$$

where $I_0(\kappa)$ is the modified Bessel function of order zero, μ is the measure of location, i.e. the mean direction ($\mu = \theta_{\mathrm{MD}}$), and κ is the concentration parameter. Fig. B.2 shows the von Mises distribution with $\mu = 180°$ and different κ values. The higher the value of κ, the more concentrated are the values around the mean direction μ. When $\kappa = 0$, $\mathcal{VM}(\theta;\mu,\kappa)$ is equivalent to the uniform distribution [89].

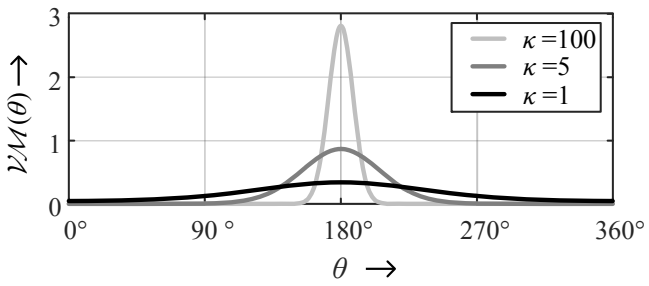

Figure B.2.: Von Mises distribution with $\mu = 180°$ and different κ values.

B.2. Symmetrical components for harmonic currents

Three-phase networks (phases A, B and C) usually have unsymmetrical currents with a high amount of harmonics. These currents can be represented as:

$$\begin{aligned} i_{\mathrm{A}}(t) &= \sqrt{2}\sum_{h=1}^{\infty} I_{\mathrm{A}}^{(h)} \sin\left(hwt + \varphi_{\mathrm{A}}^{(h)}\right) \\ i_{\mathrm{B}}(t) &= \sqrt{2}\sum_{h=1}^{\infty} I_{\mathrm{B}}^{(h)} \sin\left(hwt + \varphi_{\mathrm{B}}^{(h)}\right) \\ i_{\mathrm{C}}(t) &= \sqrt{2}\sum_{h=1}^{\infty} I_{\mathrm{C}}^{(h)} \sin\left(hwt + \varphi_{\mathrm{C}}^{(h)}\right) \end{aligned} \tag{B.4}$$

where $I^{(h)}$ and $\varphi^{(h)}$ are the RMS magnitude and phase angle for the h^{th} harmonic respectively. The phase angles $\varphi^{(h)}$ are referenced to the zero crossing of the voltage signal in phase A. If the currents are balanced, the following conditions are satisfied:

$$I_{\mathrm{A}}^{(h)} = I_{\mathrm{B}}^{(h)} = I_{\mathrm{C}}^{(h)}, \tag{B.5}$$

$$\varphi_{\mathrm{B}}^{(h)} = \varphi_{\mathrm{A}}^{(h)} - h\frac{2\pi}{3}, \tag{B.6}$$

$$\varphi_{\mathrm{C}}^{(h)} = \varphi_{\mathrm{A}}^{(h)} + h\frac{2\pi}{3} \tag{B.7}$$

If there are differences between magnitudes and phase angles between the phases, then the network has unbalance. The unbalance is better assessed using the symmetrical components instead of the original phasors. This method is preferred to take into account not only the differences between magnitudes but also the contributions of the angular displacement (differences between the phase angles φ_{A}, φ_{B} and φ_{C}) to unbalance. The symmetrical components are calculated based on the Fortescue transformation, but an additional permutation matrix is added to rearrange the symmetrical components according to the harmonic order as follows:

$$\underline{\mathbf{i}}_{b,u1,u2}^{(h)} = \mathbf{P}^{h+2} \cdot \underline{\mathbf{T}}_{120}^{-1} \cdot \underline{\mathbf{i}}_{\mathrm{A,B,C}}^{(h)} \tag{B.8}$$

$$\begin{bmatrix} \underline{I}_{\mathrm{b}}^{(h)} \\ \underline{I}_{\mathrm{u1}}^{(h)} \\ \underline{I}_{\mathrm{u2}}^{(h)} \end{bmatrix} = \begin{bmatrix} 0 & 1 & 0 \\ 0 & 0 & 1 \\ 1 & 0 & 0 \end{bmatrix}^{h+2} \cdot \begin{bmatrix} 1 & 1 & 1 \\ \underline{\mathrm{a}}^2 & \underline{\mathrm{a}} & 1 \\ \underline{\mathrm{a}} & \underline{\mathrm{a}}^{\,2} & 1 \end{bmatrix}^{-1} \cdot \begin{bmatrix} \underline{I}_{\mathrm{A}}^{(h)} \\ \underline{I}_{\mathrm{B}}^{(h)} \\ \underline{I}_{\mathrm{C}}^{(h)} \end{bmatrix} \tag{B.9}$$

where $\underline{I}_{\mathrm{A}}^{(h)}$, $\underline{I}_{\mathrm{B}}^{(h)}$ and $\underline{I}_{\mathrm{C}}^{(h)}$ are the harmonic current phasor of the harmonic order h. $\underline{I}_{\mathrm{b}}^{(h)}$ is the balanced component, $\underline{I}_{\mathrm{u1}}^{(h)}$ is the first unbalanced component and $\underline{I}_{\mathrm{u2}}^{(h)}$ is the second unbalanced component, which are the symmetrical components. The matrix $\underline{\mathbf{T}}_{120}$ is the transformation

matrix to calculate the symmetrical components (Fortescue transformation) with $\underline{\mathrm{a}} = \frac{-1}{2} + j\frac{\sqrt{3}}{2}$ [65]. Finally, the matrix $\mathbf{P}$ is a permutation matrix that reorganize the original symmetrical components according to the harmonic order.

This change in the original Fortescue transformation allows the calculation of the symmetrical components for each harmonic (positive, negative and zero sequence components), but it reorganizes the results leaving the "characteristic" symmetrical component of each harmonic as the balanced component. Table B.1 shows the relation between the traditional Fortescue transformation and the balanced and unbalanced components for the first 15$^{\text{th}}$ harmonics as example.

Table B.1.: Relation between the original Fortescue transformation and the proposed transformation

	Harmonic order h							
	1	3	5	7	9	11	13	15
$\underline{I}_{\mathrm{b}}^{(h)}$	+	0	-	+	0	-	+	0
$\underline{I}_{\mathrm{u1}}^{(h)}$	-	+	0	-	+	0	-	+
$\underline{I}_{\mathrm{u2}}^{(h)}$	0	-	+	0	-	+	0	-

If the transformation from symmetrical components to phase currents is required, the following transformation is applied:

$$\underline{\mathbf{i}}_{\mathrm{A,B,C}}^{(h)} = \underline{\mathbf{T}}_{120} \cdot \mathbf{P}^{-(h+2)} \cdot \underline{\mathbf{i}}_{\mathrm{b,u1,u2}}^{(h)} \tag{B.10}$$

B.3. Normalization methods

Normalization methods consist of different transformations that are applied to scale the original data to a smaller range. Normalization is useful to compare different data sets, especially time series, with different scales, and to improve the accuracy and efficiency of different analysis algorithms. The most common normalization methods are:

- Min-max normalization (or range-based normalization) changes the original scale of the data and fits it to the interval [0 1]. Let the minimum and maximum values of the time series be denoted by $y_{[\min]}$ and $y_{[\max]}$, respectively. Then, the original time series value $y(t)$ is mapped to the new value $y_{\mathrm{norm}}(t)$ in the range [0 1] as follows:

$$y_{\mathrm{norm}}(t) = \frac{y(t) - y_{[\min]}}{y_{[\max]} - y_{[\min]}} \tag{B.11}$$

  This normalization performs a linear transformation of the original time series and it preserves the relationships among the original data values.

- Z-score normalization (or Zero-mean normalization) uses the mean and standard deviation of the series. Let $y_{[\mu]}$ and $y_{[\sigma]}$ represent the mean and standard deviation of the values in the time series. Then, the time series value $y(t)$ is mapped to a new value $y_{\text{norm-z}}(t)$ as follows:

$$y_{\text{norm-z}}(t) = \frac{y(t) - y_{[\mu]}}{y_{[\sigma]}} \tag{B.12}$$

B.4. Distance and similarity measures

There are two main types of measures used to estimate the resemblance between curves: distance measures and similarity measures [85]. Distance measures evaluate the proximity of two objects. The most used distance measures are:

- Euclidean distance

  Let $\boldsymbol{x} = (x_1, x_2, ..., x_n)$ and $\boldsymbol{y} = (y_1, y_2, ..., y_n)$ each be a n-dimensional vector representing two different time series defined on the same time interval. The Euclidean distance is computed as:

$$DM_{\text{E}} = \sqrt{\sum_{i=1}^{n} (x_i - y_i)^2} \tag{B.13}$$

- Minkowski distance This distance is a generalization of Euclidean distance which is defined as:

$$DM_{\text{M}g} = \sqrt[g]{\sum_{i=1}^{n} (x_i - y_i)^g} \tag{B.14}$$

  where g is a positive integer. The well known Manhattan and Chebychev distances are obtained when $g = 1$ and $g = \infty$ respectively.

- Euclidean distance between the Fourier coefficients

  The Euclidean distance can also be calculated using the Fourier coefficients of each of the time series. The Euclidean distance between the time series $\boldsymbol{x}$ and $\boldsymbol{y}$ with Fourier coefficients $\boldsymbol{x_f} = \langle (p_0, q_0)...(p_{n-1}, q_{n-1}) \rangle$ and $\boldsymbol{y_f} = \langle (r_0, s_0)...(r_{n-1}, s_{n-1}) \rangle$ is [109]:

$$DM_{\text{FFT}} = \sqrt{\sum_{i=0}^{n-1} (p_i - r_i)^2 + (q_i - s_i)^2} \tag{B.15}$$

  It is common to retain only a subset of the Fourier coefficients. The Euclidean distance between the first f_C coefficients is:

$$DM_{\text{FFT}} = \sqrt{\sum_{i=0}^{f_C} (p_i - r_i)^2 + (q_i - s_i)^2} \tag{B.16}$$

  This distance measure can be decomposed in order to obtain detailed information about the similitude of the Fourier components of the time series. One of the many possibilities is to divide the DM_{FFT} between the distance of the constant components (first component of the Fourier series with frequency of 0 Hz, that is $i = 0$), and the distance between the other Fourier components:

$$DM^2_{\text{FFT}} = DM^2_{\text{CC}} + DM^2_{\text{COMP}} \tag{B.17}$$

$$DM_{\text{CC}} = \sqrt{(p_0 - r_0)^2 + (q_0 - s_0)^2} = (p_0 - r_0) \tag{B.18}$$

$$DM_{\text{COMP}} = \sqrt{\sum_{i=1}^{f_C} (p_i - r_i)^2 + (q_i - s_i)^2} \tag{B.19}$$

  DM_{CC} indicates the difference between the constant component (offset) of the time series, while DM_{COMP} indicates the difference between the other f_C coefficients. DM_{COMP} indicates how similar are the two time series without considering the offset.

If a more detailed analysis of the features of the time series is needed, then the difference of each component can be calculated. In this case it is better to express the components $\boldsymbol{x_f}$ and $\boldsymbol{y_f}$ with their polar equivalent (magnitudes and angles), that means $\boldsymbol{x_f} = \langle (m_0, \alpha_0) ... (m_{n-1}, \alpha_{n-1}) \rangle$ and $\boldsymbol{y_f} = \langle (l_0, \beta_0) ... (l_{n-1}, \beta_{n-1}) \rangle$, where $m_n = \sqrt{p_n - q_n}$, $l_n = \sqrt{r_n - s_n}$, $\alpha_n = \tan^{-1}(q_n/p_n)$ and $\beta_n = \tan^{-1}(s_n/r_n)$.

Similarity measures compares two vectors $\boldsymbol{x}$ and $\boldsymbol{y}$ usually looking on the correlation between both vectors instead on the distance between them. The most used similarity measures are listed below [60, 126]:

- Cosine measure

  Given two vectors $\boldsymbol{x}$ and $\boldsymbol{y}$, the cosine measure is represented using the inner product as:

  $$SM_{\mathrm{C}} = \frac{\boldsymbol{x}^T \boldsymbol{y}}{\| \boldsymbol{x} \| \| \boldsymbol{y} \|} \tag{B.20}$$

  where

  $\boldsymbol{x}^T \boldsymbol{y} = \sum_{i=1}^{n} x_i y_i$ is the inner product between $\boldsymbol{x}$ and $\boldsymbol{y}$

  $\| \boldsymbol{x} \| = \sqrt{\sum_{i=1}^{n} x_i^2}$ is the length of $\boldsymbol{x}$

  $\| \boldsymbol{y} \| = \sqrt{\sum_{i=1}^{n} y_i^2}$ is the length of $\boldsymbol{y}$

  The cosine measure determines whether the vectors are pointing in roughly the same direction. If $SM_{\mathrm{C}} = 0$ the vectors are at $90°$ to each other and have no match. The closer the value SM_{C} to 1, the greater the match between vectors.

- Pearson's correlation coefficient

  $$SM_{\mathrm{P}} = \frac{\sum_{i=1}^{n} (x_i - \mu_x)(y_i - \mu_y)}{\sqrt{\sum_{i=1}^{n} (x_i - \mu_x)^2 \sum_{i=1}^{n} (y_i - \mu_y)^2}} \tag{B.21}$$

  where μ_x and μ_y are the mean values of vectors $\boldsymbol{x}$ and $\boldsymbol{y}$ respectively. SM_{P} takes values between -1 (negative correlation) and 1 (positive correlation). A value $SM_{\mathrm{P}} = 0$ indicates that there is no linear correlation between both vectors.

In order to illustrate the use of these measures, Fig. B.3 shows three different cases and Table B.2 shows the obtained distance and similarity measures for each case. The first case shows two similar time series with different offset, the second case correspond to two time series with some temporal drift and the third case correspond to two completely different time series.

Distance measures DM_{E}, $DM_{\mathrm{M}\infty}$ and DM_{FFT} are higher for the the first case due to the high offset difference between the time series, and only DM_{CC} and DM_{COMP} can accurately indicate the cause of the differences. Similarity measure SM_{C} variate in a lower range than SM_{P} and it also quantifies the offset of the time series. Only SM_{P} seems to be able to show the correlation and similarity between the time series without considering the offset. It is clear that any of the distance or similarity measures can determine by their own the absolute resemblance between two time-series.

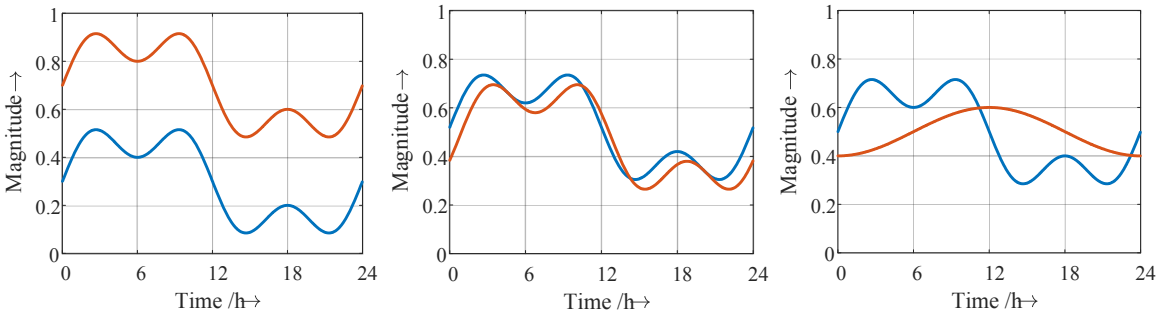

(a) Case 1 (b) Case 2 (c) Case 3

Figure B.3.: Distances of two curves

Table B.2.: Distance and similarity measures of cases defined in Fig. B.3

Case	Distance					Similarity	
	DM_{E}	$DM_{\mathrm{M}\infty}$	DM_{FFT}	DM_{CC}	DM_{COMP}	SM_{C}	SM_{P}
1	15.18	0.40	0.4	0.4	0.00	0.966	1,00
2	2.45	0.14	0.082	0.071	0.04	0.995	0.95
3	6.57	0.29	0.245	0.00	0.245	0.944	0.00

For some analyses it is useful to know the maximum possible distance that can be calculated between curves. Once the maximum is known, a range of acceptance or rejection of the similarity between curves can be defined. In case of two normalized n-dimensional vectors (time-series curves) in the interval $[0, 1]$, the maximum distance measures of Table B.3 are obtained. For similarity measures SM_{C} and SM_{P} the range of variation is always between $[0, 1]$, where 1 means a perfect similarity between curves.

Table B.3.: Maximum values of distance measures for time-series normalized between $[0, 1]$

$DM_{\mathrm{E,max}}$	$DM_{\mathrm{Mg,max}}$	$DM_{\mathrm{FFT,max}}$	$DM_{\mathrm{COMP,max}}$	$DM_{\mathrm{DC,max}}$
$\sqrt{n}$	$\sqrt[q]{n}$	$\sqrt{2}$	$\sqrt{2}$	1

Most of the distance and similarity measures are usually affected by the noise level of the signal. Fig. B.4 exemplary shows the variation of the distance and similarity measures of the time series in Fig. B.3b when a random noise is added. The noise is defined with a uniform distribution with limits $[-a \;\; a]$, where a is varied between 0 and 0.08 with steps of 0.01. The error between the distance and similarity measures is calculated with respect to the case without noise ($a = 0$).

The most affected measure with the noise is $DM_{\mathrm{M}\infty}$, which with a small noise can generate errors of 10%. DM_{E}, DM_{FFT} and DM_{COMP} are also highly affected by the noise, but they can still give accurate results when the noise is small. The similarity measures and DM_{CC} are more robust to noise. In order to reduce the effect of noise it is recommended to first smooth the signals though filters or using moving average techniques [137].

Another factor that can influence the results is the scale of the time series. This is a common problem when electricity consumption patterns from different networks are compared, because the consumption is related to the amount and type of customers in the network which produces a different amplitude scaling for each network. To remove the effect of scale, it is recommended to normalize the data before computing the distance or similarity measures [132].

There are other distance and similarity measures and more sophisticate methods to evaluate

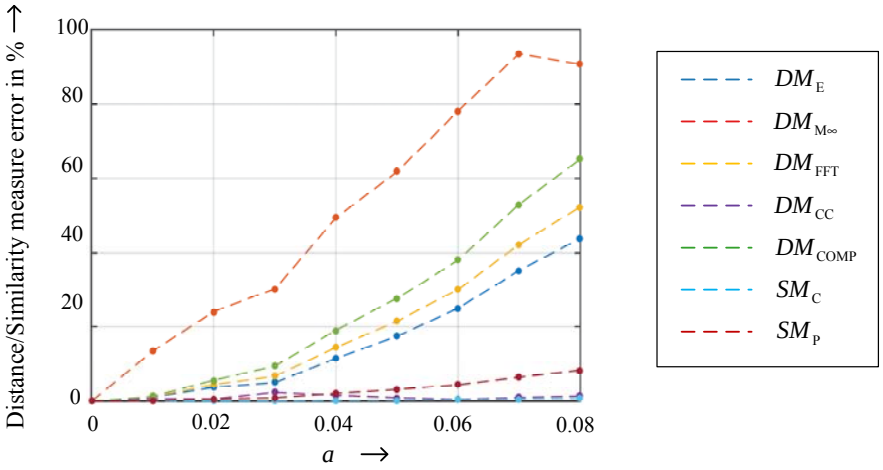

Figure B.4.: Change in distance measures with the increase of signals noise

the similitude between time series data. For example, the dynamic time warping distance is a iterative algorithm that aligns the two series so that their difference is minimized [132]. This method is widely used for speech and signature recognition. Other methods are based on statistical values or probability tests to check if two curves come from the same distribution (e.g. [73, 80]). Each method compares different characteristics of the time series; therefore, the method must be carefully chosen to compare the important characteristics of the time series depending on the application. In case of daily patterns of electricity consumption and harmonic emission, the method must preserve the time-stamp characteristic (peaks and valleys cannot be shifted), and it must be robust to noise and amplitude scaling.

C. Appendix chapter 5 - Model of residential low-voltage networks

C.1. Parameters normalized balanced current

Table C.1.: Parameters for normalized balanced current

	3rd harmonic				**5th harmonic**			
	Values		Confidence intervals		Values		Confidence intervals	
	N_μ	N_σ	N_μ	N_σ	N_μ	N_σ	N_μ	N_σ
$C_0^{(h)}$	0.35	0.023	[0.34 , 0.36]	[0.019 , 0.030]	0.49	0.066	[0.47 , 0.52]	[0.053 , 0.088]
$C_1^{(h)}$	0.29	0.034	[0.28 , 0.31]	[0.028 , 0.045]	0.20	0.044	[0.18 , 0.21]	[0.035 , 0.059]
$C_2^{(h)}$	0.15	0.017	[0.15 , 0.16]	[0.014 , 0.023]	0.07	0.032	[0.06 , 0.08]	[0.025 , 0.042]
$C_3^{(h)}$	0.06	0.014	[0.05 , 0.06]	[0.012 , 0.019]	0.02	0.011	[0.02 , 0.03]	[0.009 , 0.015]
$\theta_1^{(h)}$	1.30	0.135	[1.25 , 1.35]	[0.109 , 0.176]	1.90	0.311	[1.77 , 2.02]	[0.246 , 0.423]
$\theta_2^{(h)}$	1.77	0.198	[1.70 , 1.84]	[0.159 , 0.262]	1.19	0.676	[0.92 , 1.46]	[0.533 , 0.927]
$\theta_3^{(h)}$	2.08	0.364	[1.95 , 2.20]	[0.295 , 0.475]	1.94	0.937	[1.58 , 2.30]	[0.741 , 1.275]
$\alpha_\mathrm{b}^{(h)}$	0.94	0.018	[0.93 , 0.94]	[0.015 , 0.024]	0.95	0.015	[0.94 , 0.96]	[0.012 , 0.021]

	7th harmonic				**9th harmonic**			
	Values		Confidence intervals		Values		Confidence intervals	
	N_μ	N_σ	N_μ	N_σ	N_μ	N_σ	N_μ	N_σ
$C_0^{(h)}$	0.46	0.062	[0.43 , 0.49]	[0.048 , 0.089]	0.41	0.050	[0.39 , 0.43]	[0.040 , 0.066]
$C_1^{(h)}$	0.19	0.026	[0.18 , 0.20]	[0.019 , 0.038]	0.21	0.060	[0.19 , 0.23]	[0.048 , 0.079]
$C_2^{(h)}$	0.09	0.016	[0.08 , 0.09]	[0.013 , 0.024]	0.14	0.031	[0.13 , 0.15]	[0.024 , 0.041]
$C_3^{(h)}$	0.04	0.016	[0.03 , 0.04]	[0.012 , 0.022]	0.04	0.016	[0.03 , 0.04]	[0.013 , 0.021]
$\theta_1^{(h)}$	1.22	0.384	[1.03 , 1.41]	[0.288 , 0.576]	1.28	0.345	[1.15 , 1.41]	[0.274 , 0.467]
$\theta_2^{(h)}$	1.73	0.352	[1.56 , 1.91]	[0.264 , 0.527]	1.81	0.292	[1.70 , 1.93]	[0.231 , 0.398]
$\theta_3^{(h)}$	1.77	0.491	[1.52 , 2.03]	[0.366 , 0.747]	2.91	1.028	[2.51 , 3.31]	[0.813 , 1.399]
$\alpha_\mathrm{b}^{(h)}$	0.95	0.021	[0.94 , 0.96]	[0.016 , 0.031]	0.96	0.016	[0.95 , 0.97]	[0.013 , 0.022]

	11th harmonic				**13th harmonic**			
	Values		Confidence intervals		Values		Confidence intervals	
	N_μ	N_σ	N_μ	N_σ	N_μ	N_σ	N_μ	N_σ
$FC_0^{(h)}$	0.41	0.063	[0.37 , 0.44]	[0.046 , 0.100]	0.40	0.039	[0.36 , 0.44]	[0.024 , 0.096]
$FC_1^{(h)}$	0.17	0.056	[0.14 , 0.20]	[0.042 , 0.087]	0.22	0.054	[0.17 , 0.27]	[0.035 , 0.118]
$FC_2^{(h)}$	0.12	0.018	[0.11 , 0.13]	[0.013 , 0.029]	0.09	0.016	[0.07 , 0.10]	[0.010 , 0.035]
$C_3^{(h)}$	0.03	0.014	[0.03 , 0.04]	[0.010 , 0.023]	0.05	0.009	[0.04 , 0.06]	[0.006 , 0.023]
$\theta_1^{(h)}$	1.48	0.614	[1.16 , 1.81]	[0.453 , 0.950]	1.60	0.111	[1.42 , 1.77]	[0.063 , 0.414]
$\theta_2^{(h)}$	1.92	0.327	[1.73 , 2.11]	[0.237 , 0.527]	2.16	0.416	[1.72 , 2.59]	[0.259 , 1.020]
$\theta_3^{(h)}$	2.74	1.081	[2.12 , 3.37]	[0.784 , 1.741]	2.88	0.685	[2.03 , 3.74]	[0.410 , 1.969]
$\alpha_\mathrm{b}^{(h)}$	0.91	0.069	[0.87 , 0.95]	[0.049 , 0.113]	0.91	0.035	[0.87 , 0.96]	[0.021 , 0.102]

	15th harmonic			
	Values		Confidence intervals	
	N_μ	N_σ	N_μ	N_σ
$FC_0^{(h)}$	0.41	0.059	[0.38 , 0.44]	[0.044 , 0.087]
$FC_1^{(h)}$	0.20	0.045	[0.18 , 0.22]	[0.034 , 0.068]
$FC_2^{(h)}$	0.10	0.025	[0.09 , 0.12]	[0.019 , 0.037]
$C_3^{(h)}$	0.05	0.017	[0.05 , 0.06]	[0.013 , 0.025]
$\theta_1^{(h)}$	0.84	0.264	[0.71 , 0.97]	[0.199 , 0.390]
$\theta_2^{(h)}$	1.42	0.647	[1.12 , 1.72]	[0.492 , 0.944]
$\theta_3^{(h)}$	1.80	0.355	[1.62 , 1.97]	[0.266 , 0.532]
$\alpha_{\mathrm{b}}^{(h)}$	0.93	0.042	[0.91 , 0.95]	[0.031 , 0.063]

C.2. Parameters balanced and unbalanced harmonic phase angles

Table C.2.: Parameters for phase angles

	3rd harmonic				**5th harmonic**			
	Values		Confidence intervals		Values		Confidence intervals	
	N_μ	N_σ	N_μ	N_σ	N_μ	N_σ	N_μ	N_σ
$\mu_{\mathrm{b}}^{(h)}$	196	7.2	[193 , 198]	[5.8 , 9.4]	-36	10.4	[-40 , -33]	[8.4 , 13.7]
$\kappa_{\mathrm{b}}^{(h)}$	65	34.9	[53 , 78]	[28.2 , 46.0]	73	43.7	[59 , 88]	[35.4 , 57.0]
$\mu_{\mathrm{u1}}^{(h)}$	154	103.3	[119 , 188]	[84.0 , 134.2]	191	106.6	[156 , 227]	[86.7 , 138.4]
$\kappa_{\mathrm{u1}}^{(h)}$	2	1.1	[2 , 3]	[0.9 , 1.5]	2	1.1	[2 , 2]	[0.9 , 1.5]
$\mu_{\mathrm{u2}}^{(h)}$	163	91.1	[133 , 194]	[74.1 , 118.3]	187	98.9	[154 , 220]	[80.4 , 128.5]
$\kappa_{\mathrm{u2b}}^{(h)}$	2	1.6	[2 , 3]	[1.3 , 2.1]	3	2.1	[3 , 4]	[1.7 , 2.8]

	7th harmonic				**9th harmonic**			
	Values		Confidence intervals		Values		Confidence intervals	
	N_μ	N_σ	N_μ	N_σ	N_μ	N_σ	N_μ	N_σ
$\mu_{\mathrm{b}}^{(h)}$	139	20.2	[132 , 147]	[16.0 , 27.1]	-32	19.4328	[-39 , -26]	[15.8 , 25.3]
$\kappa_{\mathrm{b}}^{(h)}$	17	10.9	[13 , 21]	[8.7 , 14.5]	47	28.842	[37 , 58]	[23.3 , 38.0]
$\mu_{\mathrm{u1}}^{(h)}$	165	114.1	[127 , 203]	[92.8 , 148.2]	178	91.0246	[147 , 208]	[74.0 , 118.2]
$\kappa_{\mathrm{u1}}^{(h)}$	2	1.4	[2 , 3]	[1.1 , 1.9]	3	1.89325	[2 , 4]	[1.5 , 2.5]
$\mu_{\mathrm{u2}}^{(h)}$	160	110.2	[123 , 196]	[89.6 , 143.1]	161	97.0351	[128 , 193]	[78.9 , 126.0]
$\kappa_{\mathrm{u2b}}^{(h)}$	3	1.6	[2 , 3]	[1.3 , 2.1]	3	1.45735	[2 , 3]	[1.2 , 1.9]

	11th harmonic				**13th harmonic**			
	Values		Confidence intervals		Values		Confidence intervals	
	N_μ	N_σ	N_μ	N_σ	N_μ	N_σ	N_μ	N_σ
$\mu_{\mathrm{b}}^{(h)}$	134	27.4	[124 , 144]	[22.0 , 36.5]	221	69.2477	[197 , 246]	[55.7 , 91.6]
$\kappa_{\mathrm{b}}^{(h)}$	15	9.0	[12 , 18]	[7.2 , 11.7]	5	3.50932	[4 , 6]	[2.8 , 4.7]
$\mu_{\mathrm{u1}}^{(h)}$	152	102.7	[117 , 187]	[83.3 , 133.9]	200	93.1719	[169 , 231]	[75.8 , 121.0]
$\kappa_{\mathrm{u1}}^{(h)}$	2	1.3	[2 , 3]	[1.1 , 1.8]	3	1.71639	[2 , 3]	[1.4 , 2.3]
$\mu_{\mathrm{u2}}^{(h)}$	188	117.4	[149 , 227]	[95.5 , 152.5]	140	76.8086	[114 , 166]	[62.1 , 100.6]
$\kappa_{\mathrm{u2b}}^{(h)}$	3	2.1	[2 , 4]	[1.7 , 2.8]	2	1.39892	[2 , 3]	[1.1 , 1.9]

	15th harmonic			
	Values		Confidence intervals	
	N_μ	N_σ	N_μ	N_σ
$FC_0^{(h)}$	0.41	0.059	[0.38 , 0.44]	[0.044 , 0.087]
$\mu_{\mathrm{b}}^{(h)}$	181	129.4	[138 , 224]	[105.2 , 168.1]
$\kappa_{\mathrm{b}}^{(h)}$	7	5.6	[5 , 9]	[4.5 , 7.5]
$\mu_{\mathrm{u1}}^{(h)}$	184	105.9	[149 , 219]	[86.1 , 137.6]
$\kappa_{\mathrm{u1}}^{(h)}$	2	1.3	[2 , 3]	[1.1 , 1.8]
$\mu_{\mathrm{u2}}^{(h)}$	213	117.0	[174 , 252]	[95.2 , 152.0]
$\kappa_{\mathrm{u2b}}^{(h)}$	3	2.0	[2 , 3]	[1.6 , 2.6]

C.3. Scaling

Table C.3.: Regression results C1

X	h	Values			Confidence intervals			R^2_{adj}	
		p	q	r	p	q	r	eq. 5.21	eq. 5.22
b	3	0.115	0.989	0.594	[0.088,0.141]	[0.946,1.033]	[0.586,0.603]	0.967	0.970
	5	0.074	0.980	0.419	[0.053,0.095]	[0.925,1.034]	[0.405,0.432]	0.951	0.884
	7	0.144	0.720	0.522	[0.083,0.206]	[0.639,0.801]	[0.502,0.542]	0.866	0.812
	9	0.139	0.689	0.447	[0.077,0.201]	[0.604,0.775]	[0.436,0.458]	0.822	0.896
	11	0.061	0.718	0.678	[0.037,0.085]	[0.644,0.793]	[0.661,0.696]	0.903	0.918
	13	0.012	0.958	0.684	[0.006,0.017]	[0.871,1.045]	[0.658,0.71]	0.946	0.849
	15	0.020	0.825	0.642	[0.007,0.033]	[0.705,0.945]	[0.617,0.668]	0.743	0.770
u1	3	0.474	0.390	0.978	[0.378,0.569]	[0.35,0.43]	[0.975,0.982]	0.875	0.997
	5	0.183	0.424	0.965	[0.138,0.228]	[0.375,0.472]	[0.959,0.971]	0.861	0.993
	7	0.104	0.449	0.951	[0.08,0.127]	[0.406,0.493]	[0.942,0.961]	0.910	0.982
	9	0.058	0.525	0.899	[0.04,0.076]	[0.464,0.586]	[0.882,0.916]	0.861	0.937
	11	0.045	0.475	0.961	[0.032,0.057]	[0.418,0.531]	[0.953,0.97]	0.873	0.982
	13	0.005	0.935	0.904	[0.003,0.008]	[0.837,1.032]	[0.887,0.921]	0.834	0.948
	15	0.016	0.684	0.927	[0.008,0.025]	[0.584,0.783]	[0.917,0.938]	0.811	0.979
u2	3	0.418	0.421	0.979	[0.321,0.516]	[0.375,0.467]	[0.976,0.982]	0.859	0.997
	5	0.134	0.523	0.940	[0.096,0.173]	[0.467,0.579]	[0.929,0.951]	0.871	0.974
	7	0.125	0.424	0.949	[0.084,0.166]	[0.36,0.489]	[0.939,0.959]	0.779	0.981
	9	0.079	0.440	0.943	[0.055,0.103]	[0.38,0.5]	[0.933,0.953]	0.822	0.977
	11	0.007	0.905	0.964	[0.004,0.009]	[0.829,0.981]	[0.957,0.972]	0.880	0.991
	13	0.018	0.658	0.937	[0.011,0.025]	[0.581,0.735]	[0.927,0.947]	0.884	0.983
	15	0.024	0.603	0.924	[0.011,0.037]	[0.499,0.706]	[0.91,0.938]	0.665	0.950

Table C.4.: Regression results C2

X	h	Values			Confidence intervals			R^2_{adj}	
		p	q	r	p	q	r	eq. 5.21	eq. 5.22
b	3	2.341	0.364	0.657	[0.884,3.799]	[0.261,0.467]	[0.645,0.668]	0.712	0.96
	5	0.597	0.496	0.53	[0.085,1.11]	[0.355,0.637]	[0.507,0.554]	0.691	0.829
	7	0.006	1.162	0.613	[0.002,0.011]	[1.045,1.279]	[0.584,0.641]	0.877	0.818
	9	0.286	0.505	0.563	[0.1,0.473]	[0.397,0.612]	[0.548,0.578]	0.719	0.913
	11	0.104	0.573	0.682	[-0.017,0.225]	[0.382,0.764]	[0.661,0.702]	0.349	0.891
	13	0.082	0.550	0.777	[-0.028,0.192]	[0.331,0.77]	[0.745,0.81]	0.208	0.836
	15	0.265	0.354	0.82	[-0.046,0.576]	[0.16,0.549]	[0.78,0.861]	0.626	0.875
u1	3	0.876	0.276	0.965	[0.4,1.352]	[0.185,0.367]	[0.957,0.974]	0.654	0.988
	5	0.387	0.282	0.893	[0.098,0.677]	[0.157,0.407]	[0.871,0.916]	0.562	0.924
	7	0.060	0.563	0.92	[-0.012,0.131]	[0.367,0.759]	[0.902,0.938]	0.517	0.965
	9	0.421	0.132	0.936	[0.092,0.749]	[0,0.265]	[0.92,0.951]	0.075	0.96
	11	0.318	0.133	0.932	[0.069,0.566]	[0.001,0.265]	[0.916.0.949]	0.417	0.948
	13	0.571	0.065	0.962	[-0.117,1.258]	[-0.139,0.27]	[0.948,0.977]	-0.006	0.975
	15	0.610	0.007	0.987	[-0.522,1.741]	[-0.31,0.323]	[0.977,0.997]	0.899	0.997
u2	3	0.708	0.297	0.968	[0.34,1.077]	[0.21,0.384]	[0.959,0.976]	0.694	0.987
	5	0.314	0.315	0.946	[0.052,0.576]	[0.176,0.454]	[0.933,0.959]	0.521	0.98
	7	0.048	0.568	0.974	[0.003,0.093]	[0.416,0.721]	[0.966,0.982]	0.667	0.993
	9	0.126	0.347	0.916	[0.015,0.237]	[0.2,0.493]	[0.889,0.943]	0.451	0.86
	11	0.270	0.170	0.97	[-0.003,0.542]	[-0.001,0.34]	[0.962,0.977]	-0.059	0.99
	13	0.210	0.187	0.962	[-0.063,0.483]	[-0.031,0.406]	[0.942,0.981]	0.802	0.981
	15	0.809	-0.033	0.961	[-0.39,2.008]	[-0.287,0.221]	[0.948,0.975]	0.607	0.988

C.4. Model validation

Figure C.1.: Comparison of the different statistics of harmonic magnitudes and phase angles obtained with measurements of residential networks (points) and estimated data (grey bar) - 9th, 11th and 13th harmonics - Customer configuration C1

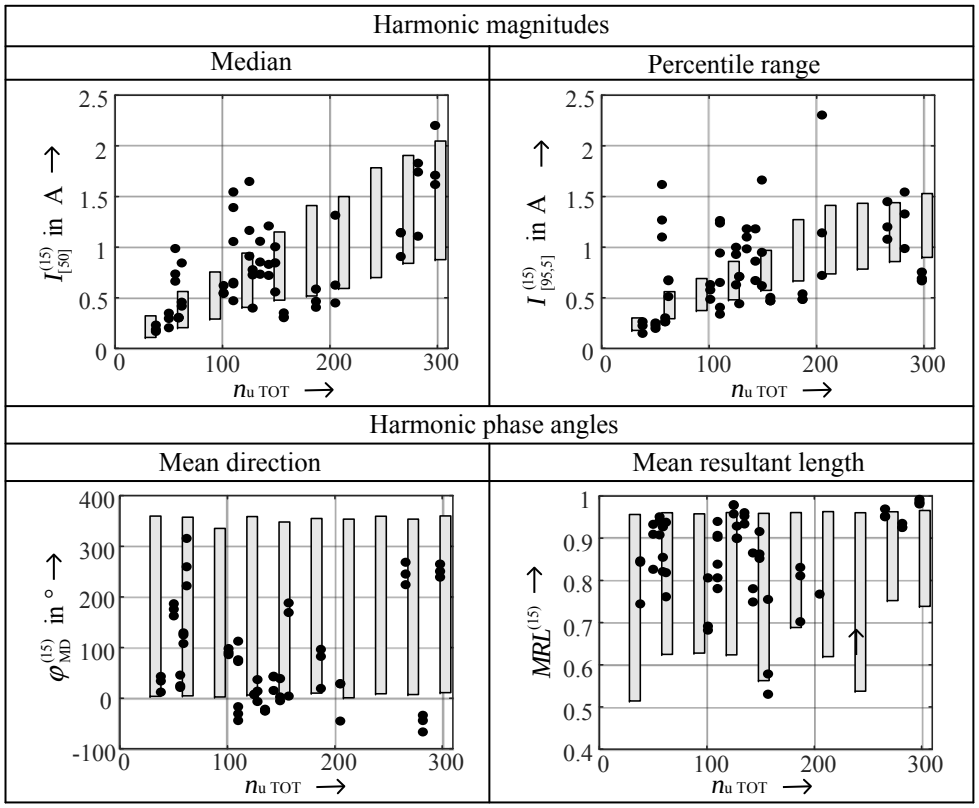

Figure C.2.: Comparison of the different statistics of harmonic magnitudes and phase angles obtained with measurements of residential networks (points) and estimated data (grey bar) - 15th harmonic - Customer configuration C1

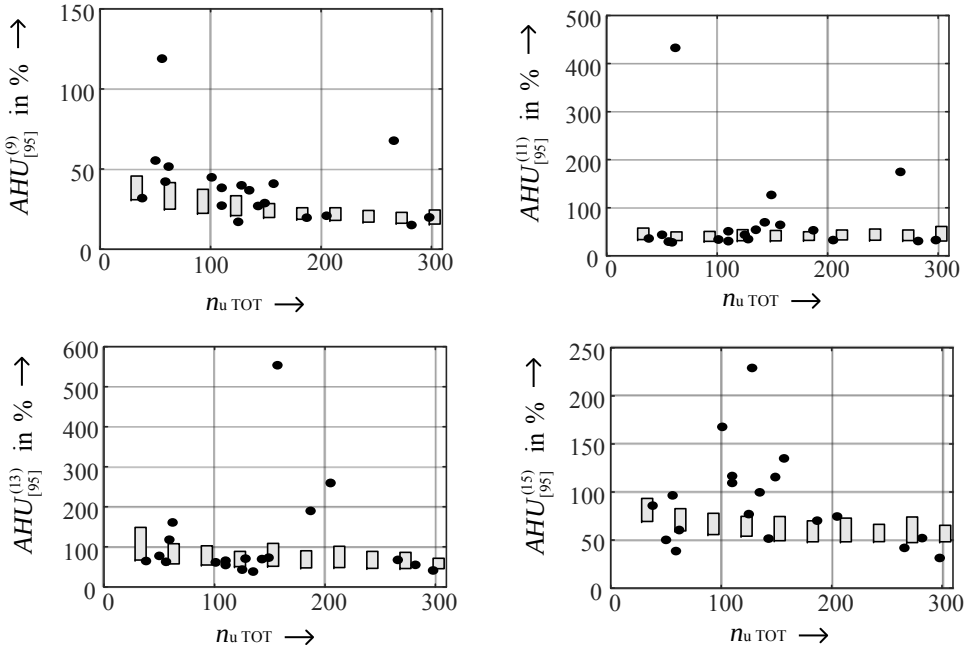

Figure C.3.: Comparison of the 95th percentile of the *AHU* factors obtained with measurements of residential networks (points) and estimated data (grey bar) - 9th, 11th, 13th and 15th harmonics - Customer configuration C1

Figure C.4.: Comparison of the different statistics of harmonic magnitudes and phase angles obtained with measurements of residential networks (points) and estimated data (grey bar) - 3rd, 5th and 7th harmonics - Customer configuration C2

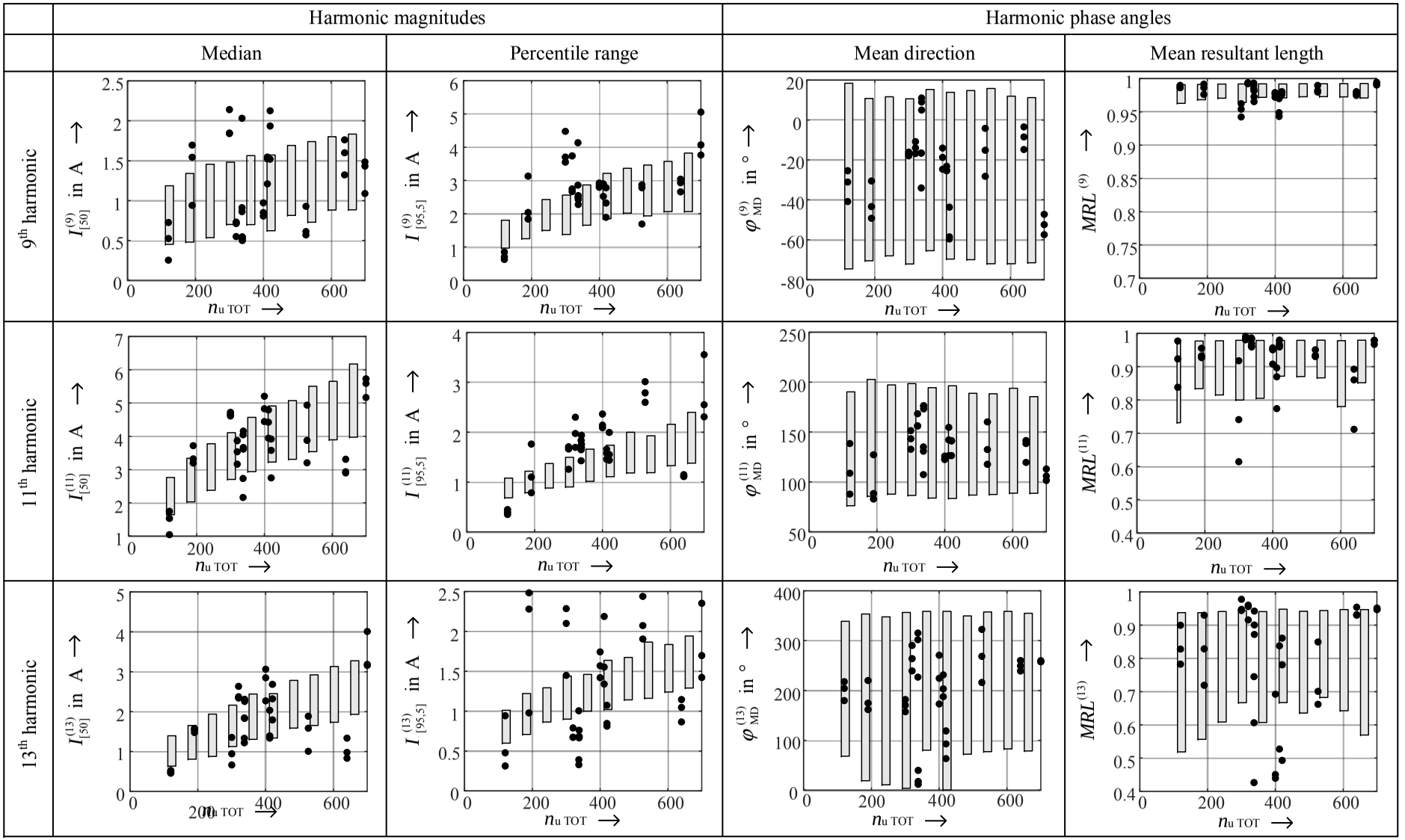

Figure C.5.: Comparison of the different statistics of harmonic magnitudes and phase angles obtained with measurements of residential networks (points) and estimated data (grey bar) - 9th, 11th and 13th harmonics - Customer configuration C2

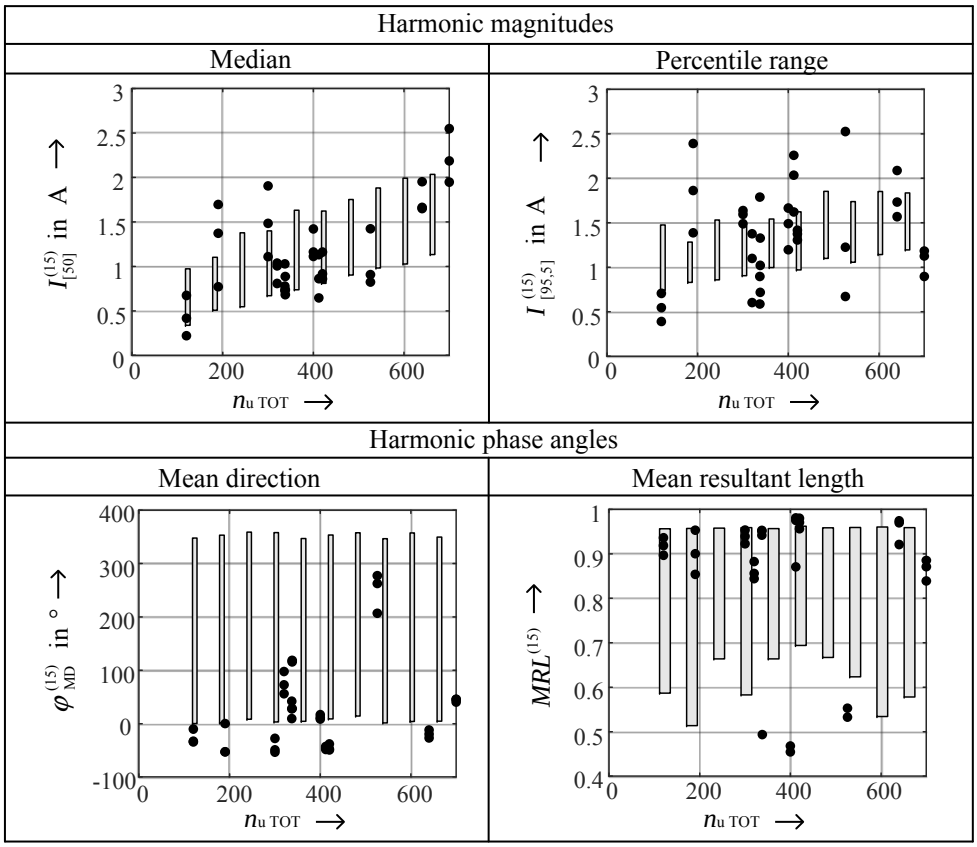

Figure C.6.: Comparison of the different statistics of harmonic magnitudes and phase angles obtained with measurements of residential networks (points) and estimated data (grey bar) - 15$^{\text{th}}$ harmonic - Customer configuration C2

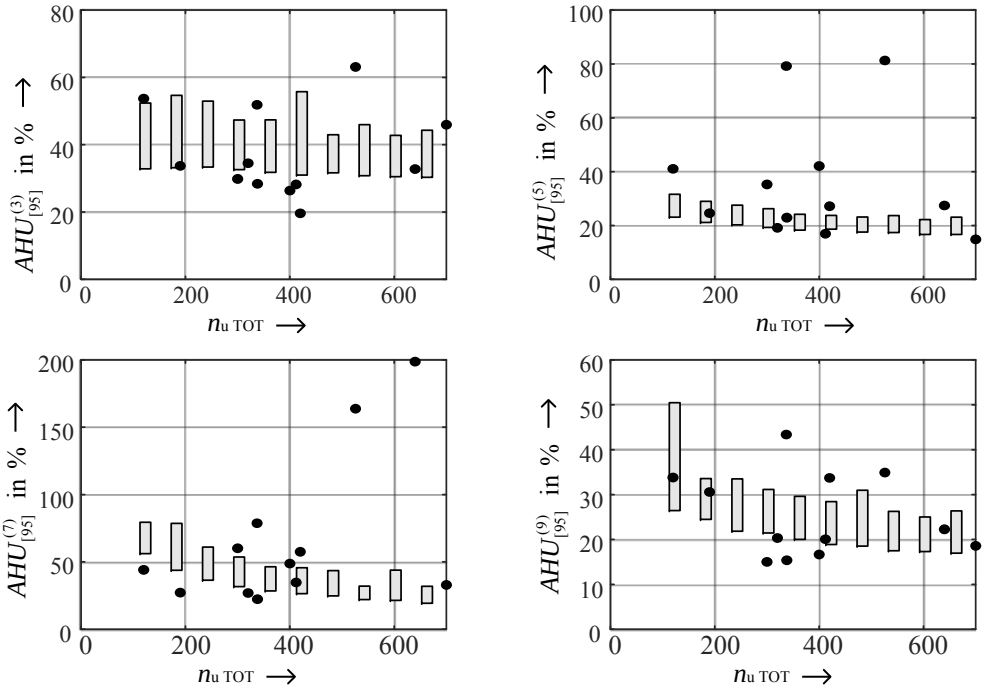

Figure C.7.: Comparison of the 95$^{\text{th}}$ percentile of the *AHU* factors obtained with measurements of residential networks (points) and estimated data (grey bar) - 3$^{\text{rd}}$, 5$^{\text{th}}$, 7$^{\text{th}}$ and 9$^{\text{th}}$ harmonics - Customer configuration C2

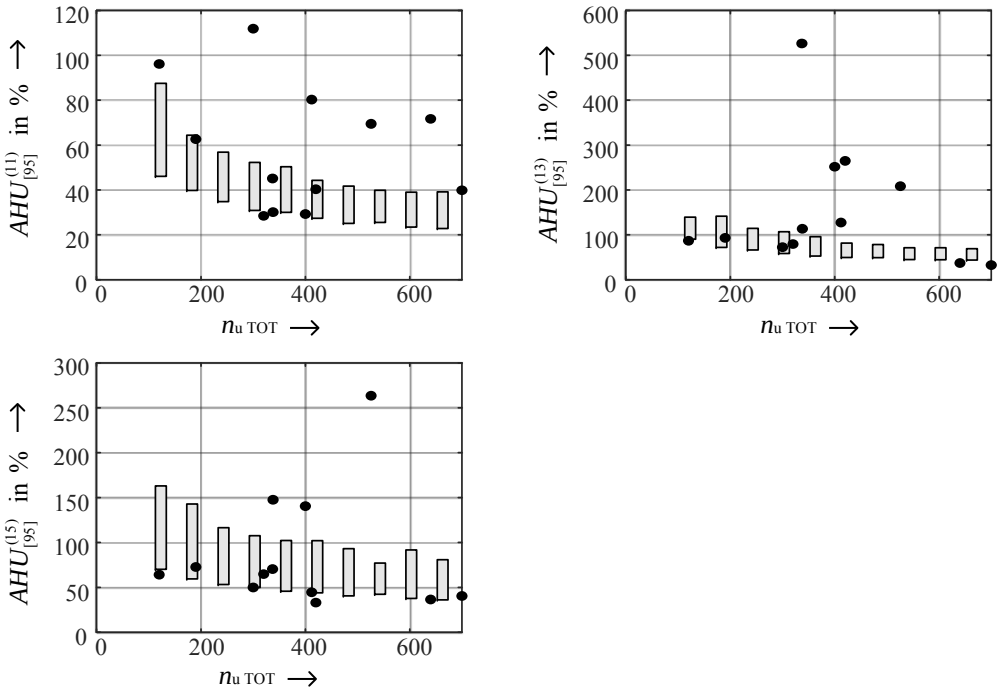

Figure C.8.: Comparison of the 95$^{\text{th}}$ percentile of the *AHU* factors obtained with measurements of residential networks (points) and estimated data (grey bar) - 11$^{\text{th}}$, 13$^{\text{th}}$ and 15$^{\text{th}}$ harmonics - Customer configuration C2

D. Appendix chapter 6 - Model of aggregate residential customers

D.1. Top-down approach

As networks with customer configuration C1 usually have less number of customers in comparison with networks with configuration C2, the cases defined to estimate the $CAF^{(h)}$ factor for each customer category are different. Tables 6.2 and D.2 summarize the selected cases for each customer topology.

Table D.1.: Cases to estimate the $CAF^{(h)}$ factor for customer topology C1

	Case												
	1	2	3	4	5	6	7	8	9	10	11	12	13
n_{cg}	30	30	30	30	30	30	30	30	30	40	40	40	40
m_{cg}	4	6	8	10	2	3	5	7	8	2	3	4	5
$n_{\text{u TOT}}$	120	180	240	300	60	90	150	210	240	80	120	160	200

	Case												
	14	15	16	17	18	19	20	21	22	23	24	25	26
n_{cg}	40	40	40	50	50	50	50	50	60	60	60	60	60
m_{cg}	6	7	8	2	3	4	5	6	2	3	4	5	6
$n_{\text{u TOT}}$	240	280	320	100	150	200	250	300	120	180	240	300	360

Table D.2.: Cases to estimate the $CAF^{(h)}$ factor for customer topology C2

	Case									
	1	2	3	4	5	6	7	8	9	10
n_{cg}	30	30	30	30	30	30	30	30	30	30
m_{cg}	4	6	8	10	12	14	16	18	20	22
$n_{\text{u TOT}}$	120	180	240	300	360	420	480	540	600	660

D.2. Customers aggregation factor

The power functions that describe the correlation between the $CAF^{(h)}$ factor and the number of groups m_{cg} for each harmonic order and each customer configuration are described as:

$$CAF^{(h)} = p \cdot (m_{\text{cg}})^q \tag{D.1}$$

The values of the parameters p and q are given in tables D.3 and D.4

Table D.3.: Regression results of $CAF^{(h)}$ factor for customer topology C1

h	Values		Confidence intervals		R^2_{adj}
	p	q	p	q	
3	1.00	-0.01	[1.00 , 1.01]	[-0.01 , -0.01]	0.99
5	1.01	-0.02	[1.01 , 1.02]	[-0.02 , -0.01]	0.83
7	1.04	-0.26	[1.04 , 1.05]	[-0.26 , -0.25]	0.99
9	1.02	-0.30	[1.02 , 1.03]	[-0.30 , -0.30]	1.00
11	1.05	-0.25	[1.04 , 1.06]	[-0.26 , -0.24]	0.99
13	1.24	0.14	[1.19 , 1.30]	[0.11 , 0.16]	0.79
15	1.17	0.22	[1.12 , 1.23]	[0.20 , 0.25]	0.92

Table D.4.: Regression results of $CAF^{(h)}$ factor for customer topology C2

h	Values		Confidence intervals		R^2_{adj}
	p	q	p	q	
3	1.01	-0.63	[1.00 , 1.01]	[-0.64 , -0.63]	1.00
5	1.02	-0.50	[1.00 , 1.03]	[-0.51 , -0.50]	1.00
7	1.04	0.18	[1.01 , 1.07]	[0.17 , 0.19]	1.00
9	1.04	-0.49	[1.03 , 1.05]	[-0.50 , -0.49]	1.00
11	1.10	-0.42	[1.08 , 1.12]	[-0.43 , -0.41]	1.00
13	1.24	-0.34	[1.16 , 1.31]	[-0.36 , -0.31]	0.99
15	1.16	-0.31	[1.06 , 1.26]	[-0.35 , -0.27]	0.98

D.3. Model validation

Figure D.1.: Comparison of the different statistics of harmonic magnitudes and phase angles obtained with measurements of residential networks (points) and estimated data (grey bar) - 9th, 11th and 13th harmonics - Customer configuration C1

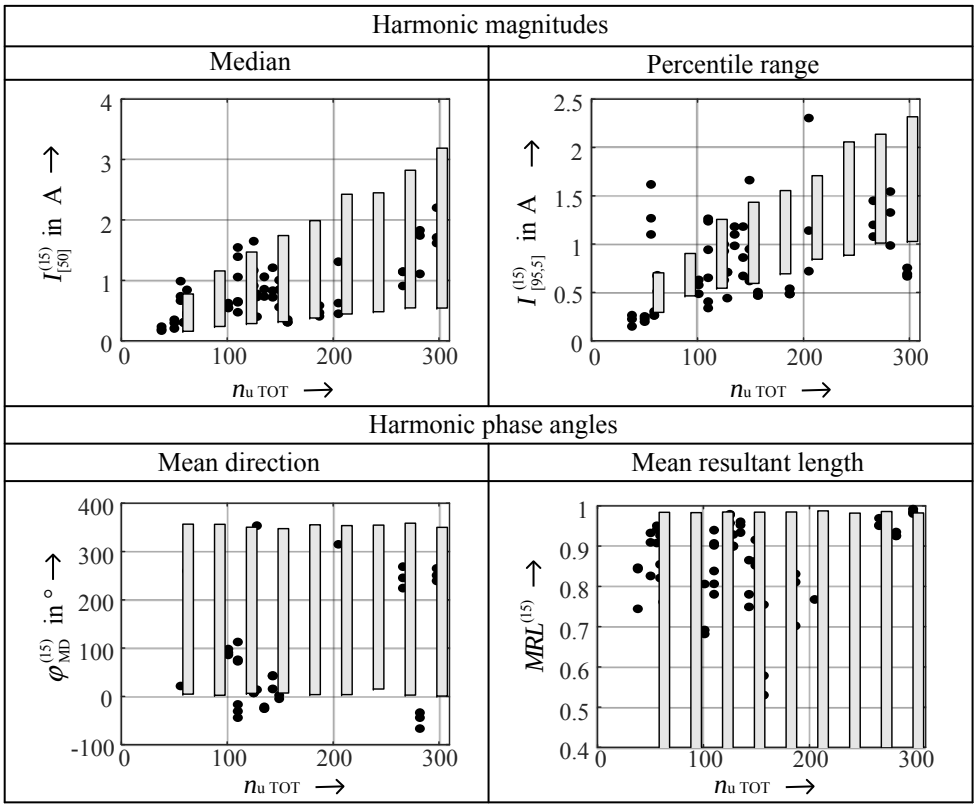

Figure D.2.: Comparison of the different statistics of harmonic magnitudes and phase angles obtained with measurements of residential networks (points) and estimated data (grey bar) - 15th harmonic - Customer configuration C1